DE-AC02-76ER01198

DOE/ER/01198/1382

TIC

MASTER

INTERSTITIAL-IMPURITY INTERACTIONS IN COPPER-SILVER AND ALUMINUM-MAGNESIUM ALLOYS

BY

HUMPHREY PAN WONG

A.B., University of California, 1975
M.S., University of Illinois, 1977

THESIS

Submitted in partial fulfillment of the requirements
for the degree of Doctor of Philosophy in Physics
in the Graduate College of the
University of Illinois at Urbana-Champaign, 1982

Urbana, Illinois

DISTRIBUTION OF THIS DOCUMENT IS UNLIMITED

PACS indices: 61.70.Yq
61.80.Fe
62.40.+i

DISCLAIMER

This report was prepared as an account of work sponsored by an agency of the United States Government. Neither the United States Government nor any agency Thereof, nor any of their employees, makes any warranty, express or implied, or assumes any legal liability or responsibility for the accuracy, completeness, or usefulness of any information, apparatus, product, or process disclosed, or represents that its use would not infringe privately owned rights. Reference herein to any specific commercial product, process, or service by trade name, trademark, manufacturer, or otherwise does not necessarily constitute or imply its endorsement, recommendation, or favoring by the United States Government or any agency thereof. The views and opinions of authors expressed herein do not necessarily state or reflect those of the United States Government or any agency thereof.

DISCLAIMER

Portions of this document may be illegible in electronic image products. Images are produced from the best available original document.

DOE/ER/01198--1382

DE82 015207

INTERSTITIAL-IMPURITY INTERACTIONS IN COPPER-SILVER AND ALUMINUM-MAGNESIUM ALLOYS

BY

HUMPHREY PAN WONG

A.B., University of California, 1975
M.S., University of Illinois, 1977

THESIS

Submitted in partial fulfillment of the requirements
for the degree of Doctor of Philosophy in Physics
in the Graduate College of the
University of Illinois at Urbana-Champaign, 1982

DISCLAIMER

This book was prepared as an account of work sponsored by an agency of the United States Government. Neither the United States Government nor any agency thereof, nor any of their employees, makes any warranty, express or implied, or assumes any legal liability or responsibility for the accuracy, completeness, or usefulness of any information, apparatus, product, or process disclosed, or represents that its use would not infringe privately owned rights. Reference herein to any specific commercial product, process, or service by trade name, trademark, manufacturer, or otherwise, does not necessarily constitute or imply its endorsement, recommendation, or favoring by the United States Government or any agency thereof. The views and opinions of authors expressed herein do not necessarily state or reflect those of the United States Government or any agency thereof.

Urbana, Illinois

DISTRIBUTION OF THIS DOCUMENT IS UNLIMITED

MGW

PACS indices: 61.70.Yq
61.80.Fe
62.40.+i

THIS PAGE

WAS INTENTIONALLY

LEFT BLANK

INTERSTITIAL-IMPURITY INTERACTIONS IN COPPER-SILVER AND ALUMINUM-MAGNESIUM ALLOYS

Humphrey Pan Wong, Ph.D.
Department of Physics
University of Illinois at Urbana-Champaign, 1982

Our purpose has been to determine the configurations and dynamical properties of complexes formed between interstitials and oversized impurities in electron-irradiated aluminum and copper. Measurements were taken of the ultrasonic attenuation (at 10 and 30 MHz) and resonant frequency (at 10 MHz) in single crystal samples of Cu-Ag and Al-Mg.

A variety of peaks appeared in both materials in plots of the logarithmic decrement versus temperature. The simultaneous presence of multiple defects was established by the different annealing behavior shown by each peak. It was found that interstitial trapping in our oversized systems was generally weaker than in previously studied undersized systems.

The principal features in Cu-Ag that must be accounted for by a model include the following: 1) Three low-temperature peaks (including the main one at 16 K, peak 1) were seen having trigonal symmetry. 2) Peak 1 annealed away at 110 K uncorrelated with any resistivity recovery. 3) Peak 1 grew at 60 K, correlated with a resistivity decrease.

For Al-Mg, the principal features associated with the main peak (peak 6) include: 1) Peak 6 was seen at a high temperature (>135 K)

having trigonal symmetry. 2) It annealed away at 127 K and seemed to correlate with a resistivity decrease. 3) The remaining peaks (1-5) grew while peak 6 annealed away.

The implications of an existing model were developed. This model was based on the predominant influence of size effects in determining impurity-interstitial interactions. Predictions were compared with the experimental results. No evidence was found for the deeply-trapped <110>-orthorhombic defect predicted by the existing model. Therefore, two alternative models were developed.

Model A uses a "canted dumbbell" at the next-nearest neighbor position to explain the results. Model B uses a point interstitial at an octahedral position. A distinction between the two which is subject to experimental check is that model A predicts that interstitial migration between different impurity atoms occurs near 127 K in Cu-Ag while model B predicts a migration temperature near 60 K.

ACKNOWLEDGEMENTS

The author gives sincere thanks to his advisor, Professor A.V. Granato for his patience, advice, and encouragement. This thesis benefited greatly from his physical insight and his way of expressing it during many invaluable discussions.

He also expresses gratitude to Drs. G.G. Setser, D.L. Johnson, and K.L. Hultman for their work in developing the apparatus and techniques used in this experiment.

Of course, much thanks and appreciation go to Mr. P. Wallace, who made the computer work, and to Mr. W. Johnson who just plain worked. Without their help and long hours, this thesis would not have been possible.

Finally, thanks and love go to Barb for her support and friendship during so much of the author's graduate career. He plans on missing her for a long, long time.

The author gratefully acknowledges the support of the United States Department of Energy under contract DE-AC02-76ER01198.

TABLE OF CONTENTS

Page

LIST OF FIGURES

C(bottom): Normal atom becomes the interstitial at octahedral site.

LIST OF TABLES

CHAPTER 1

INTRODUCTION

Our purpose has been to determine the configurations and dynamical properties of complexes formed between interstitials and oversized impurities in electron-irradiated aluminum and copper. Ultrasonic measurements offer symmetry information about defects and provide an excellent way of identifying their configuration. Previous ultrasonic studies have been conducted by Johnson(1978)[1] and Hultman(1979)[2] on aluminum alloys containing undersized impurities. However, only limited agreement was found between those studies and a model developed by Dederichs,et al.(1976)[3] in which the size effect plays a dominant role. Closer agreement is expected in the oversized case where the predicted perturbations near the oversized atom are smaller, leading to better justification for the model's use. Two oversized systems, Al-Mg and Cu-Ag, were chosen for this investigation. Al-Mg provides a natural extension to the oversized case of ultrasonic measurements already performed for several undersized aluminum alloys. Cu-Ag was selected because it had earlier been the subject of an extensive resistivity study by Cannon and Sosin(1975).[4] The results we obtained do not agree with the predictions made by Dederichs,et al., nor are they entirely consistent with the interpretation by Cannon and Sosin of their annealing results. Two models are proposed which can account for our principal results as well as the resistivity results obtained by

Cannon and Sosin.

The study of defect-impurity interactions has both scientific and technological significance and has been undertaken with a variety of techniques in metals. These include measurements of resistivity, channeling, internal friction, Mössbauer, and Perturbed Angular Correlation (PAC). The latter two are made only in special systems for which a suitable impurity is available and will not be discussed in further detail here.

Resistivity recovery measurements detect the changes in the electrical resistivity caused by radiation-induced defects and their annealing at successively higher temperatures. Interstitial concentrations, as well as migration and binding energies, can be obtained, but no symmetry information is available from resistivity studies.

Channeling measurements use backscattered ions from oriented and irradiated crystals to obtain the "apparent fraction" of solute atoms displaced by trapped defects into normally clear channels in the crystal structure. According to Swanson and Maury(1975)[5] this technique can be used to determine the configurations of defect-impurity pairs by simply comparing the displacements into different channels. However, large defect concentrations of greater than 100 ppm are required, and in practice, concentrations of about 1000 ppm are normally used. The high concentrations lead to increased interactions between defects so that conclusions from this data about the nature of isolated defects should be made with some caution. Also,

since the "apparent fraction" of solute atoms displaced represents an average over the displacements caused by all the defects in the crystal, it is only with some difficulty that the channeling technique can distinguish between defects of differing configurations which might be present in the sample simultaneously. Several different defect types have been found at defect concentrations as low as 100 ppm with the use of internal friction measurements in electron-irradiated samples (Rehn, Robrock, and Jacques, 1978).[6] Using ultrasonics, Hultman(1979)[2] has also detected the presence of several defect types in samples irradiated to Frenkel pair concentrations of only 10 ppm. Rehn, Robrock , and Jacques[6] further suggest that at the defect concentrations used in channeling experiments, defect clustering probably occurs, resulting in displacements quite different from those caused by single defect-impurity complexes. Therefore, while some symmetry information is available from the channeling measurements, precise interpretations in terms of simple defect-impurity configurations remain in doubt in many cases.

Torsional pendulum experiments (at oscillation frequencies on the order of 100 Hz) have been performed to detect the relaxations of defects formed in irradiated metals (Rehn, Robrock, and Jacques,1978).[6] The relaxations appear as peaks in a plot of the logarithmic decrement (which is a measure of internal friction) versus temperature and, for single crystals, contain information about the symmetry of the defect. Furthermore, these measurements are sensitive to the presence of only a few ppm of defects. However, looking for different symmetries requires

the preparation of different samples, a procedure which is both time-consuming and difficult.

Our measurements have been of internal friction and elastic constant changes at ultrasonic frequencies (10 and 30 MHz) in irradiated single crystals. Ultrasonic studies, unlike those of the resistivity, offer symmetry information about the defects observed and, in contrast to channeling measurements, are able to differentiate between the configurations and reorientation energies of different defects present in the sample at the same time. Also, the required concentrations are only a few parts per million which decreases the interactions between induced defects and permits the study of defects which are more nearly isolated from each other. Unlike internal friction experiments at low frequencies, use of ultrasonics allows the monitoring of each of the independent elastic constants by merely changing the polarization or direction of propagation of the sound wave. Only a single sample is necessary. Furthermore, higher frequencies allow the observation of processes (such as those involving quantum effects) at higher, more accessible temperatures. A resulting drawback however is that some relaxation peaks are pushed to a temperature higher than their annealing temperature and are consequently either not observed or are observed in the midst of annealing. A final useful feature of ultrasonics makes use of the proportionality between one component of the attenuation and the electrical conductivity at temperatures below about 100 K which causes the attenuation to rise to a plateau at about 5 K. The plateau is

produced by the residual resistivity of the sample which changes with impurity and Frenkel pair concentration. Thus, a measurement of the plateau's height permits a calculation of the number of defects introduced by the irradiation (see Hultman[2]).

Historically, resistivity measurements have played a large role in understanding some of the fundamental aspects of radiation damage in metals. Irradiation displaces atoms from their normal sites and creates Frenkel pairs which scatter conduction electrons and change the residual resistivity. This change gradually disappears as thermally activated processes at higher and higher temperatures cause trapped defects to escape and migrate through the metal until they find annihilatory sinks. These processes are grouped in distinct stages and substages which can be found in most irradiated metals (Schilling, et al[7].) There are three main stages of interest here: Stage I which takes place in aluminum and copper between 15 and 60 K, Stage II between 60 and 200 K, and Stage III between 200 and 300 K.

Stage I results from interstitial migration to vacancies. There are several substages, labeled A-E. Stages I_A-I_D are concentration independent, while I_E shifts to lower temperatures with increasing dose, and is absent in impure or cold-worked specimens. Stages I_A-I_D were discovered by Magnuson, Palmer, and Koehler[8] and supposed by them to result from annihilation of interstitial-vacancy pairs close enough so that their strain-field interaction reduced the activation energy for annihilation. Stage I_E was found by Corbett, Smith, and Walker[9] to have the same activation energy as I_D to within experimental error, and

they proposed that I_E corresponded to long-range migration of the interstitial to a vacancy sink, while I_D corresponded to short-range correlated migration of an interstitial to its own vacancy. Granato and Nilan[10] found substructure in I_D and supposed it to be partly due to weakly interacting close-pairs and partly to correlated recovery.

Stage III is generally thought to correspond to recovery caused by the recombination of migrating vacancies with interstitials trapped by impurities or other interstitials.

Stage II in very pure materials consists of a small and nearly structureless recovery. It is with the introduction of impurities that the amount of recovery becomes large and marked by distinct substages whose exact number, size, and location depend upon the amount and type of impurity present.[11,12,13,14] The impurity atoms trap migrating interstitials and hold them until higher temperatures result in either release from the trap, reconfiguration, or annihilation by a vacancy migrating in stage III[4,14].

A treatment by Eshelby(1955)[15] of the elastic interactions between point defects led to Hasiguti's[16] suggestion in 1960 that the volume change caused by an impurity atom in a cubic crystal helped determine the strength and nature of its trapping ability. He offered the suggestion that strongly undersized solute atoms would produce a single deep trap while oversized atoms were capable of several shallow traps. In fact, a similar prediction was made by Dederichs(1976),*et al.*[3] following an atomistic calculation using either a Morse, a Modified Morse, or a Born-Mayer potential to calculate possible stable positions

for the interstitial.

Until recent years, the actual geometry of an isolated interstitial was in doubt. Hasiguti(1960)[16] assumed a point interstitial for his calculations. He also supposed that it retained its identity as a point interstitial without radically affecting the positions of the atoms around it when it became trapped by an impurity. Sosin(1967),[17] while using Hasiguti's basic approach, proposed that the preferred trapping configuration might instead consist of a <100> self-interstitial dumbbell trapped at one of several possible sites around the impurity atom. Sosin's model was based on earlier calculations by Gibson, et al.(1960)[18] and Johnson(1966)[19] which showed the <100> split dumbbell to be the most stable form of the self-interstitial in pure fcc metals. This dumbbell consists of two host atoms whose axis is oriented in the <100> direction and centered on a normal lattice site. Sosin also used this model (with its several trapping locations) to explain the number of substages observed in copper alloys.

In pure metals, experimental evidence for the <100> split dumbbell configuration was first obtained using elastic constant measurements in copper by Holder, Granato, and Rehn,[20] who found a large diaelastic reduction in C_{44}, as predicted by Dederichs, Lehmann, and Scholz.[21] There is now strong experimental evidence for this configuration for both Cu and Al from elastic constant measurements[22] and from diffuse x-ray scattering measurements.[23]

A simple theoretical treatment comes from Dederichs, et

al.(1976).[3] Dederichs, et al. concluded that for fcc metals, undersized solute atoms would trap intersititals deeply, forming <100> "mixed dumbbells" with the trapped interstitial if the size difference between solute and host were not too great. Oversized solute atoms on the other hand would form shallow traps, trapping the self-interstitial dumbbell nearby but without forming a mixed dumbbell.

Thus, a model exists relating possible trapping configurations in a dilute alloy to a single parameter: namely, the size difference between impurity and host. Figure 1 illustrates the favored trapping configurations for both the undersized and the oversized case. Figure 1A shows the <100> mixed dumbbell which is believed to form for undersized impurities. The impurity is shown jumping between two equivalent sites within a "cage" formed by the host atoms. Figure 1B shows the deepest trapping configurations for a dumbbell near an oversized impurity. The dumbbell is shown jumping between two of the equivalent sites. (The remainder are depicted by the darkened ellipses.)

Experimentally, evidence for a <100> mixed dumbbell in undersized materials has come from several sources. Swanson, et al.[24] first suggested the existence of the <100> mixed dumbbell in 1973 to account for his channeling results in Al-Mn. They also proposed mixed dumbbell formation in aluminum alloys containing Fe, Zn, and Ag(1976)[25] (although Ag, in fact, is very slightly oversized.) Vogl and Mansel(1976)[26] conducted Mössbauer measurements following irradiation of $Al^{57}Co(^{57}Fe)$ and detected motion of the impurity atom within a

Figure 1. A) The <100> mixed dumbbell, consisting of an interstitial and an undersized impurity atom (shown as the smaller, darkened circle). The impurity is shown jumping between two of its 6 equivalent positions within a "cage" of host atoms.

B) The trapped <100> dumbbell in the deepest trap predicted by Dederichs, et al.[3] for an oversized impurity. It is shown jumping between two of its 12 equivalent positions. The other positions are indicated by the darkened ellipses.

A. Undersized Impurity —
⟨100⟩ Mixed Dumbbell

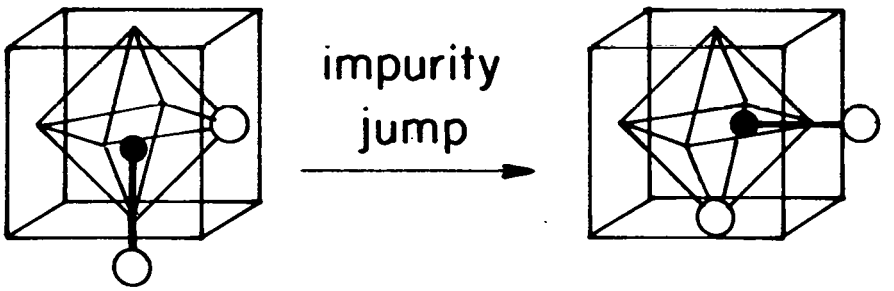

B. Oversized Impurity —
Trapped ⟨100⟩ Self-Interstitial Dumbbell

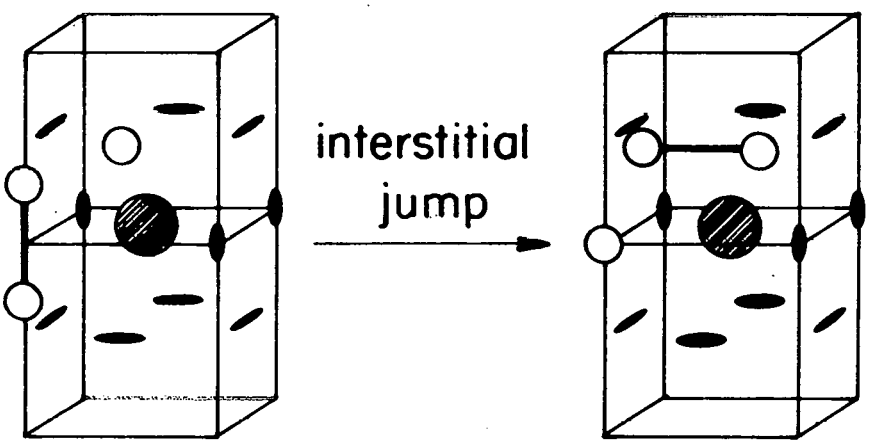

"cage" of host atoms (possibly the reorientation of a mixed dumbbell). Ultrasonic measurements by Hultman(1979)[2] provide evidence that <100> mixed dumbbells are formed in irradiated Al-Zn. However, measurements in Al-Fe[2] and in Al-Mn(Johnson,[1] 1978) suggest the importance of factors other than size effect in determining the impurity-interstitial complex. Both Fe and Mn are similarly undersized in aluminum yet both alloys produced quite different relaxation spectra. Furthermore the observations cannot be explained by the simple <100> mixed dumbbells of Dederichs, et al.'s model. So, for the case of undersized impurities, there remains substantial disagreement between experiment and theory.

In the case of oversized impurities, channeling measurements(Swanson, et al.[25], 1976) in aluminum alloys with Mg, Ga, and Sn and copper alloys with Ag, Au, and Sb indicate weak trapping by the solute atoms, i.e. only slight displacements of the solute atoms from their lattice sites were deduced, consistent with the presence nearby of a trapped self-interstitial dumbbell as described by Dederichs, et al.[3] However, the size of the apparent displacements as well as the large defect concentrations required for the channeling measurement makes any dtailed interpretation difficult.

Very little data is available on the symmetry of possible impurity-interstitial configurations in oversized materials. Internal friction measurements of Cu-In and Al-Mg by Kollers, Jacques, Robrock, and Rehn(1981)[27] indicated the presence of relaxation processes, but since they were conducted in polycrystalline samples the symmetry of those processes is unknown. Our present investigation of single

crystals is capable of gaining symmetry information about the relaxations and therefore of deciding whether they are consistent with the trapping configuration (figure 1B) suggested by Dederichs, et al.[12] and by Cannon and Sosin.[4]

Resistivity studies have been made on both Al-Mg and Cu-Ag so that the temperatures of the resistivity recovery stages in each material are known. Since it is possible in certain cases[1,2] to identify internal friction peaks with some of the radiation-induced defects which anneal away during these recovery stages, knowledge of the resistivity recovery spectra is extremely useful in planning the irradiation temperature and the annealing program for our own experiment. Cu-Ag has been studied in particular detail by Cannon and Sosin(1975)[4], who developed a simple model for the annealing and the geometry of the trapped interstitial. Their experiment studied the resistivity recovery following 1.5 Mev electron irradiation of dilute copper alloys of gold and of silver in varying concentrations. Both Cu-Ag and Cu-Au displayed similar annealing behavior. They observed four substages in stage II, but only three were large enough to be considered significant for our results. These were, for Cu-Ag, II_b at 60 K, II_c at 130 K, and II_d at 195 K.

II_b was believed to be caused primarily by the migration of interstitials from shallow traps to deep traps at the same impurity. (See figure 2A.) This was based on the fact that the fractional amount of recovery seen did not change with increasing impurity concentration. If, instead of this reconfiguration, migration away from the impurity

Figure 2. A) Cannon and Sosin's model[4] for explaining resistivity substage II_b at 60 K in Cu-Ag. The dumbbell is shown jumping from the shallow trap to the deep trap.

B) Dederichs, et al.'s results[3] for the binding energy of the defect complex consisting of a <100> dumbbell trapped by an oversized impurity located at the sites shown. Each site is labeled by its binding energy . The energy is in units of the binding energy of the mixed dumbbell. Positive energies are binding.

A.

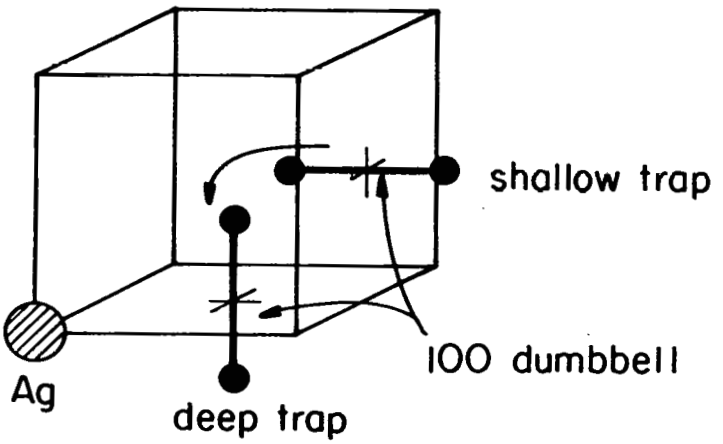

B.

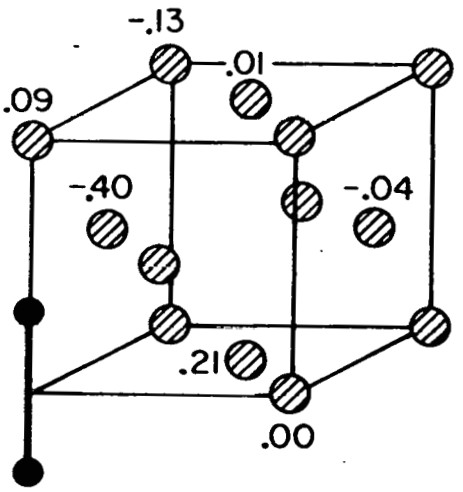

Binding energies

had taken place, some correlated recovery (caused by annihilation with the interstitial's own vacancy) would have occurred. This would have resulted in enhancement of the recovery substage with increasing impurity content because a greater fraction of the interstitials would have been trapped at impurities close to their own vacancies. This enhancement did not take place, according to Cannon and Sosin. Therefore, reconfiguration of the interstitial at the same impurity was concluded to have occurred rather than the release of the interstitial from the impurity. It should be noted, however, that other studies[14] have indicated that reconfiguration should not change the resistivity. Further discussion of this point will appear in chapter 4.

Resistivity substage II_C, at 130 K, displayed behavior consistent with interstitials being released from the Ag impurity. Upon release, the interstitials perform a random walk away from the impurity atoms; some will run into their own correlated vacancies nearby. Others will move away from their own vacancies and encounter other impurity atoms from which they escape again. Eventually, these freely migrating interstitials find either a very deep trap and are bound, or a foreign uncorrelated vacancy and are annihilated. The resulting uncorrelated recovery (at about 130 K) takes place at a somewhat higher temperature than the correlated recovery (at about 120 K) because of the additional time spent escaping impurity atoms. Since, as argued earlier, increasing impurity content should result in a greater fraction of correlated recovery occurring, one would expect a change in the shape of substage II_C with increasing Ag concentration as the lower

THIS PAGE

WAS INTENTIONALLY

LEFT BLANK

atom located at the sites indicated. The energies are in units of the binding energy of the mixed dumbbell. Values for these energies in eV can be found in Table VII. The deepest trap is marked .21. Note that the dumbbell moves and the impurity does not. Only its relative position changes.

Resistivity studies by Garr and Sosin(1967)[28] on Al-Mg were not nearly as complete as those performed on Cu-Ag. However, the presence of a major substage at 127 K guided our attention to possible changes in the ultrasonic attenuation occurring in this annealing region. Since Mg is oversized in Al by about the same amount as Ag is in Cu, Dederichs, et al.'s model predicts that the trapping configurations and energies should also be very similar. That is, the deep trap expected in Cu-Ag should also be found in Al-Mg.

Our experiment can detect relaxations of the elastic constant that are related to the reorientation of a defect between equivalent sites. We use pure shear modes of elastic waves propagating in the [110] direction and oriented in either the [001] direction (for detecting relaxations of the elastic constant C_{44}) or the $[1\bar{1}0]$ direction (for relaxations of the elastic constant C'). The corresponding applied stresses (for cubic crystals) possess symmetries which are given by the group theoretical designations T (for observing C_{44} relaxations) and E (for observing C' relaxations). The C_{44} and C' relaxations can also be observed using longitudinal waves propagating in the <111> and <100> directions respectively (see Nowick and Berry[24]).

The relaxations which occur under a particular stress are

determined by the symmetries of the defect, the crystal, and the stress applied. A defect possessing symmetry lower than that of the crystal can occupy one of several equivalent sites in the lattice. Applying the proper stress removes the degeneracy and makes some of the sites favored over others. The resulting "stress-induced ordering" produces a relaxation which is visible in measurements of the internal friction. For example, a defect with trigonal symmetry in a cubic crystal will relax under a T symmetry stress (if it relaxes at all) but will not relax under an E symmetry stress. This means that a trigonal defect could produce a C_{44} relaxation but not a C' relaxation. Other examples are given by Nowick and Berry[24] in a table relating the symmetries of the defect, the crystal, and the applied stress to the possible relaxations of the elastic constants.

The deep trapping configuration (marked by .21 in figure 2B) proposed by Dederichs, et al.[3] and by Cannon and Sosin[4] possesses <110>-orthorhombic symmetry and, according to Nowick and Berry, would relax under both E and T symmetry stresses if it relaxed at all; that is, both C' and C_{44} relaxations should be expected. Figure 3A shows the twelve equivalent positions of the trapped dumbbell around its impurity. An elementary jump performed between two of the positions is shown. Figure 3B shows the equivalent sites as squares before any stress is applied. Note that the degeneracy of the equivalent positions is removed by either a <100>- or a <111>-propagating longitudinal wave, which acts like a uniaxial stress in those directions. Sites of different energy are now distinguished by

Figure 3. A) The twelve equivalent positions for a dumbbell in the deepest trap around an oversized impurity, according to Dederichs, et al.[3] An elementary jump is shown, with the initial and final positions of the dumbbell atoms all in the same (100) plane.

B) The twelve equivalent sites are marked by squares before a stress is applied. Uniaxial stresses may be applied in the form of longitudinal waves, as shown. The degeneracy is removed, producing sites of different energies shown as triangles and squares.

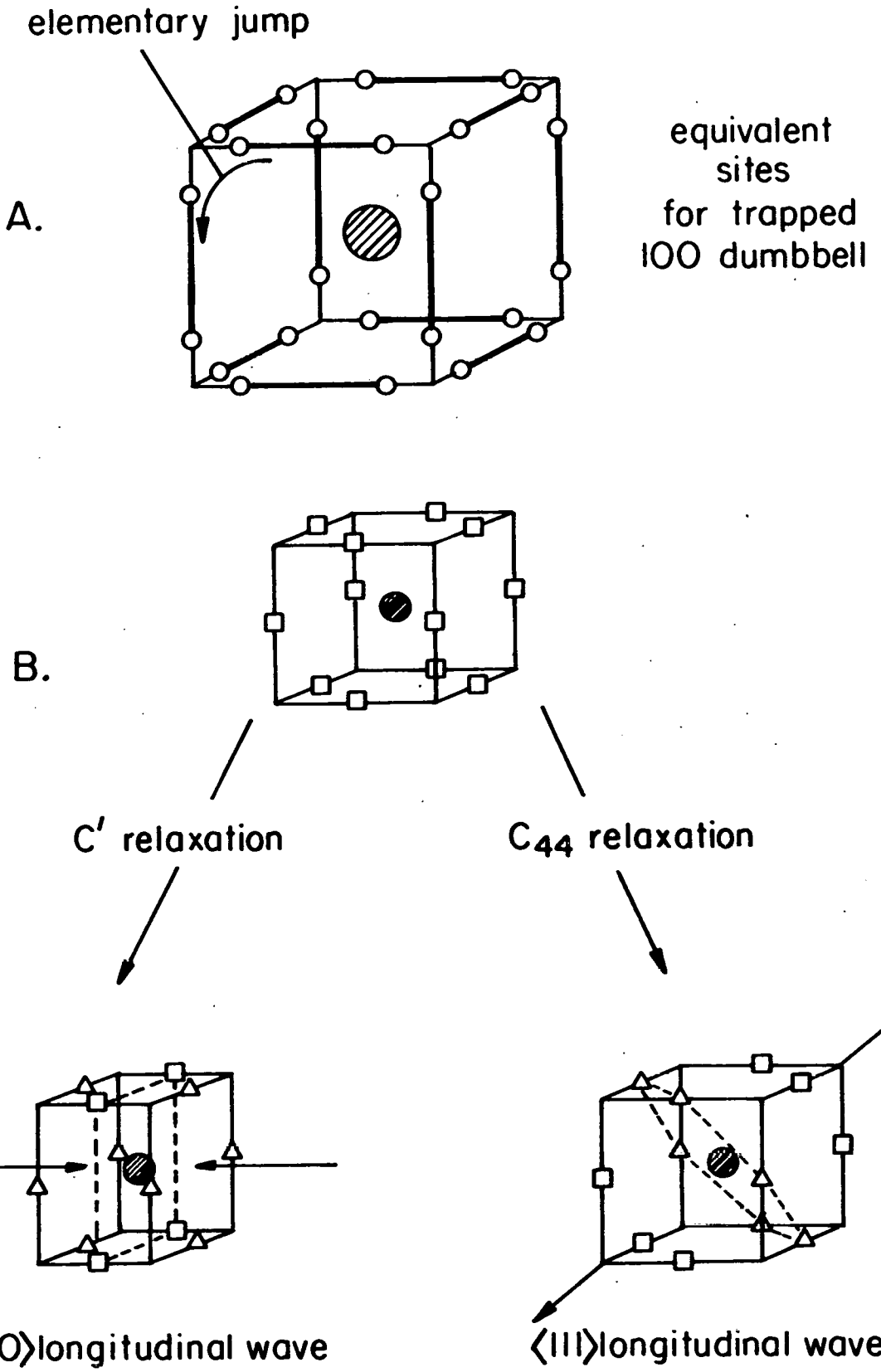
elementary jump
A.
equivalent sites for trapped 100 dumbbell
B.
C′ relaxation
C_{44} relaxation
⟨100⟩longitudinal wave
⟨111⟩longitudinal wave

triangles and squares.

We made 10 and 30 MHz measurements of the ultrasonic attenuation and the resonant frequency in single crystals of our dilute alloys. Both the T symmetry mode (elastic constant C_{44}) and the E symmetry mode (elastic constant C') were examined for internal friction peaks. Only C_{44} relaxations were present; no peaks were seen in the E symmetry (C') mode. This result is inconsistent with the relaxation of a <110> orthorhombic defect (like that shown in figure 3). Peaks in both modes were found in Al-Mg, but the annealing behavior ruled out the orthorhombic configuration predicted. Therefore, two modified versions of the predicted geometries were developed and will be presented later in this thesis.

CHAPTER 2

EXPERIMENT

We give a brief overview of the experiment first, followed by a more detailed description of the apparatus and procedure used.

Ultrasonic pulses are sent into one side of a sample via a quartz transducer. The pulses are reflected from the opposite parallel surface and return to the transducer producing an echo visible on an oscilloscope. The returning pulse bounces back and forth between the faces and forms the pattern shown in figure 4.

Due to relaxation mechanisms within the crystal, energy is absorbed from the ultrasonic pulse with each passage through the sample causing attenuation of the echoes. This attenuation is measured at 10 and 30 MHz as a function of temperature before irradiation (producing the "background" curve shown schematically in figure 5), after irradiation, and during the annealing program. Irradiation is by 2.5 Mev electrons at a fixed temperature which is above the end of Stage I so that interstitials which are formed freely migrate until they are trapped. These trapped interstitials provide new relaxation mechanisms that change the temperature dependence of the attenuation from the background curve, sometimes producing peaks caused by relaxation processes as shown in figure 5. In fact, we can obtain the number of defects introduced to the sample by monitoring the changes in the attenuation caused by the increased electrical resistivity. By raising

Figure 4. Sample with ultrasonic quartz transducer bonded in place with Nonaq stopcock grease. Pulses reflect between opposite parallel surfaces, producing echoes shown on oscilloscope screen. Electrons strike the sample opposite from the transducer.

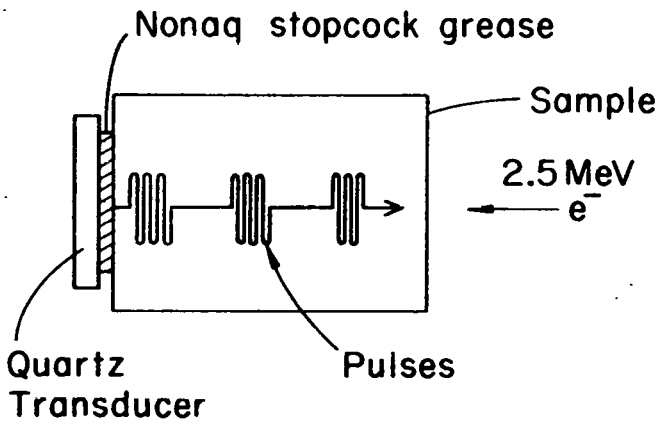

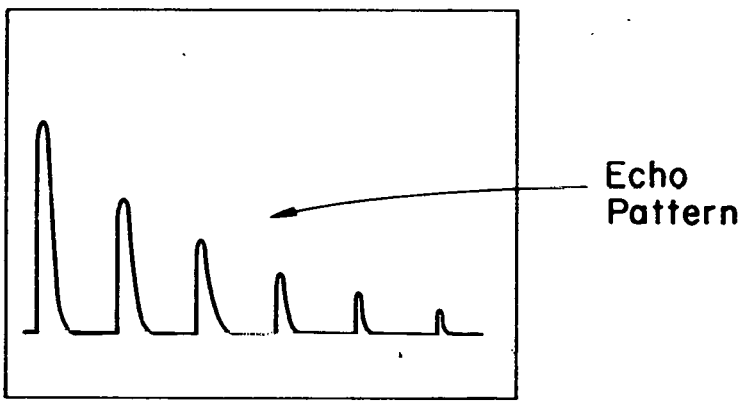

Oscilloscope screen

Figure 5. A schematic representation of the ultrasonic attenuation as a function of temperature between 5 and 200 K. Three stages of the experimental measurements are shown.

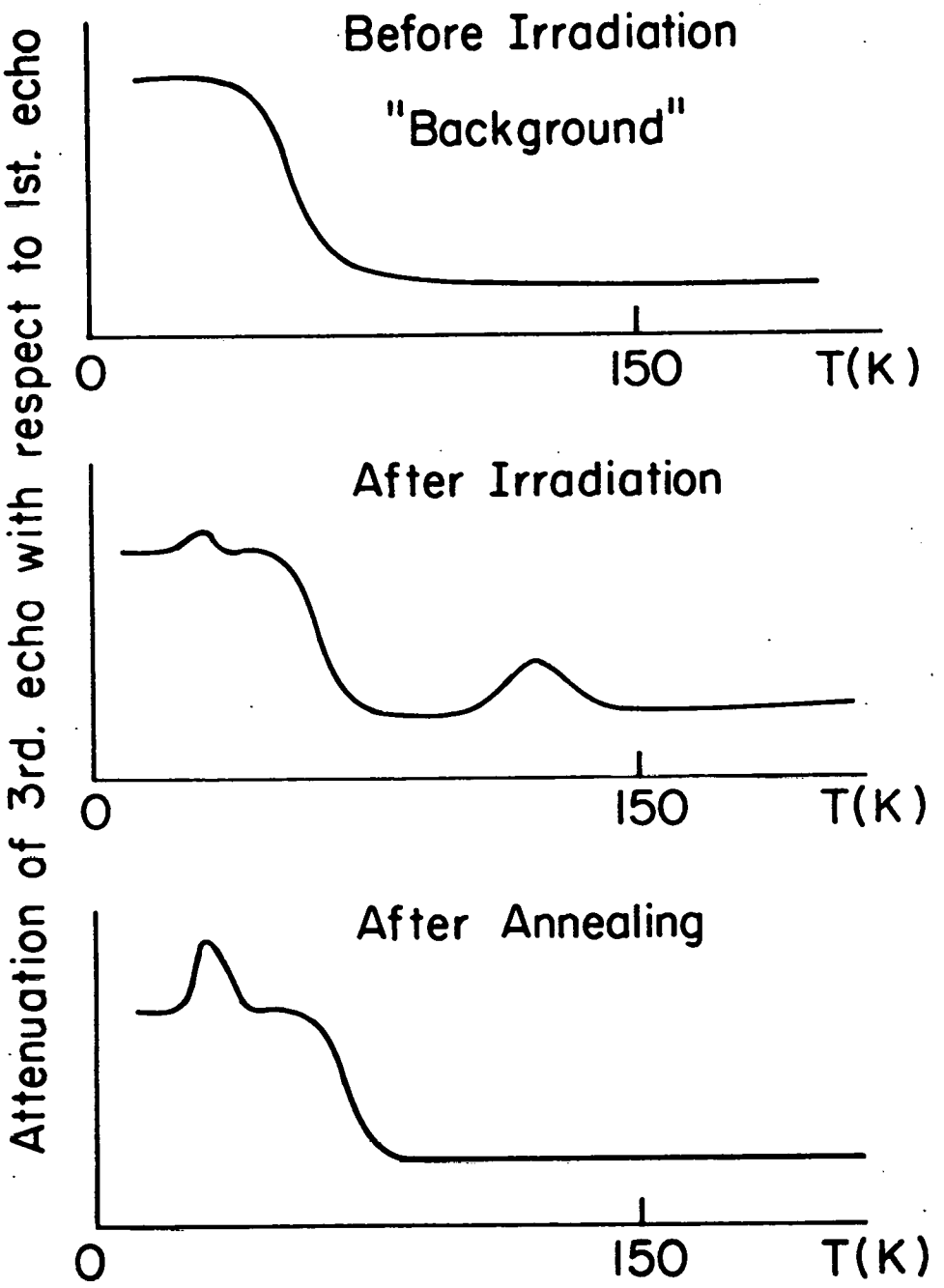
Before Irradiation
"Background"
0
150
T(K)
After Irradiation
0
150
T(K)
After Annealing
0
150
T(K)
Attenuation of 3rd. echo with respect to 1st. echo

the temperature to successively higher temperatures followed by a return to liquid helium temperatures, one can observe the gradual annealing away and/or growth of the radiation-induced attenuation changes. Measurements are also made of the changes in the sample's resonant frequency which are proportional to changes in the elastic constant. By changing the polarization of the ultrasound and observing the resulting differences, we obtain information about the symmetry of the defect. The annealing data gives us stability information, while measuring the relaxation peaks at two different frequencies provides us with the activation energy for the relaxation process.

A. Sample Preparation

Single crystal boules of Cu-Ag and Al-Mg were grown by Monocrystals Company of Cleveland Ohio. The boules were roughly oriented using Laue x-ray backscattering photographs. Ultrasonic samples were then cut from the oriented boules with a wire acid saw.[30]

The cutting solution used for Al-Mg was 50% water and 50% concentrated hydrochloric acid, while a concentrated nitric acid solution was used for Cu-Ag. The samples were then remounted on a goniometer[30] and finally oriented to an accuracy of $\pm 1/2$ degrees using the Ochs technique.[31] Excess material was removed with the acid saw before mounting the goniometer-with-sample directly onto the crystal-facing device.[30] This direct mounting preserves the orientation of the sample. Care was taken through use of these methods to avoid the introduction of dislocations to the sample; dislocation effects

are undesirable since they tend to swamp the effects attributable to point defects.

The sample rotates about the axis of orientation while being pressed very lightly against a 100% polyester cloth-covered wheel which rotates in the opposite direction. The wheel picks up a solution which attacks the sample chemically and allows current to flow from the sample to the wheel; thus the sample surface is electrochemically polished to a nearly optical finish although an "orange-peel effect" remains to mar its overall flatness.

At one time, the samples were approximately cubes with three pairs of parallel faces (Hultman[2]). However, satisfactory results have been obtained for Cu-Ag and Al-Mg with just two pairs of faces: the "ultrasonic" and the "thermal" faces.

The ultrasonic faces are used for the bonding of the transducer and for the reflection back and forth of the ultrasonic pulses. The face opposite the transducer is directly exposed to the electron beam. The thermal faces are held against the sample holder with Apiezon grease and are polished to insure good thermal contact with the holder. These faces are oriented as accurately as the ultrasonic faces since they are also used as a guide for positioning the transducer. To indicate their polarization, the shear transducers have flat portions cut from them. The "flat" is then lined up to be either parallel or perpendicular to the edge of the thermal face, depending on the mode desired.

The polishing technique used a Model 451 crystal facing instrument

by South Bay Technology. The polishing solutions, temperatures, and voltages are listed in table I. The wheel rotation was set at about 21 rpm while the sample rotation was about 20 rpm.

TABLE I. Polishing Parameters

Material	Solution	Temperature	Voltage
Cu-Ag	800 ml phosphoric acid 800 ml acetic acid 400 ml nitric acid	25°C	5 V
Al-Mg	1600 ml phosphoric acid 250 ml acetic acid 150 ml nitric acid 8.31 gm $Cu(NO_3)_2$	85°C	7.5 V

One should not expect perfect results with these parameters; they should serve only as starting values which can be varied to give the desired polish. In our case, this was one which would accomodate a quartz transducer bonded to the surface with a very small quantity of Nonaq stopcock grease (Fisher Scientific Co.). The bond had to permit a "clean" pattern of echoes at frequencies as high as 90 MHz at room temperature and survive thermal cycling between 2 K and 170 K. A clean pattern is one in which each echo rises from a flat baseline undisturbed by the presence of "ringing" phenomena caused by an unbonded section of the transducer (a problem which becomes more pronounced with increasing frequency.) With very few exceptions, if the bond survived the first excursion down from room temperature to 4.2 K at 1 K/minute without major changes in the attenuation pattern, then it

lasted throughout the irradiation and annealing program.

In appearance, the polished surface of aluminum was mirrorlike with a fine "orange-peel" texture which is a common result of chemical polishing. The flatness was judged first by observing the reflection of overhead lights from the polished face while holding the sample at half-arm's length. With Do-All optical flats, the flatness was estimated to be typically 6 microns.

10 MHz, quarter-inch quartz transducers were purchased from Valpey-Fisher (Hopkinton, MA). They were of the overtone type, unplated with no leads, with both sides polished parallel and optically flat. For examining the E and T symmetry modes, we used shear type AC-cut transducers.

The bonding procedure is a critical step in the experiment since a bond breaking at an inopportune moment results in much wasted time and money. Both the sample and the transducer are carefully cleaned with acetone (reagent grade seems to be best) and wiped with tissue. Kleenexes worked well for aluminum since they were soft enough to scratch the metal surface only slightly. The sample was cleaned first and heated to about 40°C by being placed on a hot aluminum block. A cleaned transducer was heated on the sample surface as well as a minute drop (about .5 mm wide) of Nonaq grease. The Nonaq had been heated to about 50°C and outgassed in a rough vacuum. The transducer was then placed atop the grease droplet and pressure applied to squeeze the grease into a thin, uniform layer. The transducer is then wrung down against the sample with a combination of light pressure downward and a

rotary motion alternating between clockwise and counterclockwise directions. Light pressure is used to avoid scratching the surface and also to produce a more uniform bonding layer. The final wringing down is accompanied by a gradual increase of pressure up to the desired orientation of the transducer. Heating the sample lowered the viscosity of the Nonaq and enabled the thinnest bonds to be made; on the other hand, excess heating was found to degrade the Nonaq and resulted in poor bonds. The bond could be inspected visually through the unplated transducer and examined with a Sperry attenuation comparator at different frequencies using the criteria stated earlier for a "clean" pattern.

B. Apparatus

The prepared sample is mounted in the sample holder as shown in figure 6, and the holder is placed into the sample chamber of our cryostat.[1] Figure 7 (after Johnson[1]) displays the physical arrangement of the sample and the beam interface tube. A 2.5 Mev electron beam is provided by the Van de Graaf facility of the Materials Research Laboratory. The beam strikes a thin aluminum scattering foil C and passes through the water cooled collimators D and E. About 10% of the incident beam reaches the sample after collimation. Beam currents generally run from 2 to 9 microamps depending on the holding temperature and the cooling power. The cooling power is available in the form of liquid helium brought through the capillary tube M and vaporized directly beneath the sample holder. The beam was aligned by

Figure 6. Three views of the sample holder.

(1) Plunger pressing against the quartz transducer and feeding r.f. pulses into it.

(2) Block containing the platinum, carbon, and silicon thermometers.

(3) Ultrasonic sample.

(4) resistivity sample.

(5) Hole cut in the holder to allow electrons to strike the ultrasonic sample.

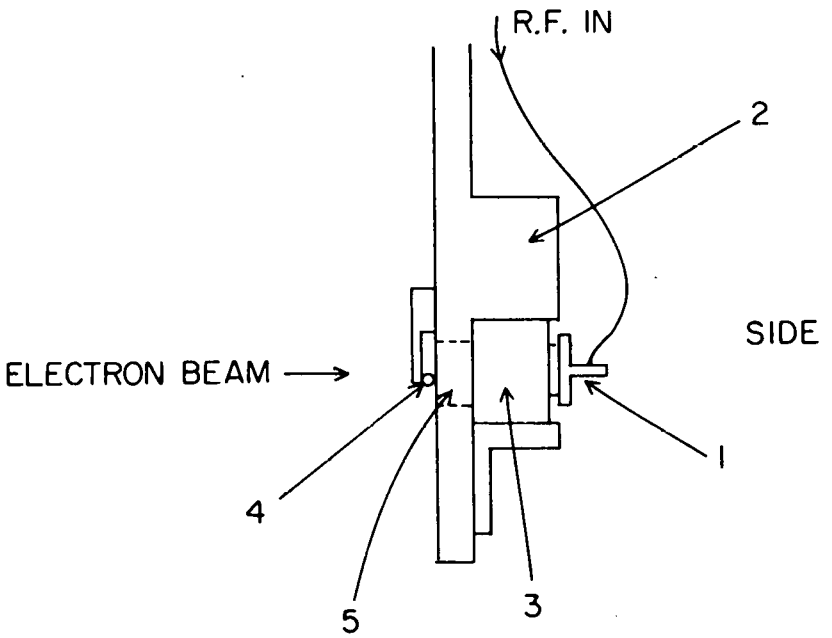
R.F. IN
2
SIDE
ELECTRON BEAM
1
4
5
3

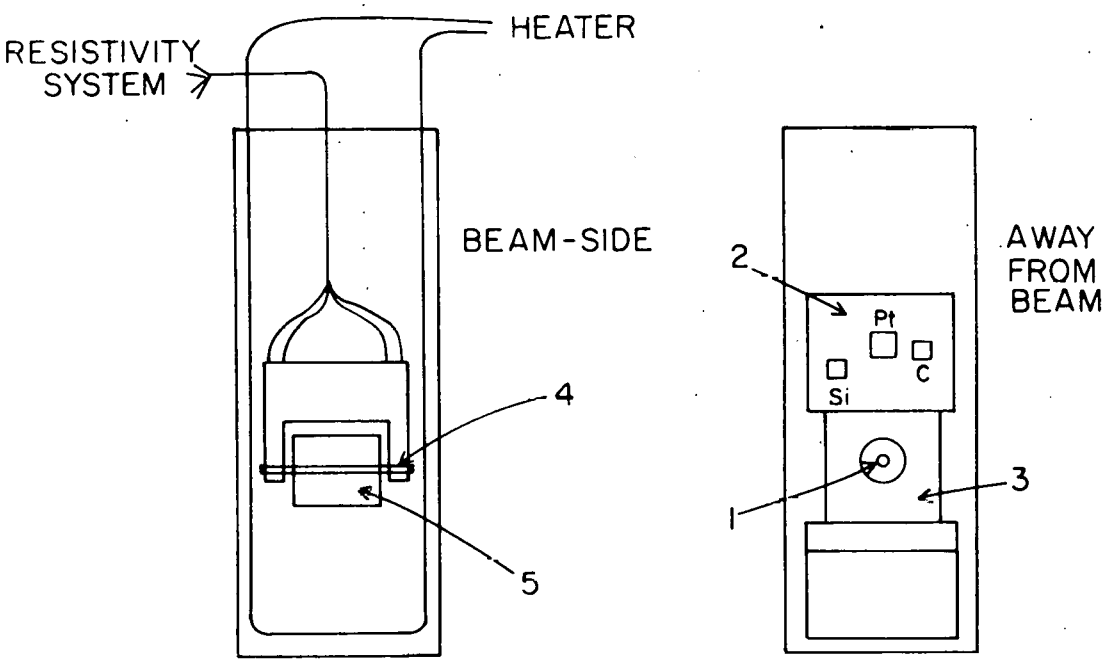
RESISTIVITY SYSTEM
HEATER
BEAM-SIDE
4
5
2
Pt
C
Si
AWAY FROM BEAM
1
3

Figure 7. Cross-section of Cryostat, sample holder, and electron beam interface.
(A) e^- beam entry port
(B) BeO disc, beam alignment flap
(C) scattering foil
(D) first aperture
(E) second aperture
(F) current monitor flap
(G) gate valve
(H) LN_2 shield
(I) sample chamber window
(J) cooling coils
(K) bypass valve
(L) viewing port
(M) liquid He capillary tube and vaporizer
[After Johnson[1]]

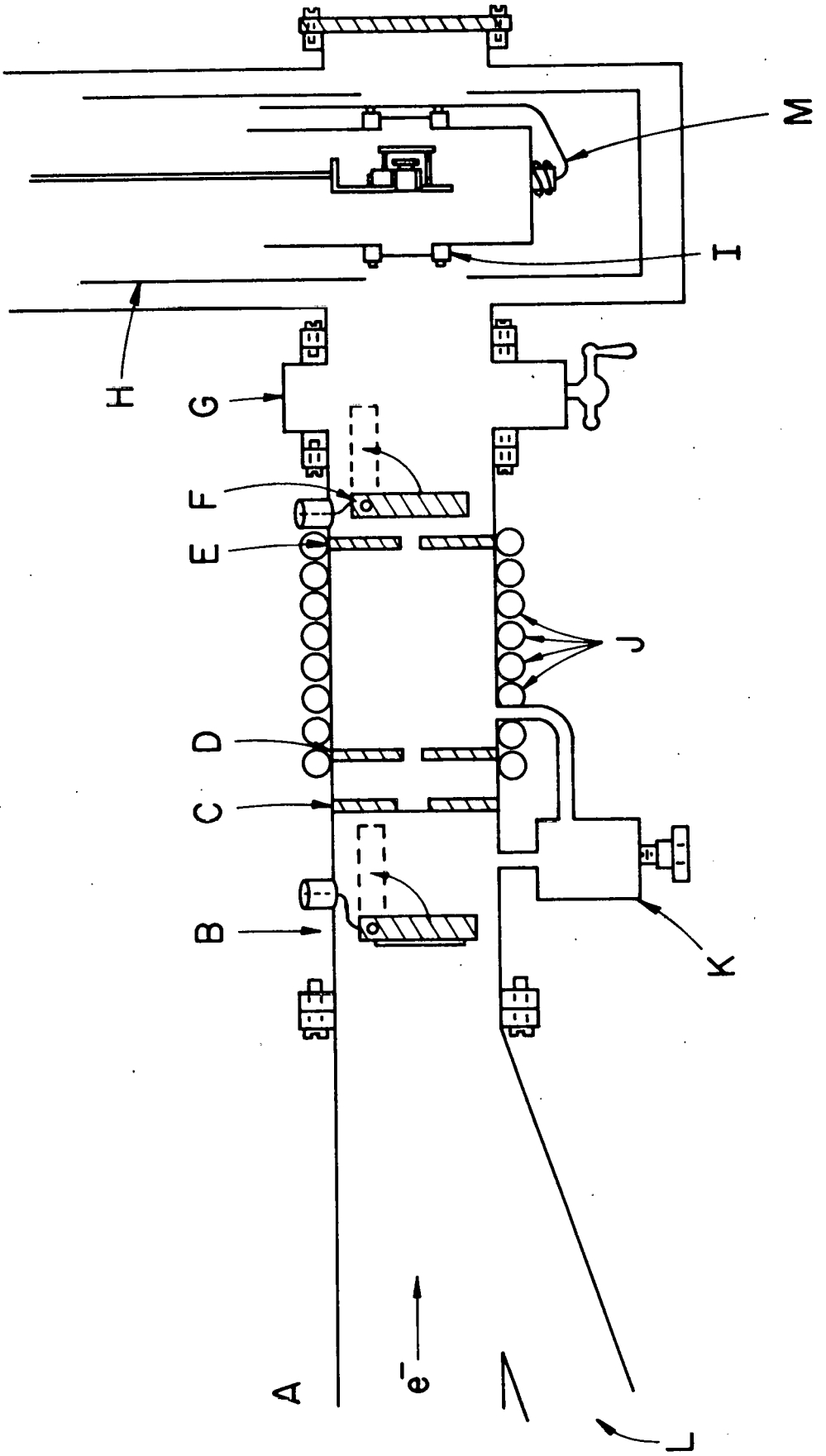
M
I
H
G
F
E
J
D
C
B
K
A
e⁻
L

maximizing the current falling on the current flap F after the collimators; this is a simplification of the original technique in which a BeO disc (which fluoresced under electron impact) was used in conjunction with a T.V. camera to line up the beam.[1] The current flap was lowered periodically to help estimate the total dose, but this has been found to give inconsistent results. Methods are now being developed to measure the total electron flux more reliably by using a combination of continuous current measurement and more meticulous alignment of the sample holder itself.

We measured the temperature of the sample with three thermometers. Platinum and carbon thermometers were used in a system described by Johnson[1] and Hultman[2] and depicted in figure 8 (after Hultman). The platinum sensor was used for temperatures above 25 K, while the carbon sensor was used to record temperatures below 25 K. This manual system was used intermittently during our experiments and usually only for measurements of the resonant frequency. A new computer-based temperature control/measurement system centered around an LSI-11 is being developed (figure 9). The manual system now serves mainly as a back-up temperature controller in case the computer system fails. Details will be presented in another thesis.

During our experiments, the computer used a silicon thermometer from Lake Shore Cryotronics. This thermometer became uncalibrated upon exposure to the gamma radiation arising from the 2.5 Mev electron bombardment. It was recalibrated against the platinum thermometer and was found to be in error by as much as +1.5 K near 60 K; but below 30

Figure 8. Manual platinum temperature control system
A(top): control loop schematic
B(lower left): platinum thermometer bridge schematic
C(lower right): integrating/differentiating controller schematic

[After Hultman[2]]

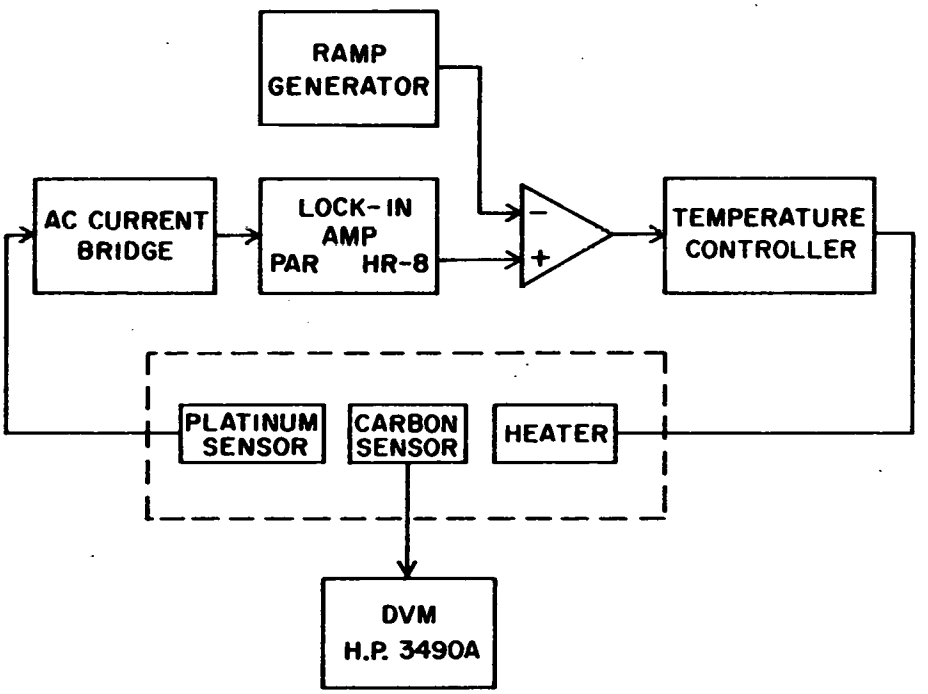

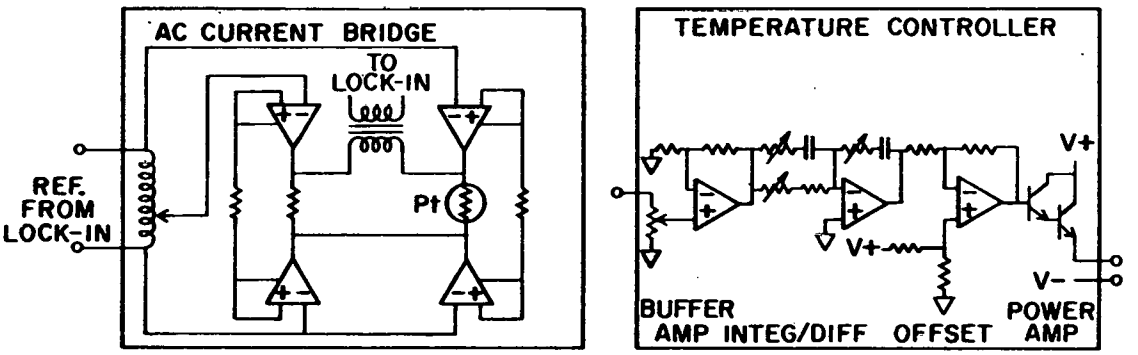

TEMPERATURE CONTROL SYSTEM

Figure 9. Hybrid LSI-Manual Temperature control schematic
A(top): LSI-11 and peripheral equipment
B(left): sample holder and thermometry
C(right): interface between computer and temperature controller
D(bottom): manual platinum temperature control

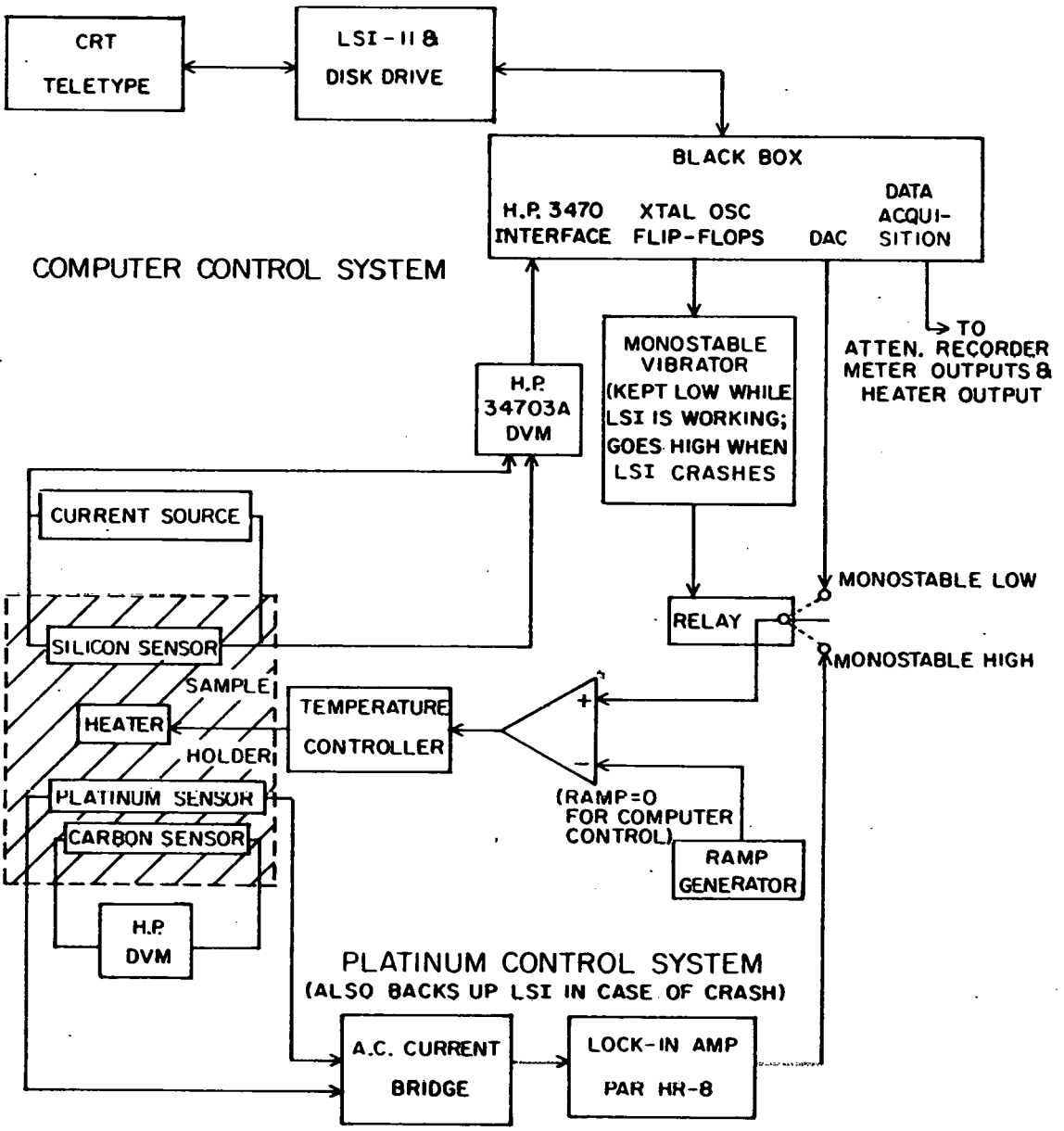
CRT
TELETYPE
LSI-11 &
DISK DRIVE
BLACK BOX
H.P. 3470 INTERFACE
XTAL OSC FLIP-FLOPS
DAC
DATA ACQUI-SITION
COMPUTER CONTROL SYSTEM
TO ATTEN. RECORDER METER OUTPUTS & HEATER OUTPUT
MONOSTABLE VIBRATOR (KEPT LOW WHILE LSI IS WORKING; GOES HIGH WHEN LSI CRASHES
H.P. 34703A DVM
CURRENT SOURCE
MONOSTABLE LOW
RELAY
MONOSTABLE HIGH
SILICON SENSOR
SAMPLE HOLDER
HEATER
TEMPERATURE CONTROLLER
+
−
PLATINUM SENSOR
CARBON SENSOR
(RAMP=0 FOR COMPUTER CONTROL)
RAMP GENERATOR
H.P. DVM
PLATINUM CONTROL SYSTEM
(ALSO BACKS UP LSI IN CASE OF CRASH)
A.C. CURRENT BRIDGE
LOCK-IN AMP PAR HR-8

K it was incorrect by only .2 K, and above 110 K the silicon thermometer was within .1 K of its original calibration. These errors were not important in the temperature ranges of interest.

Simultaneous measurements were made of the ultrasonic attenuation at both 10 and 30 MHz using equipment purchased from Matec, Inc. (Warwick, R.I.) The advantages of such a system over the method used by Johnson are discussed by Hultman. They include savings in both time and helium use as well as allowing more accurate observation of the relative behavior of the 10 and 30 MHz attenuation. A schematic diagram of the system is shown in figure 10 (after Hultman).

Two pulse-echo and attenuation recorder packages from Matec (one for 10 and the other for 30 MHz) were externally triggered on alternate phases of a 200 Hz square wave. The r.f. signals from each package were led into separate impedance-matching networks which both fed into the quartz transducer bonded to the sample. There was considerable interaction between the networks which affected the amount of energy actually coupled into the sample; however, it was assumed that there was no corresponding effect upon the radiation-induced changes in the attenuation. In any case, both impedance-matching networks were tuned to maximize the 10 and 30 MHz pulse-echo patterns. We could discern changes in the attenuation as small as .02 dB out of 10 dB.

The resonant frequency (or velocity) measurements were taken with the set-up shown in figure 11 (after Hultman). A sampled-continuous wave technique was used as described by Johnson. The excitation frequency is modulated at about 16 Hz around an odd harmonic of the

Figure 10. Attenuation system schematic [After Hultman[2]]

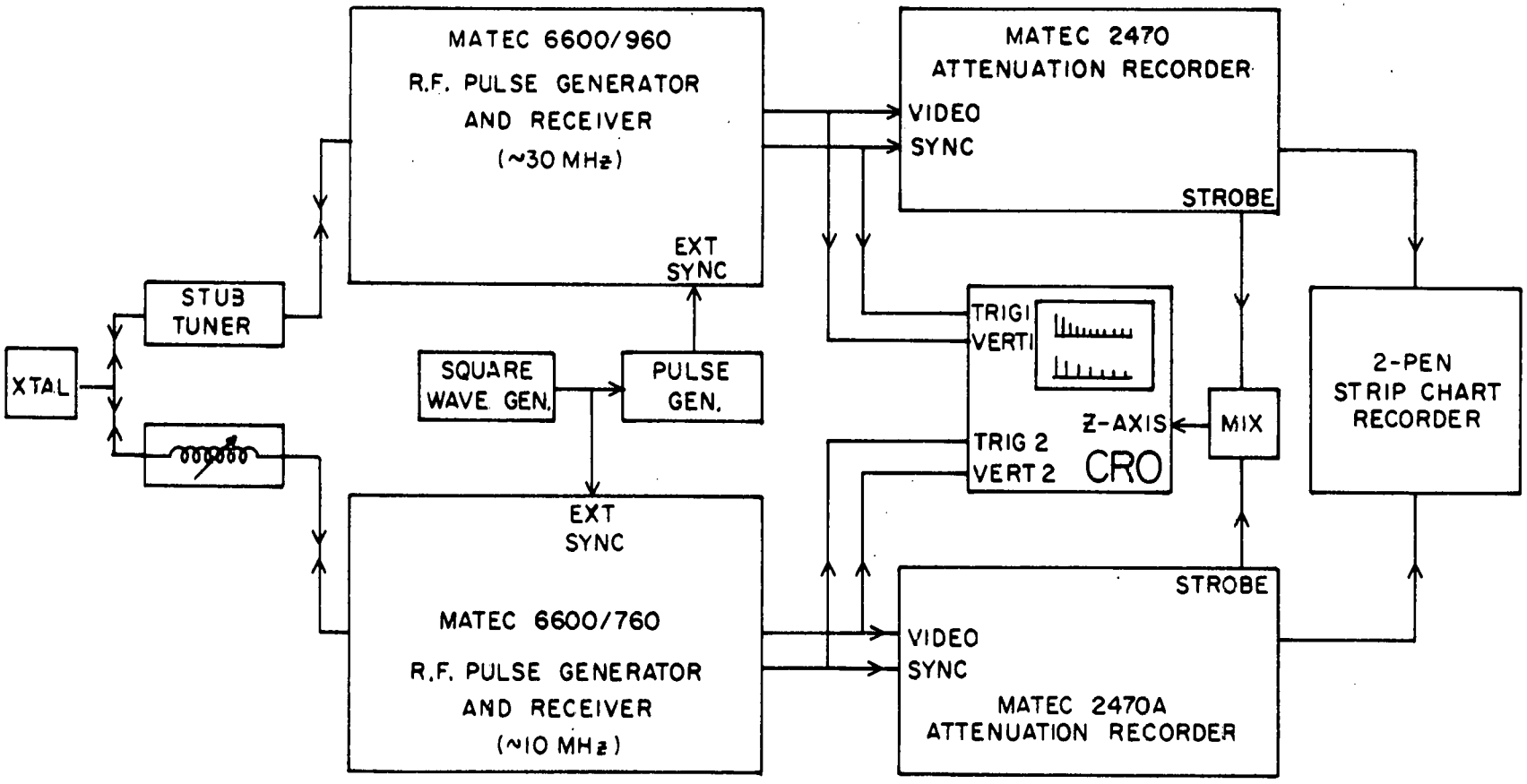

Attenuation System

Figure 11. Velocity system schematic [After Hultman[2]]

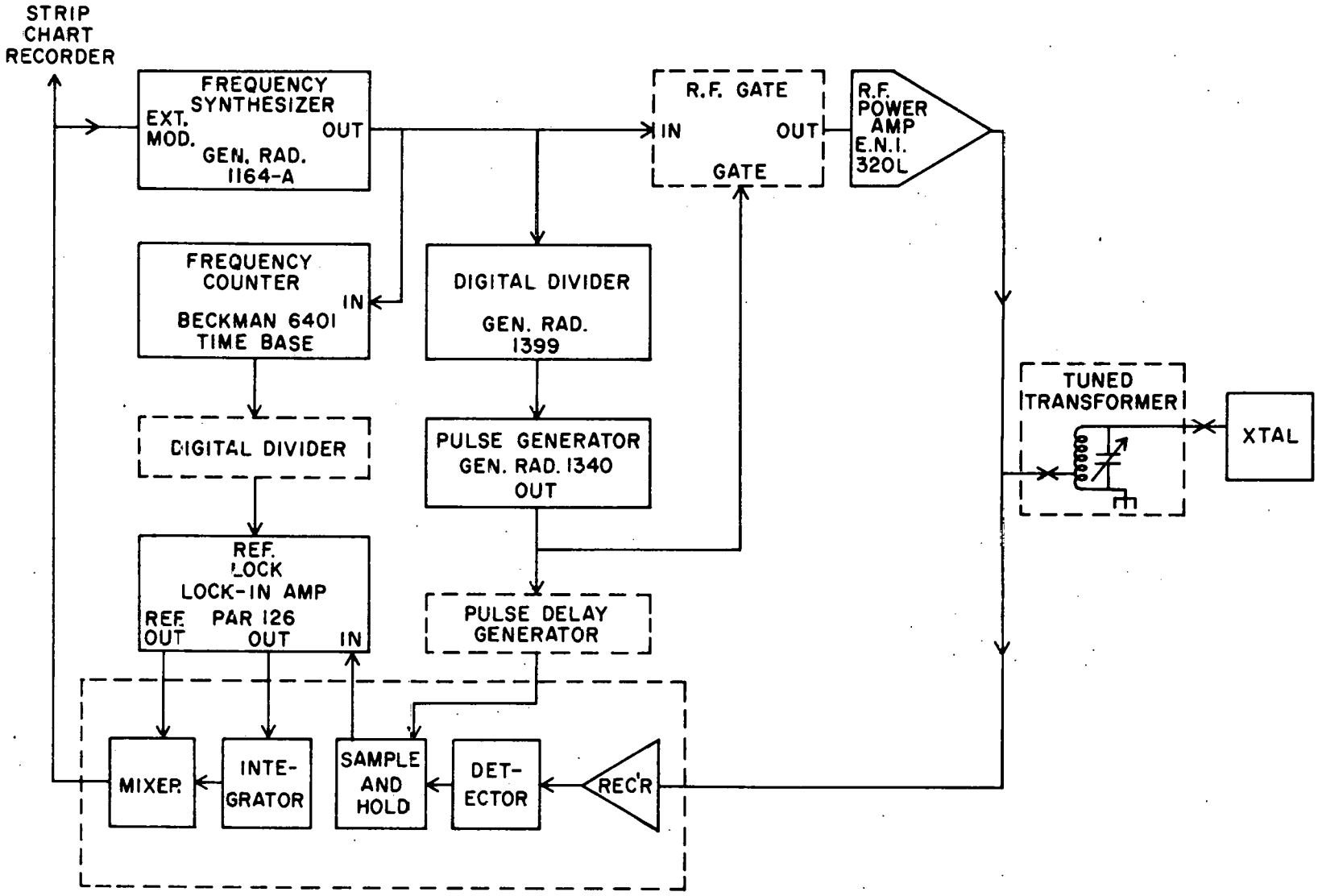

Velocity System

resonant frequency of the sample. These harmonics are approximately 100 KHz apart and are easy to find near the 10 MHz resonant frequency of the transducer. Periodically, the signal to the power amplifier is gated-off and the decay of the standing wave's strain amplitude in the sample is observed. This strain is measured after a set delay time (that follows the gating-off of the input signal) and is processed synchronously with the modulation frequency. A feedback signal is derived from this which determines the central frequency about which the excitation frequency is varied. It is assumed that the strain amplitude as a function of frequency is fairly symmetric about odd harmonics of the resonant frequency and is maximized there. The frequency of the chosen harmonic is then read from the digital counter. At temperatures below 40 K, our resolution is better than 10 Hz out of 10 MHz or one part in a million.

The resonant frequency f is related to the elastic constant C and the sound velocity v in the sample by the equations,

(1) $$f=nv/2L \quad \text{and} \quad v=\sqrt{C/\rho}$$

where n is an odd integer, L is the sample length, and ρ is the sample density. This leads to the expression,

(2) $$2\Delta f/f = \Delta C/C + \Delta L/L$$

Thus, the relative modulus change $\Delta C/C$ is twice the relative

frequency change, since length changes can be neglected here.[1,2]

Resistivity measurements were made with the 4-terminal AC current bridge described by Johnson.[1] The sample was a thin wire spark-cut from a slice of the single crystal boule that had been electrochemically polished to a thickness of about 10 mils. The ratio of the room temperature resistivity to the residual resistivity at 4.2 K was used in conjunction with the change in the electronic component of the ultrasonic attenuation to determine the number of defects created in the sample.

C. Procedure

The contributions of various mechanisms to the total attenuation are assumed to be linear in nature. Therefore, the changes attributable to the radiation-induced defects can be found by subtraction of the background (pre-irradiation) attenuation curve as a function of temperature from the post-irradiation curve. The background attenuation was measured while linearly ramping the sample's temperature down from about 180 K to 2 K at 1 K/min.(see figure 5) The attenuation was high in the temperature region above 240 K probably because the Nonaq grease bond between transducer and sample had not frozen yet. Around 240 K , the bond froze for the first time and the attenuation became fairly flat, though it still tended to decrease until about 190 K. From 190 K to 100 K, the attenuation was flat except for occasional small jumps which may have been caused by the bond readjusting itself to the first thermal stresses it had ever

encountered in its frozen state. From 100 K to 15 K, the attenuation rose again because of an electronic contribution proportional to the increase of electrical conductivity in this temperature range. This rise in the attenuation at low temperatures was first observed by Bömmel[32] and has been discussed by Hultman as well as by others.[33,34,35] The change in the residual resistivity(ρ_0) can be calculated from the decrease following irradiation(ΔA_σ) in the attenuation rise(A_σ), by using equation 3:

$$\Delta\rho_0 = \rho_0(\Delta A_\sigma/A_\sigma)/[1-(\Delta A_\sigma/A_\sigma)] \tag{3}$$

We can then obtain the number of defects induced in our sample by using published values of the change in resistivity per unit concentration of Frenkel pair.

From 15 K to 2 K, the attenuation flattens out again due to the slow temperature dependence of the conductivity. The 2 K point was reached by first flooding the sample chamber with liquid helium and then pumping on the sample chamber to reduce the temperature. 10 and 30 MHz backgrounds were similar except for the larger electronic contribution which was expected for the higher frequency. After the first ramp downward was completed, the sample was heated to about 180 K and cooled off again to obtain a final background that was usually freer of the jumps which appeared in the first background.

The resonant frequency was also measured before irradiation in the range from 40 K to 5 K using the manual platinum temperature

controller. Below 20 K, the background is fairly flat, while above 35 K the strong temperature dependence of the elastic modulus causes the frequency to drop off sharply, roughly as T^4. Resistivity measurements were also made before irradiation at 5 ,10 and sometimes 4.2 K.

Irradiation temperatures for Al-Mg were set at 50 K, but the actual sample temperature was higher due to a thermal gradient between the place where the beam struck the sample and the thermometer.

A new method for monitoring the irradiation temperature was used for the later Cu-Ag runs and all of the following runs. This method utilized the strong monotonic temperature dependence of the resonant frequency above 35 K (about 1000 Hz/K compared to a frequency resolution in this region of 100 Hz out of 10 MHz). A background measurement of the resonant frequency was taken at temperatures in the region of the desired irradiation temperature. The velocity system was then used to continuously monitor the resonant frequency during the irradiation. In this manner, the temperature of the sample is directly measured, eliminating the problem of thermal lags or gradients. It was found that the sample temperature could be as much as 30 K higher than the temperature set with the control system; this differential depended upon the temperature, the beam current, and the helium flow rate.

For Cu-Ag, the desired irradiation temperature for most of the runs was 50 K or lower. This was required in order to study the nature of the resistivity annealing substage at 60 K observed by Cannon and Sosin[4]. The later runs used the frequency measurement as a temperature

gauge during irradiation and we performed irradiations as low as 40 K with annealing steps to 80 K followed by 80 K irradiations with annealing steps to 240 K.

The irradiations with 2.5 Mev electron lasted for several days using beam currents ranging from 4 microamps at 40 K to 9 microamps at 80 K. Since all the electrons are stopped a few millimeters deep in the samples, the attenuation effects seen are representative of a volume averaged defect concentration. These volume averaged concentrations were typically around 9 ppm, but for two Cu-Ag runs, the concentrations became as high as 18 ppm. Using a procedure outlined by Johnson,[1] the local defect concentrations can be calculated. For Cu-Ag, these local concentrations ranged from about 70 ppm to 170 ppm. For Al-Mg, these local concentrations were less than about 35 ppm.

The isochronal annealing program was intended to crudely approximate the use of a constant heating rate as an annealing technique. The sample is heated so as to produce a temperature ramp which is linear with respect to time. The sample is "ramped" up to an annealing temperature where it is held for a fixed time before it is ramped back down to helium temperature. The attenuation measurement is made continuously during the upward and downward ramps as well as during the anneal itself, and is interrupted only in order to perform the frequency measurement at low temperatures. This process is repeated for each annealing point.

The ramps upward were usually conducted at a rate of 2 K/minute to a temperature 10 K below the anneal point. We then continued to the

annealing temperature at 1 K/min., held at the annealing temperature for 10 minutes, and then ramped down at 1 K/min. to 10 K below the anneal point. From there, we would ramp down to around 60 K at either 2 K/min. or 1 K/min. The 1 K/min. rate was used whenever a more precise temperature measurement was desired: for example, whenever there was the possibility of a relaxation peak between 60 K and the anneal temperature. From 60 K down to helium temperatures, the 1 K/min. cooling rate was used.

The annealing points were initially selected on the basis of known resistivity substages in Al-Mg and Cu-Ag but were ultimately determined by the growth or disappearance of the relaxation peaks observed. In regions where annealing of the relaxation peaks takes place, the annealing temperatures were 5 K apart below 160 K and 10K apart above 160 K. This distinction was justified because annealing takes place over a wider temperature range with increasing temperature (Granato and Nilan[10]). In between these annealing regions, annealing points were chosen to be as much as 40 K apart although a 20 K separation was more likely when the annealing behavior was not well-known. Annealing continued until 240 K where bond changes started to make our frequency measurements less reliable. It was found that very little remained of any relaxation peak after an anneal to 240 K and that most peaks disappeared before this final anneal.

CHAPTER 3

EXPERIMENTAL RESULTS

A. Scope of the measurements

The ultrasonic attenuation and resonant frequency were measured in samples of Al-Mg and Cu-Ag, before and after irradiation.

Three distinct effects were observed: 1) the conductivity-related rise in the attenuation below 100 K (see for example the "background" curve in figure 5), 2) changes in the frequency caused by diaelastic effects, and 3) relaxation peaks in the attenuation (see the "after irradiation" curve in figure 5) and related changes in the frequency caused by paraelastic effects.

The rise in the attenuation below 100 K is caused by the interaction of the sound wave with the conduction electrons and is proportional to the electrical conductivity. The shear wave attenuation A_σ(Np/cm) is given in the low frequency limit (electron mean free path << ultrasonic wavelength) by[2]

$$(4) \qquad A_\sigma = (2\pi^2 f^2/\rho v^3)(3\pi^2 N^2)^{2/3}(\hbar^2\sigma/5e^2)$$

where f is the frequency of the sound wave, ρ is the sample density, v is the sound velocity, N is the number of electrons of charge e per unit volume, and σ is the electrical conductivity (all in Gaussian units). However, both Lax[36] and Hultman[2] have observed a discrepancy

between the calculated and the experimental values for the attenuation. This discrepancy may be caused by the assumption[2] that the mean free path is the same for both acoustic and electronic processes, or by a failure of the free electron approximation upon which equation 4 is based. Our own results appear in table II.

TABLE II. Conductivity-Related Attenuation

Run	Sample	Mode	A_σ(Np/cm)[calc]	A_σ[calc]/A_σ[exptl]
I	Al-Mg	C'	.1408	1.22
II	Al-Mg	C_{44}	.1064	1.58
III	Al-Mg	C_{44}	.1064	1.67
IV	Cu-Ag	C'	.3432	1.51
V	Cu-Ag	C_{44}	.0604	1.03
VI	Cu-Ag	C_{44}	.0604	1.09
VII	Cu-Ag	C_{44}	.0604	1.17
VIII	Cu-Ag	C'	.3432	1.24

Diaelastic and paraelastic effects are descriptive terms analogous to those given to related magnetic effects. They both involve the response of a defect possessing an elastic dipole moment in an externally applied strain field.

The diaelastic effect is caused by a leaning (without reorientation or diffusion between sites) of dipolar defects in response to an ultrasonic strain. The strain induces a dipole moment proportional to the strain. This effect is measurable in our experiment as a relatively large decrease in the resonant frequency from the background value. This diaelastic effect can be expressed as

a relative frequency change which is independent of temperature and frequency in the range of our measurements. It is the effect that provided the first experimental evidence for <100> split interstitials in pure Cu.

The paraelastic effects are caused by the stress-induced ordering and relaxation of pre-existing elastic dipoles between orientations which were equivalent before application of the ultrasonic strain. Unlike the case of the diaelastic effect, actual diffusion of the defects takes place from one site to another. In a crystal containing many defects, this process again leads to a reduction of the elastic constants. It also produces an attenuation effect. A different process occurs for each defect type that undergoes relaxation. The temperature and frequency dependence of the attenuation and modulus changes caused by a single defect type are given by the well-known Debye equations:

$$\Delta C/C = (R/\pi)\,[1+(\omega\tau)^2]^{-1} \tag{5}$$

$$\Delta = (R\omega\tau)\,[1+(\omega\tau)^2]^{-1} \tag{6}$$

where $\Delta C/C$ is the relative modulus change, Δ is the logarithmic decrement, R/π is the relaxation strength, ω is the frequency, and τ is the relaxation time constant. The decrement Δ is related to our measured attenuation α(dB/μsec) by

(7) $$\Delta = .115\ \alpha/f(\text{MHz})$$

For a classical thermally activated relaxation, τ is given by the Arrhenius expression

(8) $$\tau^{-1} = \nu_0 \exp(-H/kT)$$

where ν_0 is a frequency factor and H is the activation enthalpy for the relaxation (reorientation) process. The relaxation strength is given by[37]

(9) $$R/\pi = \beta c v_0 C^2 (\delta\lambda)^2/kT$$

where β is a numerical factor of the order of unity, c is the atomic fraction of defects present for the defect type undergoing relaxation, C is the elastic constant appropriate to the mode being examined, v_0 is the atomic volume, and $\delta\lambda$ is the shape factor of the defect derived from differences between the principal values of the λ-tensor. (The λ-tensor describes the strain produced in the crystal per unit concentration of the defect.) Therefore, paraleastic effects give rise to peaks in the attenuation as a function of temperature and to dispersions in the modulus as a function of temperature. Diaelastic effects also produce changes in the modulus, but they are distinguished from the paraelastic changes by their independence of temperature and frequency in the temperature range studied.

Nowick and Heller[37] have discussed the relaxation effects expected for various defect configurations, while the possible diaelastic effects due to split interstitials have been treated by Dederichs, et al.[3]

Tables III and V provide summaries of some basic data for the Al-Mg and Cu-Ag runs in the order in which they were performed.

TABLE III. Summary of Al-Mg Runs

	Date	Mode	Irrad Temp (K)	Selected Echoes 10MHz/30MHz	Time Between Echoes (μs)	Thickness (mm)	Volume Averaged Dose (ppm,F.P.)
Run I	Nov 1978	C'	55	2nd+8th/2nd+4th	54/18	13.9	5.8
Run II	Feb 1979	C_{44}	50	2nd+14th/2nd+4th	94/15.5	13.16	4.3
Run III	Jun 1980	C_{44}	60	2nd+12th/2nd+6th	70/28	11.73	4.5

Dose figures are given in terms of the induced Frenkel pair concentration. Equation 3 gives the radiation-induced change in the bulk resistivity corresponding to the observed changes in the conductivity-related rise in the attenuation. The Frenkel pair concentration is then obtained by using published values of the resistivity change per atomic % of Frenkel pairs present: 2μΩ-cm/at.% for copper[38] and 4μΩ-cm/at.% for aluminum[39]. However, the absolute values of the concentrations obtained in this fashion were found to be

less precisely known than the relative heights of the attenuation peaks between different runs. From equation 9 (which gives the proportionality between the relaxation strength and the defect concentration), we know that the relative heights of the peaks should also give the relative defect concentrations from run to run. For example, in order to reach the final tabulated values for Cu-Ag (C_{44} mode), we assumed that the calculated defect concentration for run 5 was the most accurate and then used the relative heights of peak 1 (see figure 19) to establish the Frenkel defect concentrations in the other runs. A similar procedure was followed for the remaining runs.

Pre-irradiation resistivity measurements were taken of both Al-Mg and Cu-Ag. The residual resistivity measured in each case was compared with the known resistivity contribution per atomic % of Mg in Al (.46 $\mu\Omega$-cm)[39] and of Ag in Cu (.14 $\mu\Omega$-cm)[40] in order to obtain the impurity concentrations. Those concentrations were 893 at. ppm of Mg in Al and 1370 at. ppm of Ag in Cu.

B. Al-Mg results

The 10 MHz ultrasonic attenuation in the C_{44} mode as a function of temperature is shown in figure 12 for Al-Mg(run III). This attenuation was measured using the 2nd and 12th echoes (70 μsec separation) and is given in units of dB. The conductivity-related rise in the attenuation which occurs between 100 K and 10 K is evident in the figure. Typically, the post-irradiation value of this rise (at our doses) was 5-10% lower than the value before irradiation.

Figure 12. The attenuation in Al-Mg at 10 MHz is shown as a function of the observation temperature in the C_{44} mode. Three different 10 minute anneals between 125 and 145 K are displayed. (Data from run III.)

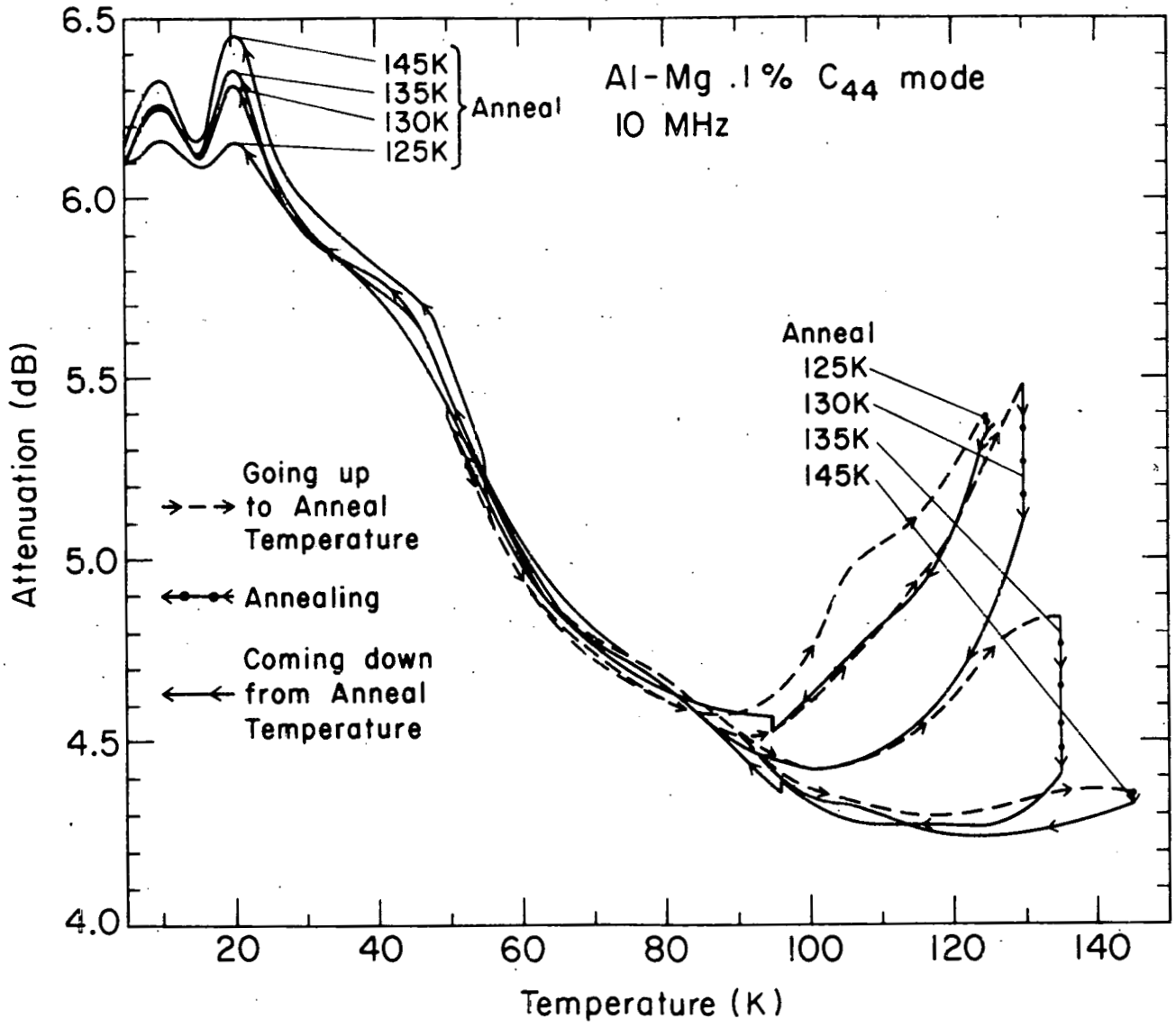
Al-Mg .1% C_{44} mode
10 MHz
145K
135K
130K
125K
Anneal
Anneal
125K
130K
135K
145K
Going up to Anneal Temperature
Annealing
Coming down from Anneal Temperature
Attenuation (dB)
Temperature (K)
6.5
6.0
5.5
5.0
4.5
4.0
20
40
60
80
100
120
140

Figure 12 displays the results of four different anneals in the region around 130 K and shows how the main peak near 135 K, peak number 6, disappeared while the three lower temperature peaks (at 8, 20, and 44 K) grew. An interpretation of this behavior will appear later in chapter 4.

Measurements in the C' mode were performed in run I, but while two small peaks (at 14 and 19 K) were present after irradiation and annealing, no peak as large as peak number 6 was observed.

Figure 13 shows the logarithmic decrement in C' and C_{44} modes (plotted with solid and dashed lines, respectively) as a function of temperature with the background values subtracted. Six decrement peaks are shown at three different points in the annealing program. Peaks 1 and 2 were seen in C'(run I), and peaks 3, 4, 5, and 6 were seen in C_{44}(run III). A seventh peak, in the C_{44} mode, appeared at 33 K (during run II) after a 50 K irradiation but disappeared after the first anneal (to 85 K) was performed. The C_{44} run shown in figure 13 was performed at a higher irradiation temperature, and this seventh peak was not seen.

Peak 6 was the largest peak, and its disappearance after the 145 K anneal coincides with the growth of the remaining peaks in both modes. It was difficult to determine the exact shape of peak 6 since the defect responsible for it anneals away in the region where the peak is seen (figure 12). In fact, the portion of the peak that we were observing dwindled visibly while we were holding the sample at the annealing temperature, allowing us to measure the annealing as a

Figure 13. The logarithmic decrement in Al-Mg at 10 MHz as a function of observation temperature in C'(run I, solid curve) and C_{44}(run III, dahed curve). Three different anneals are shown.

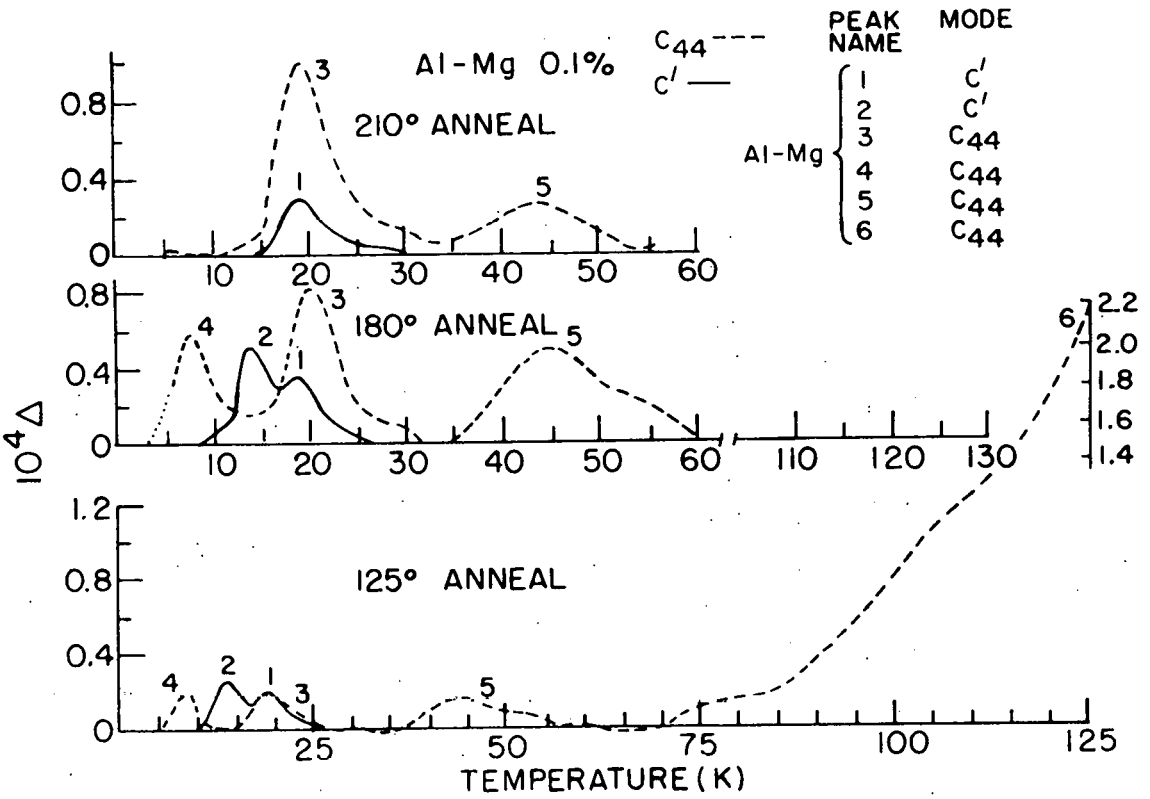
Al-Mg 0.1%
C_{44} ---
C' ——
PEAK NAME
MODE
Al-Mg
1 C'
2 C'
3 C_{44}
4 C_{44}
5 C_{44}
6 C_{44}
210° ANNEAL
180° ANNEAL
125° ANNEAL
$10^4\Delta$
TEMPERATURE (K)

function of time. Figure 14 shows the height of the peak at 130 K and 135 K (background subtracted) plotted semilogarithmically against the time held at each temperature. The results of both C_{44} runs are shown. The straight line fit shows that the annealing process is exponential in time. Since the peak height is proportional to the defect concentration, the concentration may be expressed as

$$(10) \qquad c/c_0 = \exp[-f_0 \Delta t \exp(-U/kT)]$$

where c_0 is the concentration at the start of the anneal, f_0 is the frequency factor, U is the activation energy for annealing, and Δt is the time after the start of the anneal. The activation energy U may be obtained by first plotting the slopes of the lines in figure 14 semilogarithmically against 1000/T. The activation energy may be obtained from the slope of the resulting line. This plot is shown in figure 15 using the data from both C_{44} runs. In our case, U = .326$\pm$.05 eV. This compares well with the activation energy of .33 eV found by Garr and Sosin[20] for the resistivity substage at 127 K in Al-Mg. This value can be compared with that obtained for a set of internal friction peaks found by Kollers, Jacques, Rehn, and Robrock[27] in polycrystalling Al-Mg. We estimated an activation energy of .4 ev for those peaks by first assuming a heating rate of 1 K/min to be equivalent to their set of 10 minute isochronal anneals at 10 K intervals. We then applied Granato and Nilan's[10] relation between activation energy, heating rate, and temperature of maximum annealing. The discrepancy between their

Figure 14. The logarithmic decrement at 10 MHz of peak 6 at 130 and 135 K plotted semilogarithmically against the time held at that temperature.

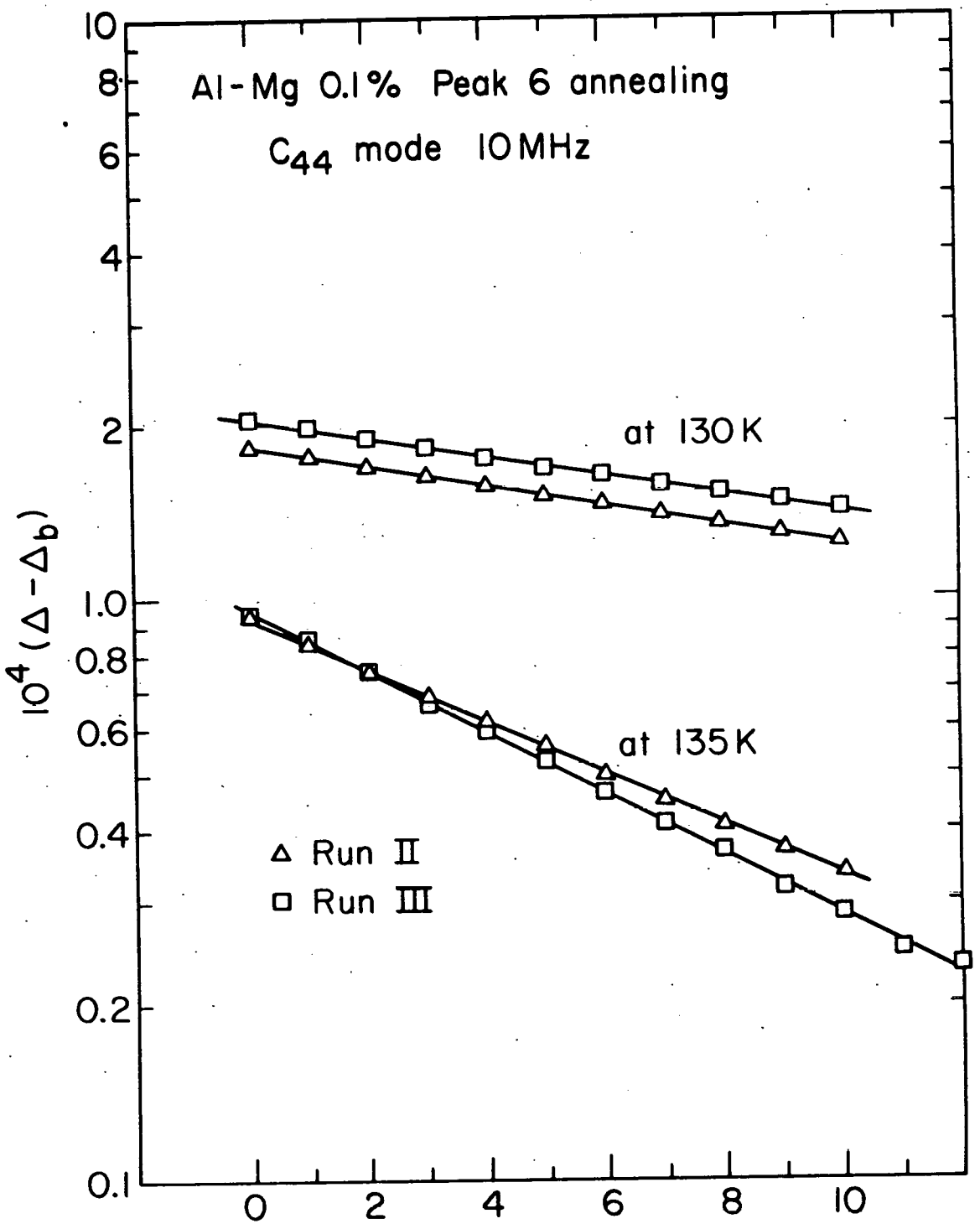
Al-Mg 0.1% Peak 6 annealing
C_{44} mode 10MHz
at 130K
at 135K
Run II
Run III
$10^4(\Delta-\Delta_0)$
10
8
6
4
2
1.0
0.8
0.6
0.4
0.2
0.1
0
2
4
6
8
10

Figure 15. The slopes of the lines from figure 14 plotted semi-logarithmically against 1000/T to obtain the activation energy for annealing.

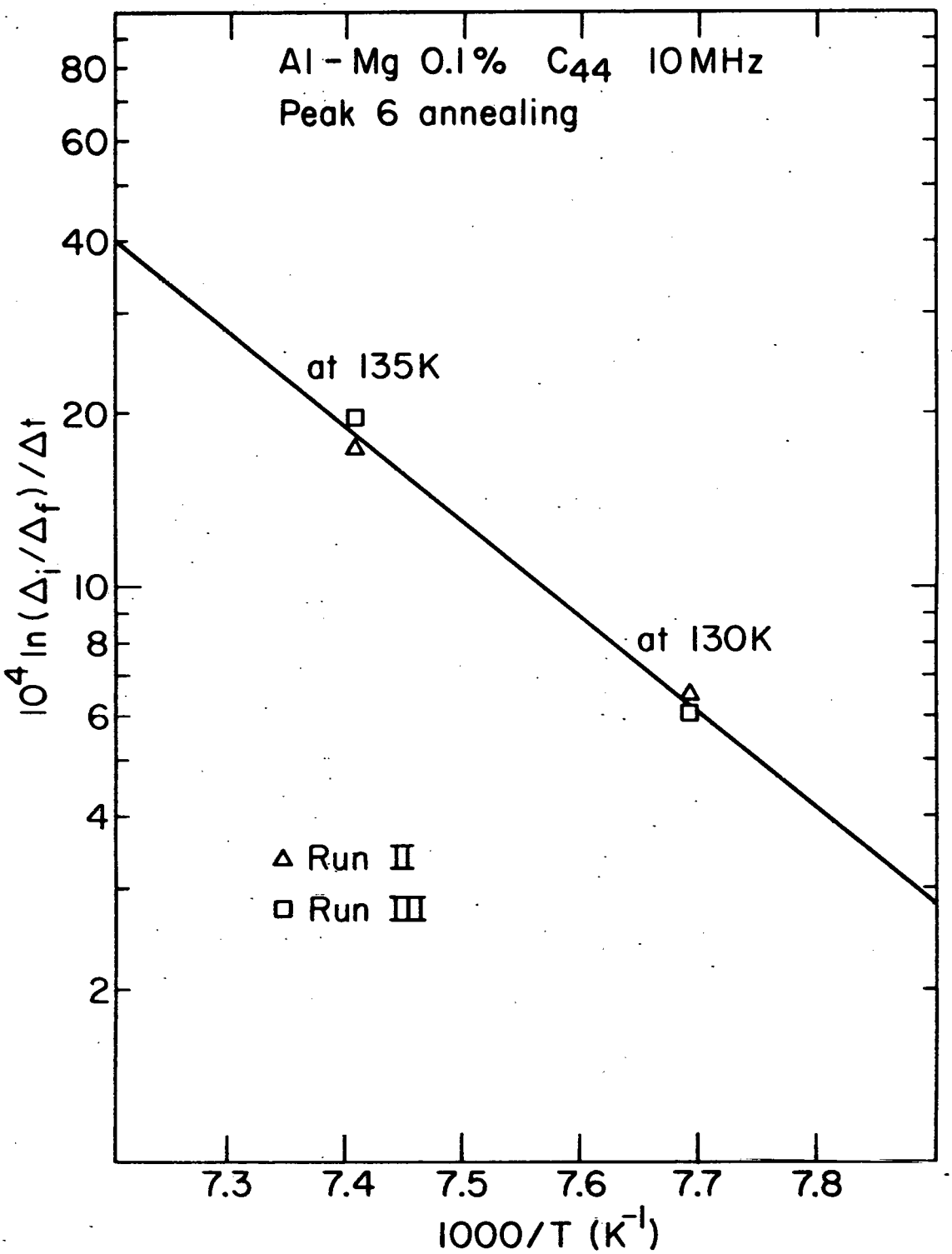
Al - Mg 0.1% C_{44} 10MHz
Peak 6 annealing
at 135K
at 130K
Δ Run II
□ Run III
$10^4 \ln(\Delta_i/\Delta_f)/\Delta t$
80
60
40
20
10
8
6
4
2
7.3
7.4
7.5
7.6
7.7
7.8
1000/T (K^{-1})

activation energy and the energy obtained for our peak 6 remains unexplained.

Kollers, Jacques, Rehn, and Robrock[27] observed five internal friction peaks using a torsional pendulum (at frequencies of 20-70 Hz) that had been irradiated with 3 MeV electrons. Of all our peaks (and despite the discrepancy noted above), only peak 6 has an annealing behavior similar to that observed by Kollers, et al.[27] for the set of peaks II, III, and IV. The remaining two peaks, I and V, annealed away near 150-160 K and did not correspond to any peaks observed by us. At our frequencies of 10 and 30 MHz, peak IV (and V as well) would only have been visible at a temperature higher than the annealing temperature. We therefore tentatively identify our peak 6 in the C_{44} mode with peaks II and III seen by Kollers, et al. Since the shape of our peak is altered by the annealing which takes place during the measurement, it is possible for peak II to overlap with peak III and be indistinguishable as a separate peak in our measurements. Using frequencies of 20-70 Hz would push the observation temperatures of our low temperature peaks to even lower values; nevertheless, some of our peaks, particularly 1, 3, and 5, should still have been visible in Kollers, et al.'s measurements. Their absence will be explained in chapter 4, but the absence in our measurements of any peaks corresponding to their peak 1 remains unexplained.

The maximum peak height for each of the peaks (except as noted for peak 6 where the height at 120 K was used) is expressed in terms of the logarithmic decrement (background subtracted) and plotted against the

annealing temperature in figures 16 and 17. Figure 16 shows the data from the first C_{44} measurements (run II), following irradiation to a Frenkel pair concentration of 4.3 ppm. Peak 3(20 K) and a peak at 33 K were seen immediately after irradiation, but the 33 K peak disappeared after the first anneal to 85 K. Peak 4(8 K) appeared at this point. The next major feature is the disappearance of peak 6 accompanied by a growth in peaks 3, 4, and 5(which first became distinguishable after the 125 K anneal). This activity coincided with a resistivity substage seen at 127 K by Garr and Sosin after electron irradiation[28] and by Dimitrov, et al. following neutron irradiation[41] of Al-Mg. No points were taken in run II between the 145 and 180 K anneals, but evidently the three remaining peaks experienced growth in this region. The dashed lines in figure 16 connecting the 190 K anneal points to the 210 K anneal points indicate that the 210 K anneal was for 20 minutes instead of the 10 minutes used for the other anneals.

This lack of detail in two annealing regions of interest (145-180 K, and 190-210 K) led to a second examination of C_{44} (run III) shown in dashed lines in figure 17. The growth of peaks 3, 4, and 5 between 145 and 180 K is seen to be fairly gradual. Between 190 and 210 K, peak 3 grew, peak 4 disappeared, and peak 5 became smaller. Above 220 K, vacancy migration begins and peaks 3 and 5 finally diappear.

A plot of the C' results(run I) is shown in figure 17 as a solid curve. Peak 1(19 K) was present immediately after irradiation and remained unchanged until the 125 K anneal. Peak 2(14 K) first appeared after the 120 K anneal. Growth of these two peaks also accompanied the

Figure 16. The maximum peak height for the C_{44} peaks at 10 MHz (in log decrement) plotted against annealing temperature. (run II data)

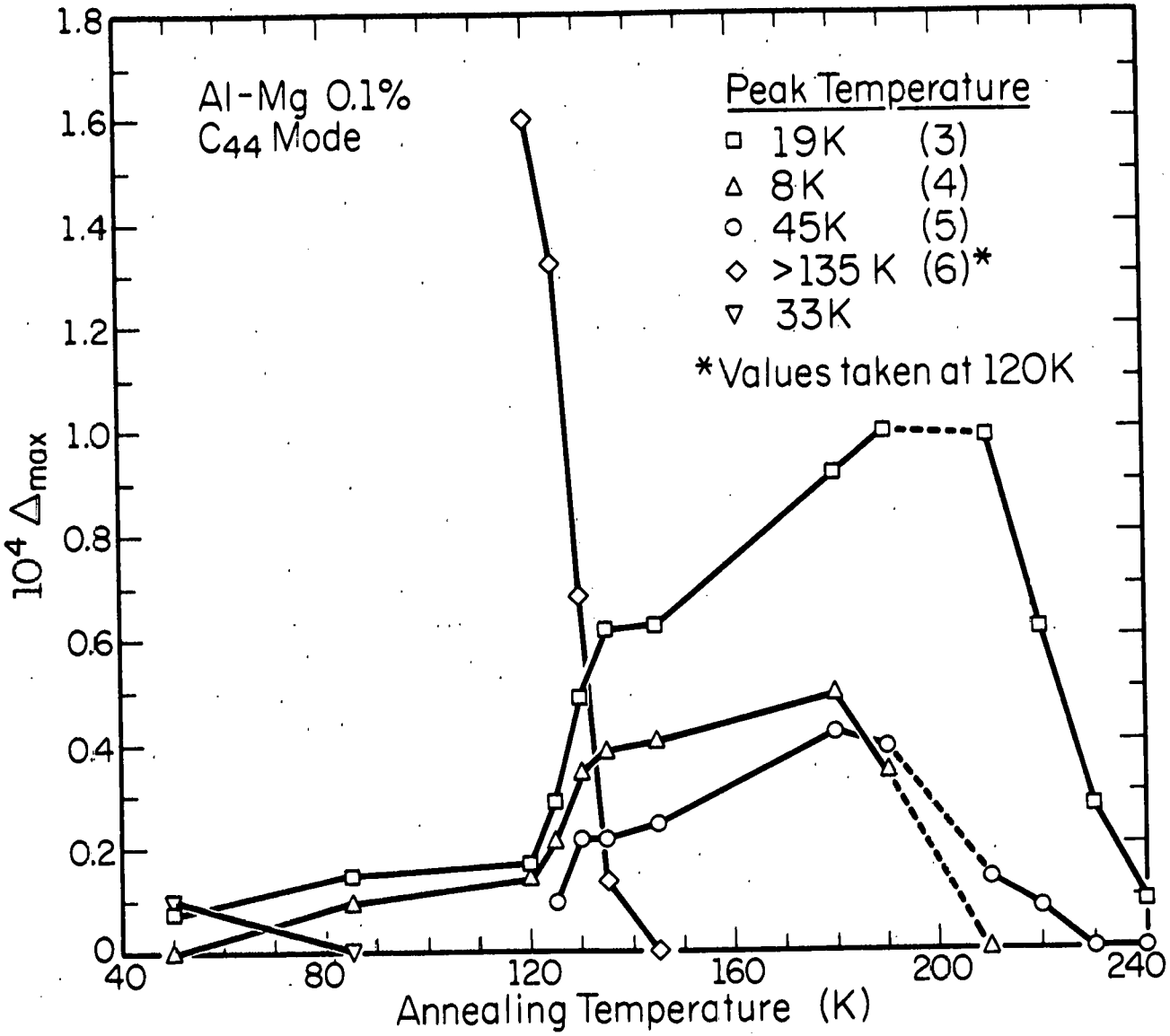
Al-Mg 0.1%
C44 Mode
Peak Temperature
19K (3)
8K (4)
45K (5)
>135 K (6)*
33K
*Values taken at 120K
$10^4 \Delta_{max}$
Annealing Temperature (K)
0
0.2
0.4
0.6
0.8
1.0
1.2
1.4
1.6
1.8
40
80
120
160
200
240

Figure 17. A(top): Maximum peak heights (in log decrement) for C' (run I) and C_{44} (run III) at 10 MHz, plotted against annealing temperature. C' is shown with a solid curve, C_{44} with a dashed curve.

B(bottom): The relative modulus change, after irradiation, plotted against the annealing temperature. C' is the solid curve, C_{44} the dashed. The dotted portion in the lower C_{44} curve represents uncertainty about the data point. The frequency used for C' was 11.04 MHz. For C_{44} it was 10.16 MHz. (Data from run 1 (C') and run III (C_{44}).)

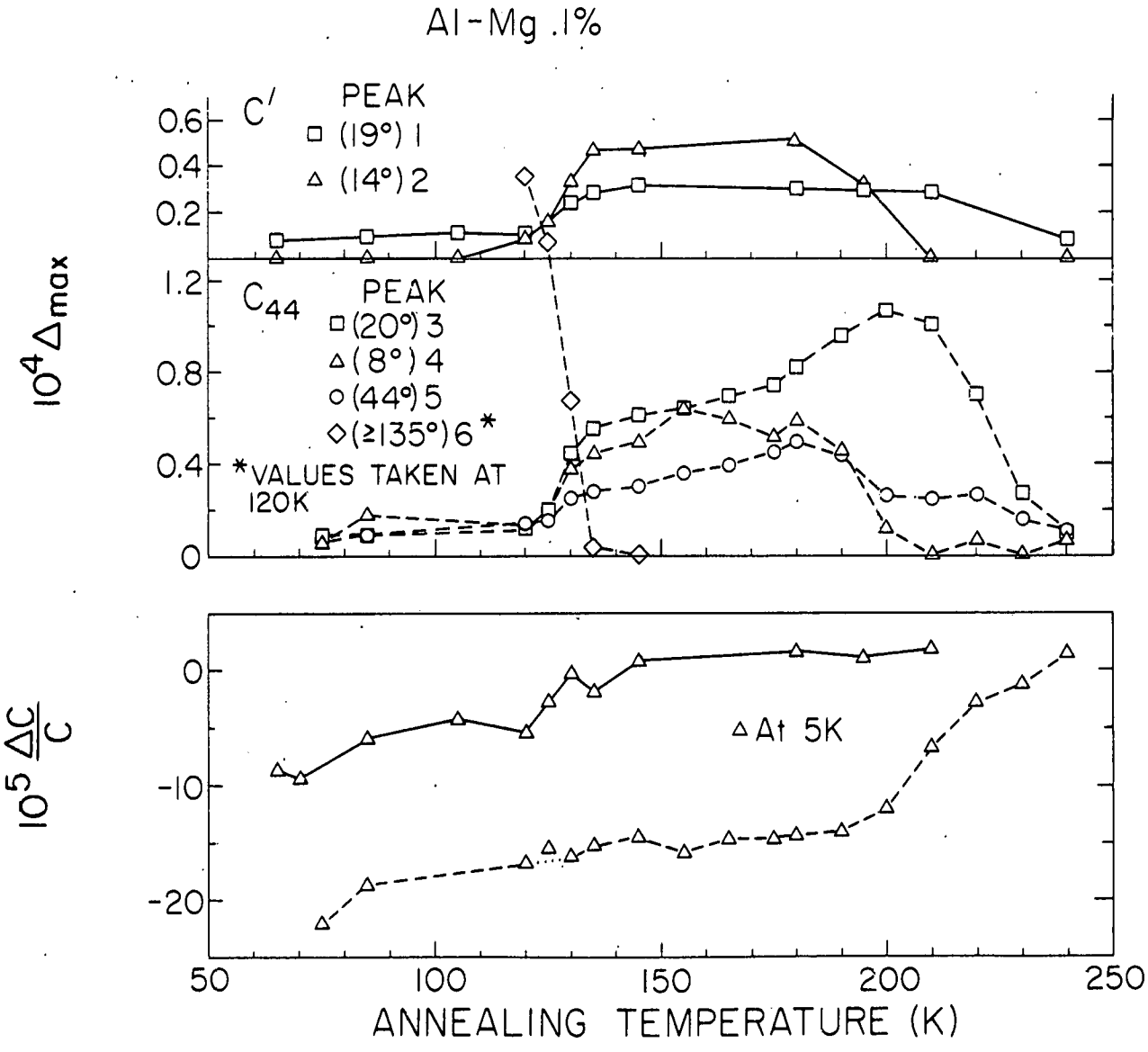
Al-Mg .1%
C′
PEAK
□ (19°) 1
△ (14°) 2
0.6
0.4
0.2
C44
PEAK
□ (20°) 3
△ (8°) 4
○ (44°) 5
◇ (≥135°) 6 *
*VALUES TAKEN AT 120K
1.2
0.8
0.4
0
$10^4 \Delta_{max}$
$10^5 \frac{\Delta C}{C}$
△ At 5K
0
-10
-20
50
100
150
200
250
ANNEALING TEMPERATURE (K)

disappearance of peak 6 in the C_{44} mode; however, very little change was seen afterward until peak 2 started to shrink following the 195 K anneal. Peak 1 remained until the onset of vacancy migration in stage III, when it also vanished.

One of the conclusions that can be made from these plots is that since no peak displayed an annealing behavior which was identical to the behavior of any other peak, each peak must correspond to a different defect type. For example, although peaks 1 and 3 (in the C' and C_{44} modes respectively) occurred at nearly the same temperature, they behaved quite differently in the annealing region between 180 and 200 K: peak 1 changed hardly at all, while peak 3 grew significantly. In this same region, peaks 2 (at 14 K) and 4 (at 8 K) both annealed away; however, peak 2 first appeared after the 120 K anneal whereas peak 4 was present immediately after irradiation. Peak 5 (at 45 K, C_{44} mode) seemed to partially anneal away around 190 K but did not entirely vanish until the onset of stage III (240 K) when vacancy migration takes place. Peak 6 disappeared near 127 K unlike any of the other peaks.

The lower portion of figure 17 shows the annealing behavior of the diaelastic effect for C'(run I) and C_{44}(run III) (solid and dashed lines, respectively) plotted as the temperature-independent part of the relative modulus change, $\Delta C/C$(at 5 K) versus the annealing temperature. As mentioned previously, this change is equal to $2\Delta f/f$, twice the relative change in the resonant frequency, where Δf is the difference between the frequency measured at 5 K after irradiation and the

frequency at 5 K before irradiation. The resonant frequency is decreased after the crystal is softened by the introduction of radiation damage, and this decrease appears as a negative diaelastic effect.

As the annealing program proceeded, the C' diaelastic effect decreased slightly after the 85 K anneal and then almost completely disappeared around the 130 K anneal. The diaelastic effect in the C_{44} mode also decreased after the 85 K anneal, but showed little change near 130 K, although a small amount of annealing would have been hidden in the noise. Not until the 200-240 K anneals did the C_{44} diaelastic effect disappear.

Plotted in figure 18 is the relative modulus change at 5 K as a function of the annealing temperature for the C_{44} mode, run II. The sample was irradiated to a Frenkel pair concentration of 4.3 ppm. The C_{44} diaelastic effect again displayed a decrease after the 85 K anneal. Near 130 K, the noise level was lower than in the other C_{44} run and a definite decrease in the diaelastic effect occurred. The C_{44} effect remained unchanged until the onset at 210 K of vacancy migration, after which the diaelastic effect annealed away. The dashed portion of the curve signifies that the 210 K anneal was 20 minutes long instead of the usual 10 minutes.

Two interesting features appeared in these annealing curves which may be related to the annealing of decrement peak 6: 1) A small decrease in the C_{44} diaelastic effect occurred near 130 K, as shown in figure 18, and 2) nearly complete recovery of the C' diaelastic effect

Figure 18. The relative modulus change for C_{44} (measured at 5 K), plotted against annealing temperature. The frequency was 11.04 MHz. The dashed portion indicates that the 210 anneal lasted for 20 minutes instead of the usual 10 minutes.

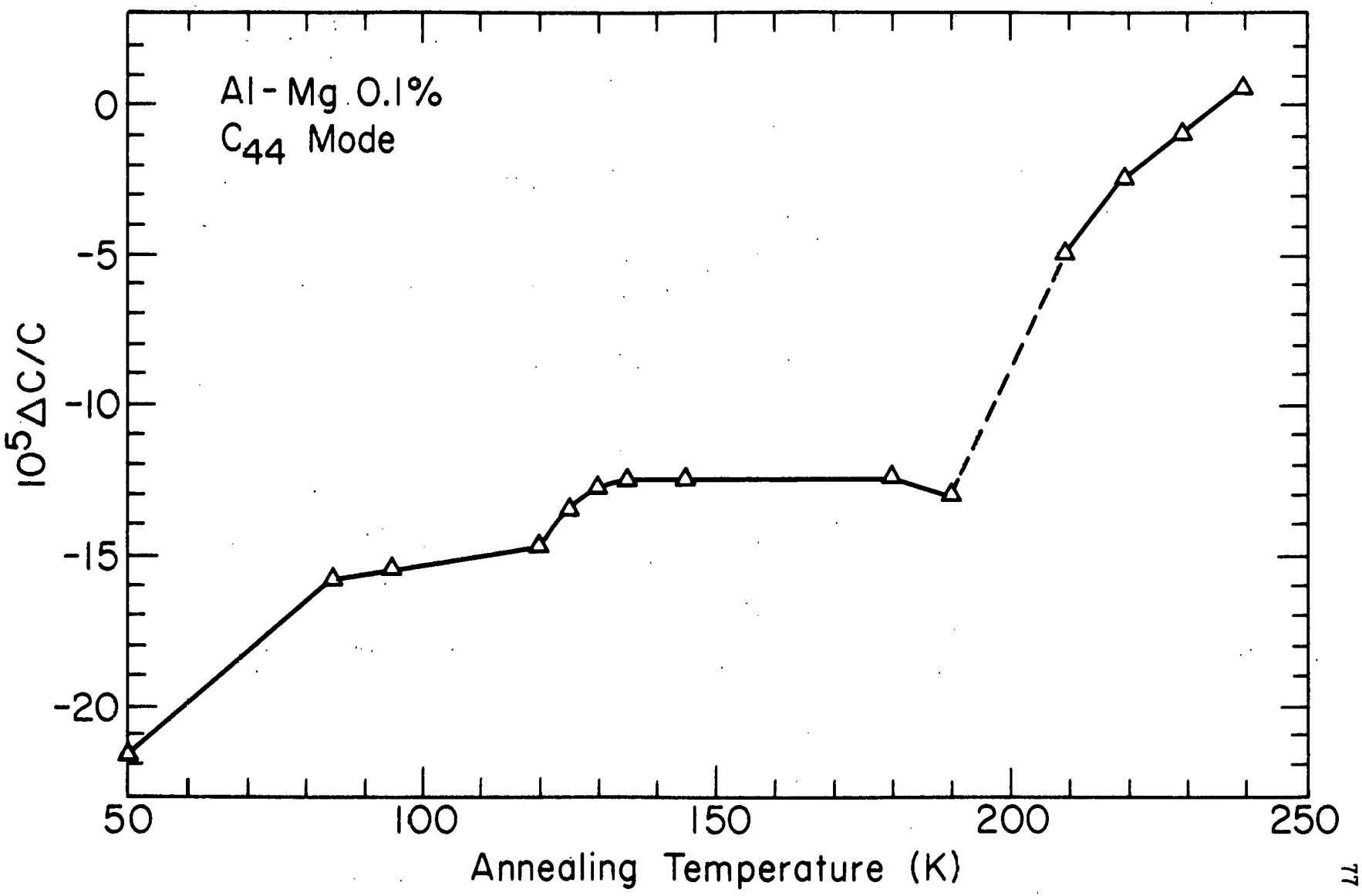
Al - Mg 0.1%
C_{44} Mode
$10^5 \Delta C/C$
0
-5
-10
-15
-20
50
100
150
200
250
Annealing Temperature (K)

occurred near 130 K, as shown in figure 17. The small decrease seen in figure 18 seems to be a real effect and is not caused by the presence at 8 K of a relaxation peak; first of all, the magnitude of an effect caused by the relaxation at 8 K would be no more than $.5 \times 10^{-5}$ which is only about 20% of the relative change actually observed in the modulus. Secondly, one would expect the dispersion caused by a relaxation to cause an apparent increase in the diaelastic effect, i.e. a change to more negative numbers.

The diaelastic effect is still not well understood theoretically so that an interpretation of these results in terms of possible defect configurations will not be attempted here.

TABLE IV. Characteristics of Attenuation Peaks in Al-Mg .1%

Peak	Mode	T_m(K) 10MHz / 30MHz	H(meV)	ν_0(1/sec)	Δ_m/c	RT_m/c (K)
1	C'	19.3 / 21.8 $\pm$.5	18$\pm$7	$10^{11.6\pm.5}$	5.2$\pm$.5	201
2	C'	14.0 / 15.9 $\pm$.5	11$\pm$2	$10^{11.8\pm.5}$	8.6$\pm$.5	241
3	C_{44}	19.8 / 22.3 $\pm$.5	17$\pm$3	$10^{12.2\pm.5}$	22.7$\pm$1	899
4	C_{44}	8.2 / 9.3 $\pm$.5	6$\pm$2	$10^{11.8\pm.5}$	11.9$\pm$.5	195
5	C_{44}	44 / 48 $\pm$1	45$\pm$14	$10^{13.6\pm.7}$	10.4$\pm$.6	915
6	C_{44}	>135			48$\pm$5	12960

Table IV summarizes the major characteristics of the relaxation peaks observed in Al-Mg.

T_m is the temperature of the peak maximum, and values are given

for both 10 and 30 MHz. From the Debye equations, the decrement peaks occur for $\omega\tau=1$ which, when combined with the Arrhenius expression for τ given in equation 6, implies that the use of two different frequencies, f_1 and f_2, causes the peak temperatures to shift accordingly from T_1 to T_2. One can use this shift to obtain H, the activation enthalpy for the relaxation:

$$(11) \qquad (H/k)[(1/T_1)-(1/T_2)] = \ln(f_2/f_1)$$

ν_0, the frequency factor, is then easily calculated from equation 6. One technique[29] for obtaining the peak shift is to plot the decrement peaks for 10 and 30 MHz as shown in figure 19. The background was subtracted and each point on the curve multiplied by its corresponding temperature in order to eliminate the inverse T dependence of the relaxation strength (see equation 9). The result was normalized and then plotted against 100/T. Since Debye peaks are normally symmetric about $\omega\tau=1$ when plotted versus $\ln \omega\tau$, the exponential dependence of τ upon the inverse temperature means that replacing $\ln \omega\tau$ with 100/T (for a given frequency) will preserve the symmetry of the peaks. The results for peak 3 (C_{44} mode) after the 190 K anneal are shown in figure 19.

The shift of the entire peak (rather than just that of the maximum) is used for the evaluation of H using equation 11. T_m was obtained by taking an average of the abscissa values at the half-maximum points on the curves. (In some cases where the peak was

Figure 19. The decrement values for peak 3 in Al-Mg, multiplied by temperature and normalized, plotted as a function of 100/T for 10 and 30 MHz, side by side. The peak shift with frequency was used to calculate the activation energy for relaxation of the peak 3 defect. A peak having the classical Debye shape was calculated and is shown as the dashed curve.

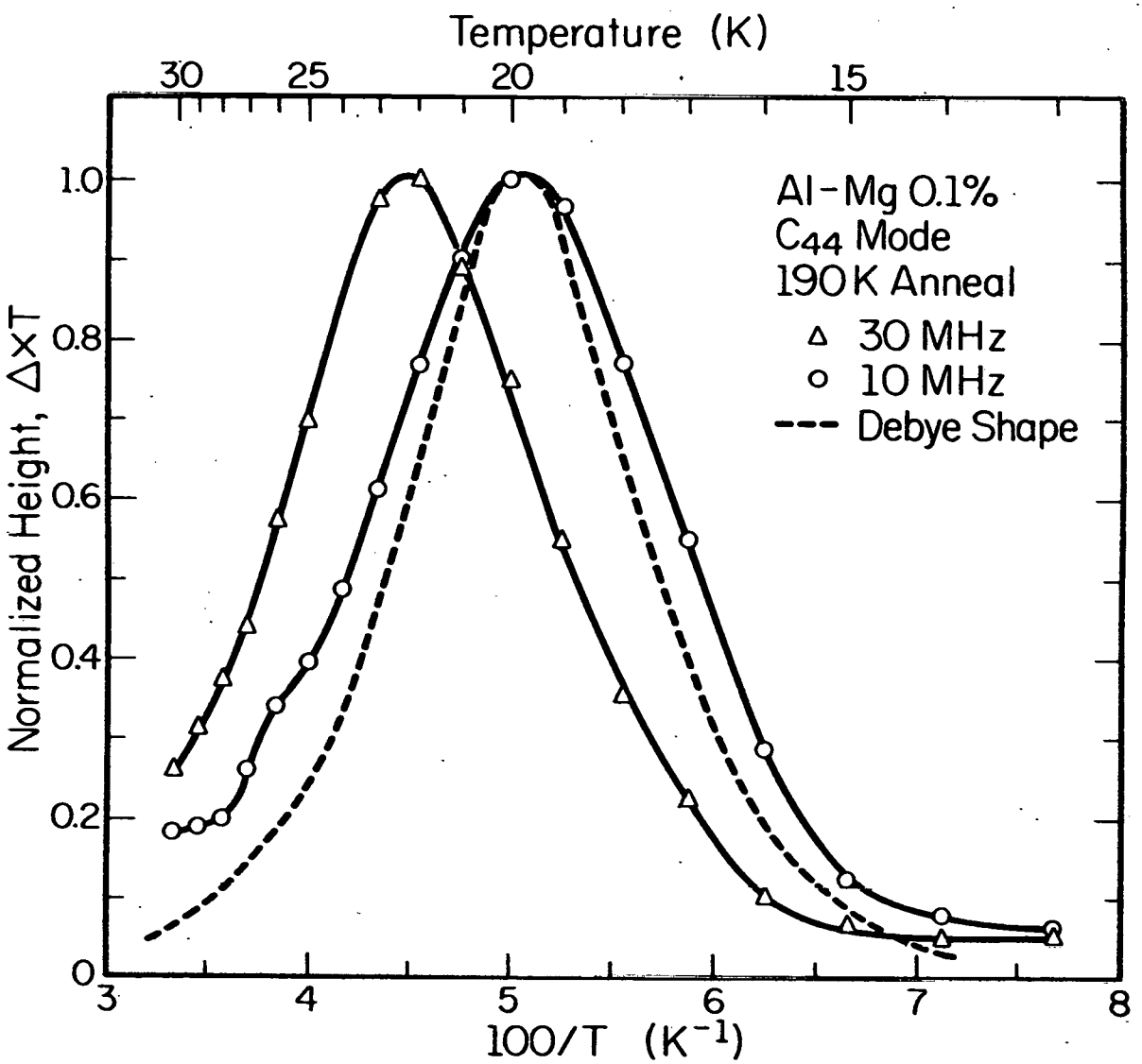
Temperature (K)
30
25
20
15
1.0
0.8
0.6
0.4
0.2
0
Normalized Height, ΔxT
Al-Mg 0.1%
C44 Mode
190K Anneal
30 MHz
10 MHz
Debye Shape
3
4
5
6
7
8
100/T (K-1)

slightly asymmetric, the nine-tenths-maximum points were also used.) The last two columns in table IV are concerned with the size of the relaxation peaks. Δ_m/c is the maximum decrement seen for each peak during the annealing program divided by the Frenkel defect concentration after irradiation (as listed in table III). RT_m/c is the temperature-compensated relaxation strength for each peak per unit concentration of Frenkel defect after irradiation, again for the maximum value observed.

From the characteristics listed in table IV and the Debye equations, the shapes of Debye peaks can be calculated and compared with the experimental peaks. For example, the curve drawn with dashed lines in figure 19 has the classical Debye shape and agrees well with peak 3. All the peaks in Al-Mg have shapes which are approximately Debye in nature except possibly peak 6 (which anneals during our observation of it.)

C. Cu-Ag results

Measurements were taken of the ultrasonic attenuation (at 10 and 30 MHz) and resonant frequency (at 10 MHz) in both C' and C_{44} modes. A summary of some basic data for the Cu-Ag runs is given in table V. No relaxations were visible in the C' mode, but several peaks were seen in the C_{44} mode. The existence of several peaks was deduced only after observation of the annealing behavior of the attenuation. This process of deduction will be outlined later in this section and involves a combination of the data shown in figures 20 and 21. Figure 20 shows

Figure 20. The log decrement in Cu-Ag at 10 MHz, plotted as a function of observation temperature for C_{44}. Three different anneals are shown. (data from run V)

PEAK STRUCTURE

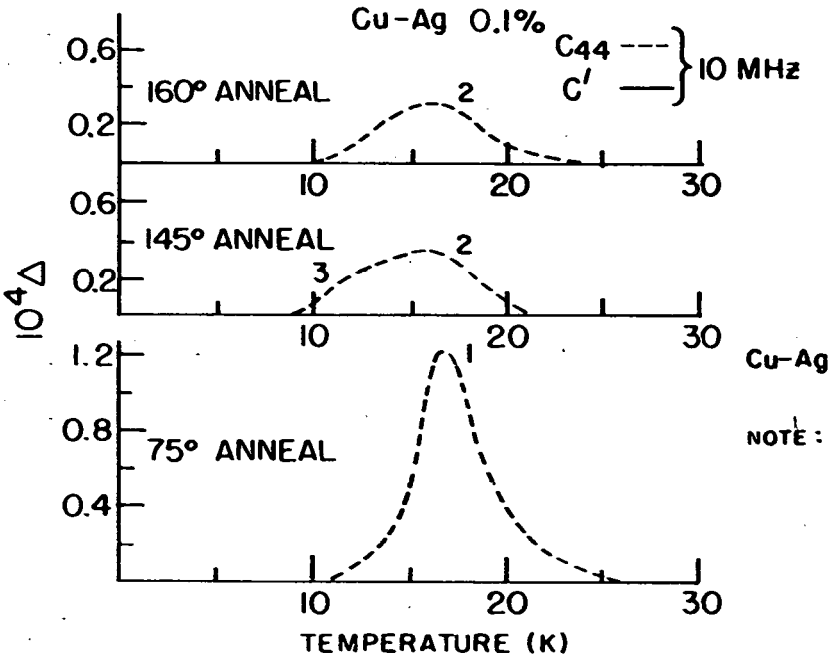

	PEAK NAME	MODE
Cu-Ag	1	C_{44}
	2	C_{44}
	3	C_{44}

NOTE: NO PEAKS WERE VISIBLE IN THE C' MODE

Figure 21. A(top): The maximum peak height for the C_{44} peaks in run V (in log decrement) plotted against annealing temperature (in K).

B(bottom): The relative modulus change for C'(solid curve), run IV and C_{44} (dashed curve), run V, plotted against annealing temperature (in K). The frequency used for C' was 10.52 MHz. For C_{44}, it was 11.17 MHz.

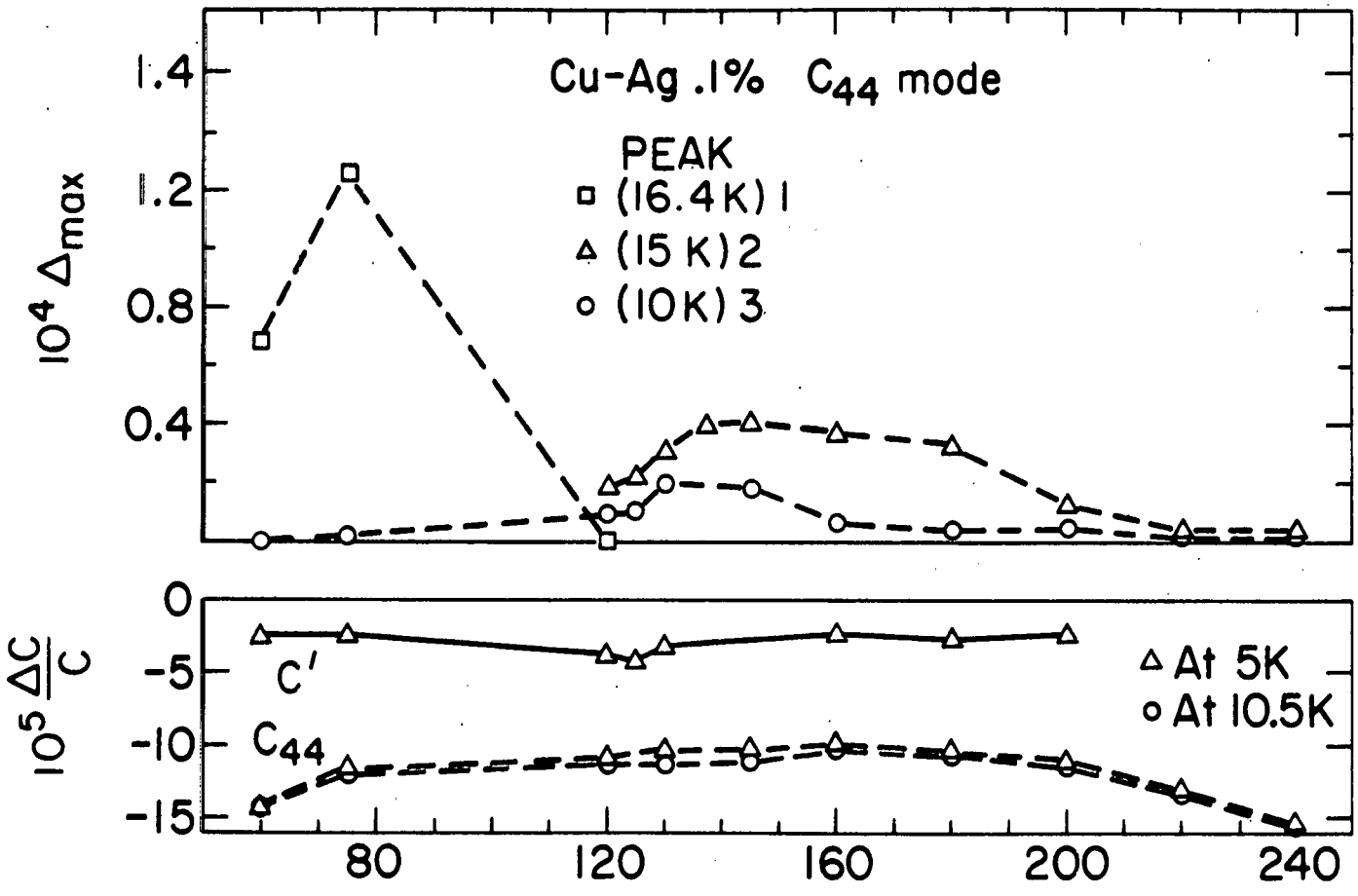
Cu-Ag .1% C_{44} mode
PEAK
(16.4 K) 1
(15 K) 2
(10 K) 3
$10^4 \Delta_{max}$
1.4
1.2
0.8
0.4
0
-5
-10
-15
$10^5 \frac{\Delta C}{C}$
C'
C_{44}
At 5K
At 10.5K
80
120
160
200
240

the 10 MHz logarithmic decrement after background subtraction plotted as a function of temperature between 0 and 30 K at three different points in the annealing program. The results are from run V. The top portion of figure 21 displays the annealing behavior

TABLE V. Summary of Cu-Ag Runs

	Date	Mode	Irrad Temp (K)	Selected Echoes 10MHz/30MHz	Time Between Echoes (μs)	Thickness (mm)	Volume Averaged Dose (ppm,F.P.)
Run IV	Jul 1980	C'	50	1st+4th/1st+2nd	30.9/10.3	8.48	3.6
V	Jul 1980	C_{44}	50	2nd+8th/1st+3rd	34/11.2	8.48	9.3
VI	Oct 1980	C_{44}	58	1st+7th/1st+3rd	33.7/11.2	8.18	5.0
VII	Mar 1981	C_{44}	40 80	1st+10th/1st+5th	49/22	8.18	4.0 18.7
VIII	Apr 1981	C'	40 80	1st+9th/1st+3rd	77.3/19.3	8.18	1.8 15.4

at 10 MHz in terms of the maximum peak height in logarithmic decrement versus the annealing temperature, again for run V. Run V served as a preliminary investigation of the C_{44} mode.

Immediately after irradiation at 50 K to a Frenkel defect concentration of 9.3 ppm, only peak 1(at 16 K) was visible. The 75 K anneal produced a two-fold increase in peak height. This suggested an association with the resistivity substage II_b observed by Cannon and

Sosin[4] at 60 K. The next substage observed by them was named II_c and occurred between 120 and 140 K; therefore, our next anneal was to 120 K. Of great interest was the fact that peak 1 was already gone after this anneal, well before the bulk of the resistivity annealing in this region had taken place. Only a small, poorly-defined peak structure was left in its place with a shoulder between 9 and 12 K and a maximum centered at 15 K rather than 16 K. One of the most intriguing features about the Cu-Ag system is that this peak structure continued to increase during the 125-145 K anneals, well after peak 1 had disappeared. If, as Cannon and Sosin supposed,[4] Ag impurities released trapped interstitials in this vicinity, the growth of this structure can be explained. However, what annealing mechanism would then account for the early disappearance of peak 1?

Figure 21 shows the growth in both the height of the shoulder and the maximum height at 15 K. In figure 20, the structure present after the 145 K anneal is shown, and the maximum is labeled peak 2 while the shoulder near 11 K is labeled peak 3. Peak 2, even though occurring at nearly the same temperature as peak 1, was believed to be a distinct peak caused by a different defect or set of defects and not simply a diminished version of peak 1. It was assumed that once the defect responsible for peak 1 started to anneal, as evidenced by the drastic reduction in peak height, the defect would continue to anneal away until peak 1 was entirely gone. Also, the maximum height of the "peak" definitely shifted from 16 K to 15 K during the 75-145 K anneals. The existence of the shoulder was verified when, upon subsequent annealing

to 160 K, the peak height between 9 and 12 K decreased noticeably. Peak 2 remained until the 200 K anneal where it finally annealed away. This behavior correlates with the resistivity substage II_d seen by Cannon and Sosin at about 190 K.

A second run was performed in the C_{44} mode (run VI, Frenkel pair concentration of 5 ppm) in order to obtain details about the behavior of peak 1 near 60 K(stage II_b), and about the temperature separation between the annealing of peak 1 and the growth of peaks 2 and 3. The observed annealing behavior is shown in figure 22 plotted as the maximum peak height in decrement (background subtracted) versus the annealing temperature. Unlike the behavior in run V, peak 1 did not grow after annealing to 80 K. Apparently, the irradiation temperature was too close to 60 K so that all of the II_b annealing took place during the irradiation. However, we were still able to check on the annealing region between 95 and 145 K. The difference between the temperature where peak 1 disappeared and that where peaks 2 and 3 grew is clearly shown in figure 22. Maximum annealing of peak 1 took place near 110 K, well before stage II_c (as seen by Cannon and Sosin), while maximum growth for peaks 2 and 3 took place near 127 K. Peak 3 again disappeared near 150 K (which did not correspond to any resistivity change observed) while peak 2 annealed out in the same temperature range as stage II_d (190 K).

To determine whether or not peak 1's growth corresponded to the resistivity stage II_b (60 K), we performed a third C_{44} run (VII) with particular emphasis on a low temperature irradiation followed by an

Figure 22. The maximum peak heights for the C_{44} peaks (in log decrement) in run VI, plotted against the annealing temperature.

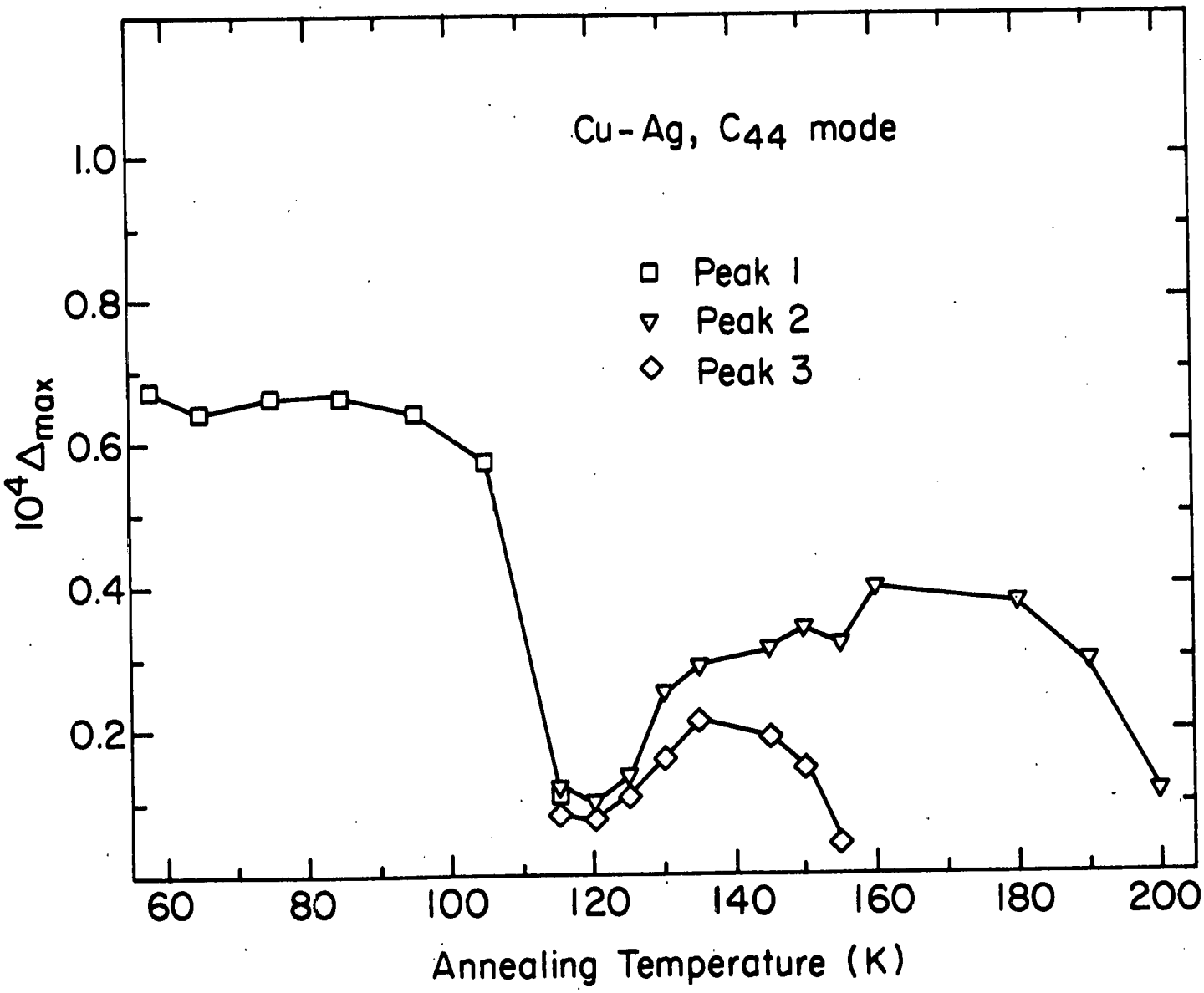
Cu-Ag, C_{44} mode
Peak 1
Peak 2
Peak 3
$10^4\Delta_{max}$
1.0
0.8
0.6
0.4
0.2
60
80
100
120
140
160
180
200
Annealing Temperature (K)

annealing program centered on 60 K. We irradiated our sample for several days at 40 K to a Frenkel pair concentration of about 4 ppm. To insure the proper irradiation temperature, we monitored the resonant frequency continuously during irradiation and made use of the strong sensitivity of the frequency to temperature changes. The results of the irradiation and annealing for 30 MHz are shown in figure 23. Shown in solid lines are the annealing curves (maximum peak height in decrement vs. annealing temperature) for the 30 MHz attenuation peaks 1 and 2 (read from the left-hand scale). Peak 3 was ignored for this run. The boxed portions represent the growth of the peak following irradiation at the temperature specified. The dash-and-dotted curve gives the Cannon and Sosin data for the amount of induced resistivity change remaining in Cu-Ag(500 ppm) as a function of annealing temperature. The resistivity points are normalized to the value after the 40 K anneal, and their values are read from the right-hand scale. They are unconnected with the 80 K irradiation, as indicated by the dashed line.

After the 40 K irradiation, we proceeded to anneal the sample upward in 4 or 5 K steps to 79 K. The growth of peak 1 correlated very well with the recovery stage II_b which was believed by Cannon and Sosin[4] to be due to a reconfiguration of the interstitial into a deeper trapping position at the same impurity.

The annealing program was followed by another irradiation, this time at 80 K to a final Frenkel pair concentration of 18.7 ppm. This higher irradiation temperature increased our effective cooling power

Figure 23. The results of run VII for the C_{44} mode:
A: Boxed portions show the maximum height of peak 1 in Cu-Ag (at 30 MHz) as a function of the total induced Frenkel pair concentration, measured after each day of irradiation.

B: Outside the boxed portions, maximum peak heights (at 30 MHz) are plotted against annealing temperature, shown by solid curves.

C: For comparison, the residual resistivity change measured in Cu-Ag(500 ppm) as a function of annealing temperature by Cannon and Sosin[4] is also shown (by the broken, dash-and-dotted line). The values were normalized to the 40 K anneal.

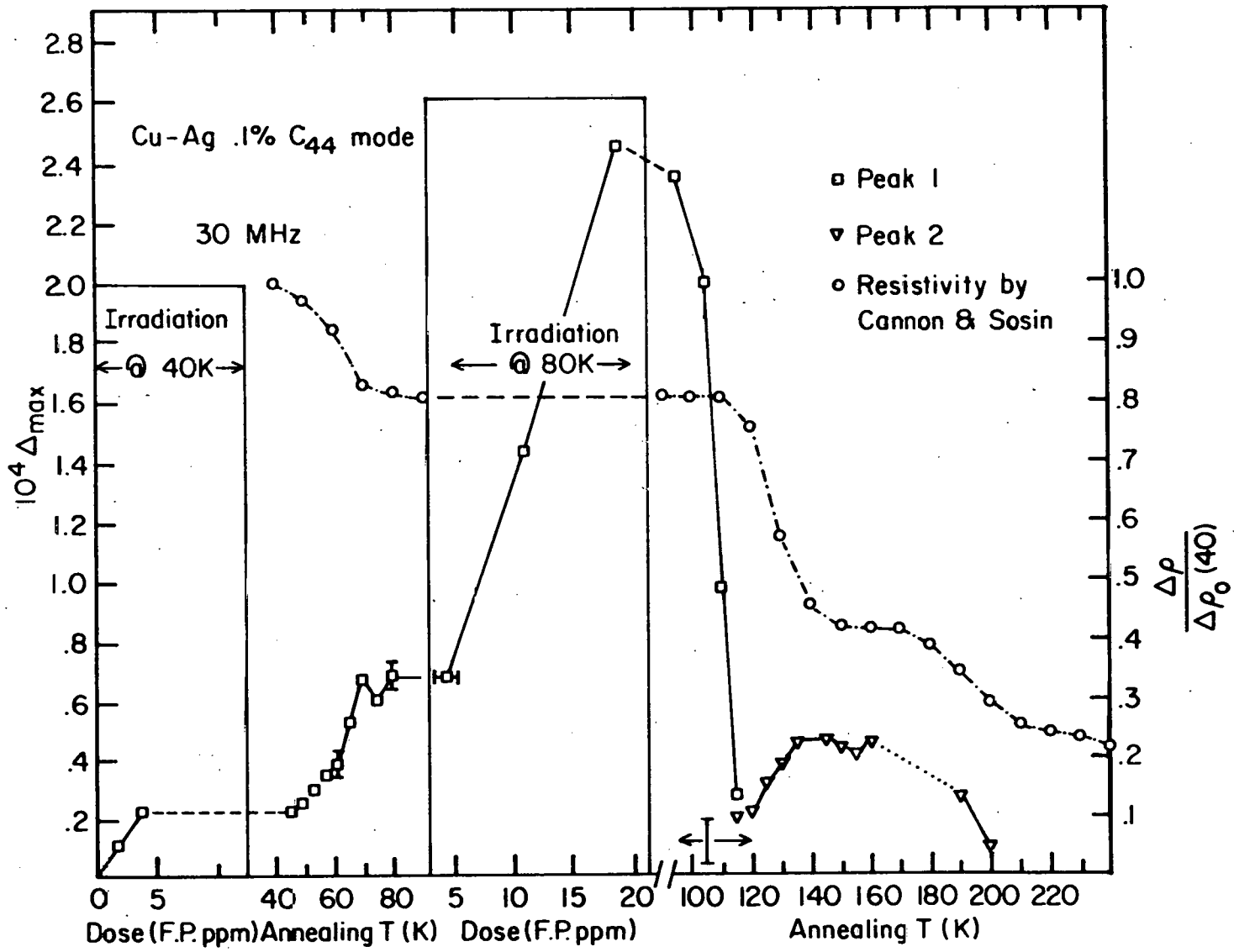
Cu-Ag .1% C_{44} mode
30 MHz
Irradiation @ 40K
Irradiation @ 80K
Peak 1
Peak 2
Resistivity by Cannon & Sosin
$10^4 \Delta_{max}$
$\frac{\Delta\rho}{\Delta\rho_0(40)}$
Dose (F.P. ppm)
Annealing T (K)
Dose (F.P. ppm)
Annealing T (K)

and allowed us to use higher beam currents. Peak 1 grew by a factor of 4. We annealed between 95 and 145 K, and after comparing our annealing data for peak 1 with Cannon and Sosin's resistivity data, we saw no distinct resistivity change associated with the disappearance of peak 1 at 110 K. Resistivity measurements performed by us on samples made from our own boule of Cu-Ag confirmed this fact.

We also verified the growth that took place in peak 2 between 120 and 145 K, significantly separated from the disappearance of peak 1 between 95 and 115 K. From figure 23, one can see a strong correlation between the growth of peak 2 and the resistivity recovery (stage II_c) observed by Cannon and Sosin. Our interpretation of these results will appear in chapter 4.

The annealing continued through 210 K with the disappearance of peak 2 taking place between 170 and 210 K, just where stage II_d in the resistivity was observed. The dotted line between 160 and 190 K in the peak 2 annealing curve indicates that no annealing points were taken in that region.

Measurements of the diaelastic effect in terms of the temperature-independent part of the relative modulus change ($\Delta C/C$) were also performed at 10 MHz in our samples. The lower portion of figure 21 shows a plot of the relative modulus change versus the annealing temperature for C' (run IV, Frenkel pair concentration of 3.6 ppm) and C_{44} (run V, 9.3 ppm Frenkel pairs) indicated by the solid and dashed lines, respectively.

The annealing curve for the C' diaelastic effect is rather flat,

showing very little change even in the annealing regions where the attenuation peaks were undergoing growth or shrinkage. The annealing curve for the C_{44} diaelastic effect shows a slight decrease of the effect (to less negative values) after the 75 K anneal, and then stays fairly flat until about 180 K. Above 180 K, the diaelastic effect gradually increases (to more negative values).

Figure 24 shows the annealing results for the C' (run VIII) and C_{44} (run VII) diaelastic effects (solid and dashed lines, respectively). Both of these runs started with a 40 K irradiation (to 1.8 ppm Frenkel pairs for C' and to 4 ppm for C_{44}) followed by annealing up to 74 K for C' and 79 K for C_{44}. The C' diaelastic effect appeared to increase slightly in this annealing region. However, there was a definite decrease in the C_{44} diaelastic effect that correlates well with the resistivity substage II_b (60 K).

An 80 K irradiation was then performed (to a final Frenkel pair concentration of 15.4 ppm for C' and 18.7 ppm for C_{44}) followed by the annealing program described earlier for the attenuation measurements. The annealing points were taken from 80 to 200 K.

In the C' mode, the diaelastic effect decreased throughout this region fairly smoothly except near 110 K and 130 K (where peak 1 disappeared and peak 2 grew in the C_{44} mode). The size of these deviations from smoothness was small, near the noise level of the system, and no conclusions are made about their possible origin. The diaelastic effect in C_{44} showed no major changes between 80 and 160 K. After 160 K, the effect gradually increased as it did in run V (figure

Figure 24. Annealing behavior of the relative modulus change for C' (solid) and C_{44} (dashed): first, following irradiation at 40 K, and then following irradiation at 80 K. Data are from runs VII(C_{44}) and VIII(C'). Measurements were at 5 K; the frequency for C' was 10.48 MHz. For C_{44}, it was 10.3 MHz.

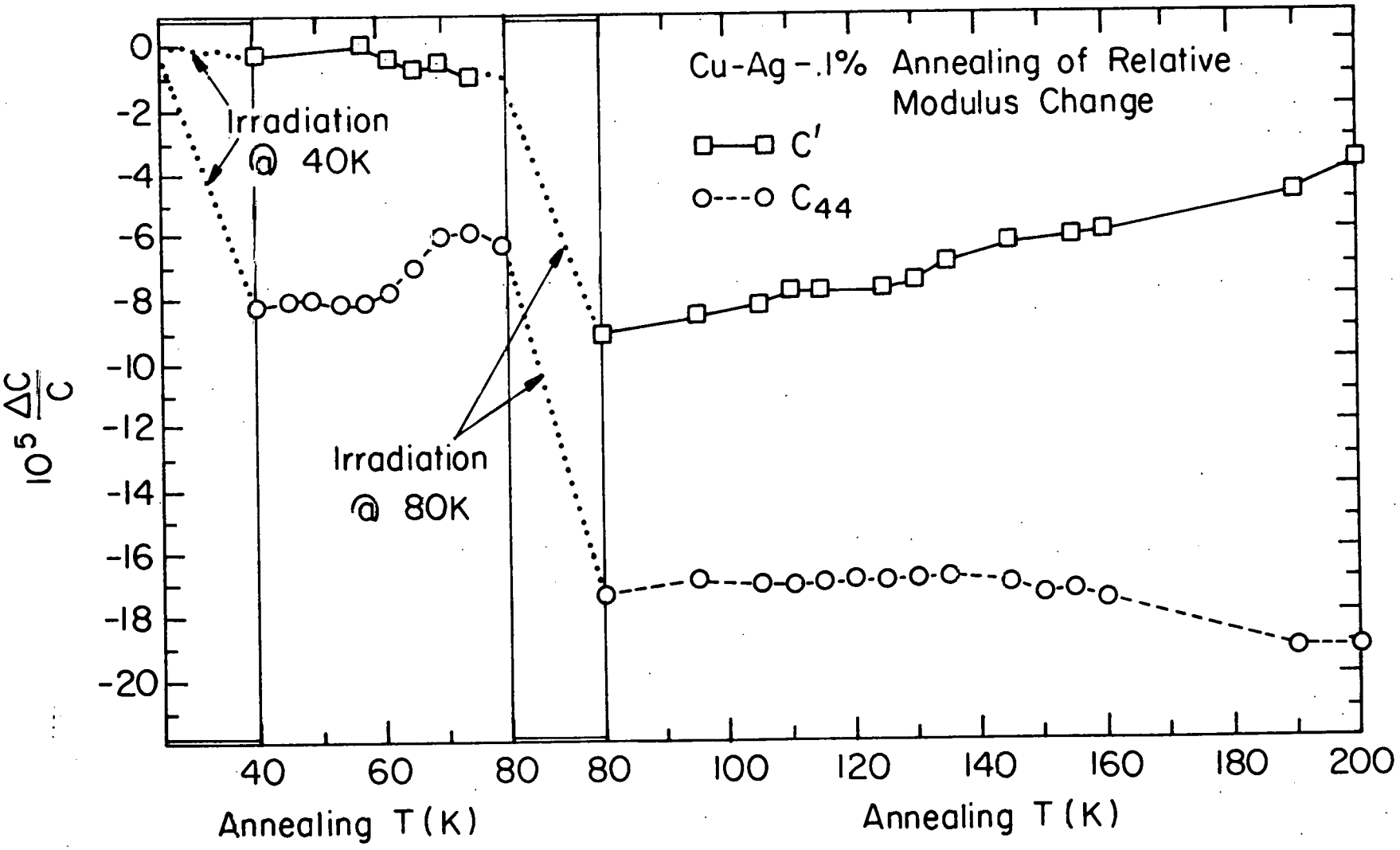
Cu-Ag -.1% Annealing of Relative Modulus Change
C′
C_{44}
Irradiation @ 40K
Irradiation @ 80K
$10^5 \frac{\Delta C}{C}$
0
-2
-4
-6
-8
-10
-12
-14
-16
-18
-20
40
60
80
80
100
120
140
160
180
200
Annealing T (K)
Annealing T (K)

21).

Figure 25 shows a plot of the diaelastic effect as a function of the Frenkel pair concentration for C' (run VIII) and C_{44} (run VII) shown with solid and dashed lines, respectively. As discussed previously, irradiation took place at 40 and 80 K. After each day of irradiation, the sample was ramped down to helium temperatures and the diaelastic measurement taken. The C' effect (after about 1.8 ppm of Frenkel pairs were introduced at 40 K) was very small. After annealing to 74 K, the effect was only slightly larger, as indicated in figure 25. Irradiation at 80 K seemed to produce a much larger effect per ppm Frenkel pair as evidenced by the steeper slope of the line drawn between the 80 K points, compared to the slope for the 40 K irradiation. However, only one point was taken after the 40 K irradiation, and since the initial pinning of dislocations might decrease the diaelastic effect in the early stages of irradiation, it is possible that the slope of the line drawn through the 40 K irradiation points later in the irradiation program could have been as large as the slope of the 80 K line.

In C_{44}, the diaelastic effect after 40 K irradiation was larger than in C' for the same dose. The annealing up to 79 K produced a decrease in the effect, as shown in figure 25. One would expect from this decrease after annealing that the diaelastic effect per ppm Frenkel pair after irradiation at 80 K would be less than that for irradiation at 40 K. This conclusion is supported by a comparison of the slopes of the lines drawn through the 80 K and 40 K points.

Figure 25. The relative modulus change for C'(solid) and C_{44} (dashed) as a function of total radiation-induced Frenkel pairs at 40 and 80 K irradiation temperatures. Data were taken at 5 K following each day of irradiation. The resonant frequency for C' was 10.48 MHz. For C_{44}, it was 10.3 MHz.

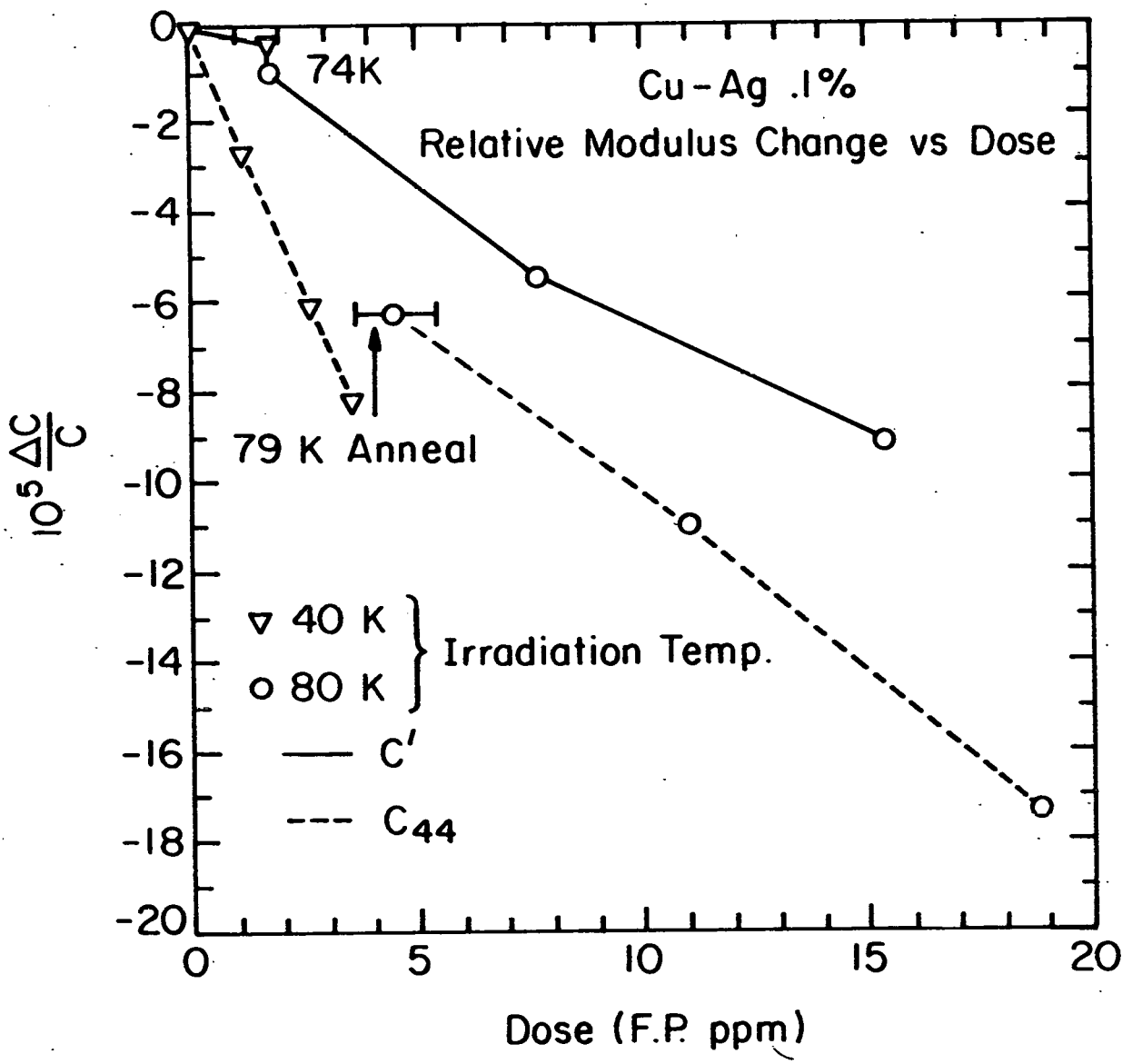
74K
Cu-Ag .1%
Relative Modulus Change vs Dose
79 K Anneal
40 K
80 K
Irradiation Temp.
C'
C44
$10^5 \frac{\Delta C}{C}$
Dose (F.P. ppm)
0
-2
-4
-6
-8
-10
-12
-14
-16
-18
-20
0
5
10
15
20

However, because the diaelastic effect is still not sufficiently well-understood, the significance of these results to the possible defect configurations remains unclear.

Table VI lists the characteristics of the peaks in Cu-Ag which were obtained in the manner discussed previously. An accurate determination of the characteristics for peak 3 was precluded by its small size and its proximity to peak 2. The numbers given for peak 2 are intended as estimates only; peak 2 was too wide to be accounted for by a single relaxation process. Figure 26 shows a plot of the normalized, temperature-compensated decrement at 10 and 30 MHz versus 100/T for peak 1 after the 95 K anneal. The dashed line is a calculated Debye peak, and it agrees well with the experimental peak observed.

TABLE VI. Characteristics of Attenuation peaks in Cu-Ag .1%

Peak	Mode	T_m(K) 10MHz / 30MHz	H(meV)	ν_0(1/sec)	Δ_m/c	RT_m/c (K)
1	C_{44}	16.3 / 18.4 $\pm$.5	14$\pm$3	$10^{12.3\pm.9}$	13.0$\pm$.5	424
2	C_{44}	15.1 / 17.1 $\pm$.5	13$\pm$3	$10^{12.1\pm.9}$	5	151
3	C_{44}	10 /----------				

Figure 25. Peak 1 in Cu-Ag, decrement values multiplied by temperature and normalized, plotted as a function of 100/T for 10 and 30 MHz, side by side. A peak having the classical Debye shape was calculated and is shown as the dashed curve.

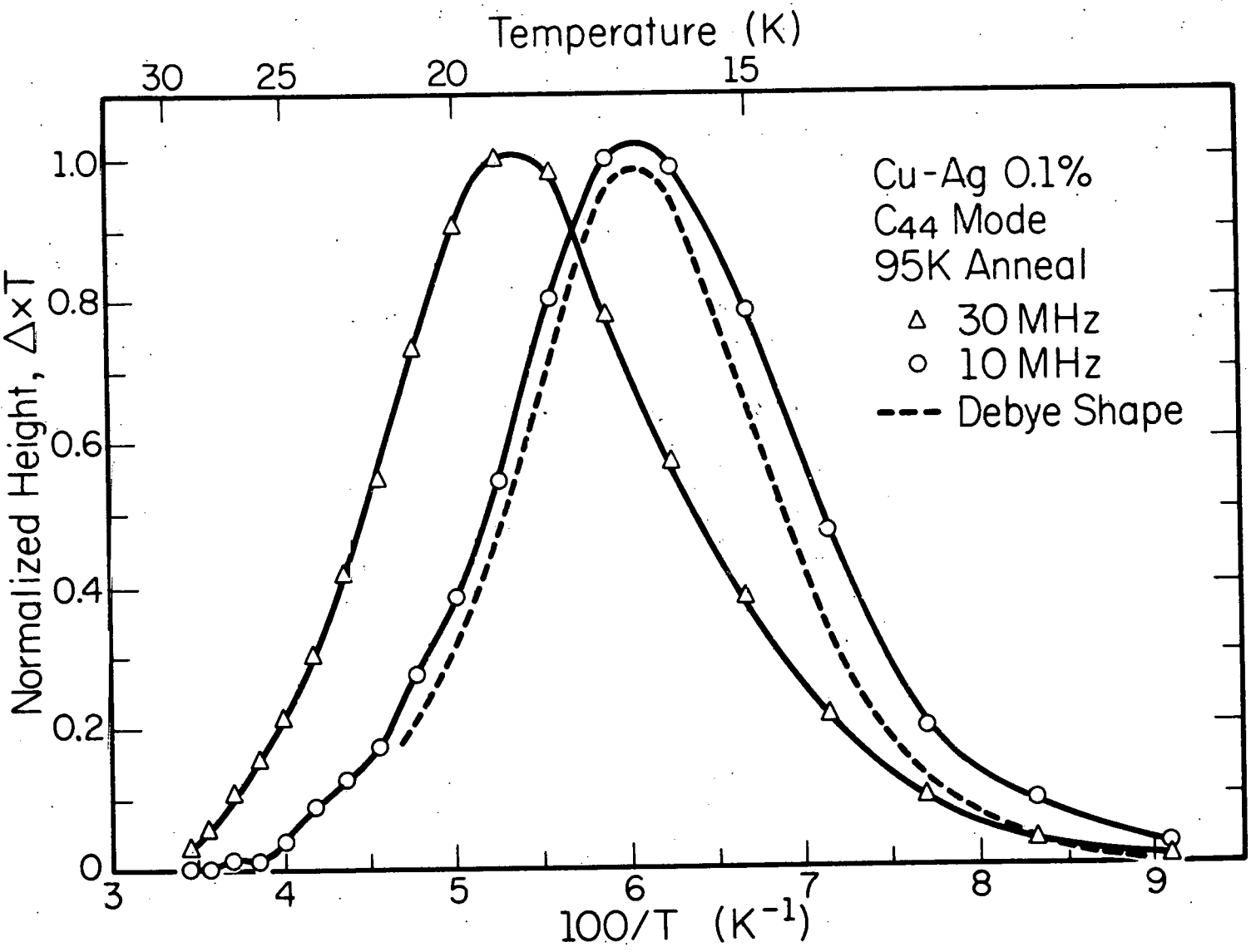
Temperature (K)
30
25
20
15
1.0
0.8
0.6
0.4
0.2
0
Normalized Height, Δ×T
3
4
5
6
7
8
9
100/T (K⁻¹)
Cu-Ag 0.1%
C44 Mode
95K Anneal
△ 30 MHz
○ 10 MHz
--- Debye Shape

CHAPTER 4

Discussion

We have found that electron-irradiation of Al-Mg and Cu-Ag introduces defects which cause a variety of peaks in the ultrasonic attenuation. Al-Mg displayed 6 peaks which were visible in both the C' and C_{44} acoustic modes, while Cu-Ag displayed 3 peaks only in the C_{44} acoustic mode.

Each of the relaxation peaks in Al-Mg showed an annealing behavior different from that of every other peak. The same is true of the three peaks in Cu-Ag: that is, peak 1 disappeared at 110 K, peaks 2 and 3 grew at about 125 K, peak 3 disappeared near 150 K, and peak 2 disappeared near 190 K. It is reasonable to conclude from the annealing behavior observed that each peak in Al-Mg and Cu-Ag corresponds to a different defect type.

Al-Mg and Cu-Ag represent two systems in which the impurity atom is strongly oversized within the host lattice: $\Delta V/V$ is 44% for Mg^{25} in Al and 36% for Ag^{39} in Cu. In these oversized systems, all of the attenuation peaks (except possibly peak 6 in Al-Mg) underwent growth during some part of the stage II annealing program. The main peaks (peak 1 in Cu-Ag and peak 6 in Al-Mg) annealed away in the middle of stage II (110 K for Cu-Ag, 130 K for Al-Mg). This is in sharp contrast with the behavior found in the undersized systems studied so far: Al-Mn (Johnson[1]) as well as Al-Zn and Al-Fe (Hultman[2]). In the

undersized case, almost all of the peaks reached their maximum heights immediately after irradiation and remained unchanged until they finally annealed away. For the strongly undersized materials Al-Mn and Al-Fe (where $\Delta V/V$ is about -30%),[39] the main peaks did not disappear until the onset of vacancy migration in stage III (210-240 K).

These differences in the annealing behavior suggest that the interstitial traps near oversized impurities tend to be shallower than the traps near oversized impurities. This behavior is roughly consistent with the results of calculations performed by Dederichs, et al.[3] Figure 2B shows the binding energies for the complexes consisting of a self-interstitial dumbbell and an oversized impurity located at the sites indicated. (Recall that the impurity does not move between these sites. Rather, the dumbbell jumps so that the relative position of the impurity is what changes. Also, the energies are given in units of the binding energy for the mixed dumbbell, which forms only in the case of the undersized impurity. Positive values are considered to be binding.) Reversing the signs gives the results for an undersized impurity. The binding energies one then obtains for the undersized complexes represent stronger binding overall than one finds in the case of the oversized impurity: these energies are 1.0, .40, .13, and .04 for the undersized impurity, and .21, .09, and .01 for the oversized impurity. Table VII gives the predicted binding energies, E_b (in eV), and the approximate expected temperatures of annealing, T_A, for these configurations in Cu-Ag and Al-Mg. The results for two models (models A and B) are listed. These models will be discussed in detail later in

TABLE VII. Binding Energies and Annealing Temperatures for Impurity Traps in Cu-Ag and Al-Mg

Trap	Cu-Ag .01	Cu-Ag .09	Cu-Ag .21	Al-Mg .01	Al-Mg .09	Al-Mg .21
MODEL A						
E_b(eV)	.03	.26	.62	.03	.25	.57
$U(eV)=E_b+E_m$	.15	.38	.73	.14	.36	.69
$T_A(K)=320\ U$	47	122	235	46	116	220
MODEL B						
E_b(eV)	.013	.12	.28	.012	.11	.26
$U(eV)=E_b+E_m$	.13	.24	.40	.13	.23	.38
$T_A(K)=320\ U$	42	76	127	41	72	120

this chapter. The binding energy of a mixed dumbbell as a function of size mismatch ($\Delta V/V$) is given by Dederichs, et al.[3] and is used to obtain E_b, the binding energy of the complex. We assume the activation energy for annealing, U, is given by E_b+E_m, where E_m is the free migration energy of the interstitial which is taken here to be .115 eV for Al and .117 eV for Cu.[42] This value for U should be regarded as an upper limit in the case of a defect moving from a shallow trap to a deeper one. This is because the energy barrier separating a shallow trap from a deep one is likely to be lower than the normal migration energy in the rest of the crystal.

The annealing temperature is calculated by first considering equation 10 again. (Implicitly, to obtain equation 10, we assumed that

the defects need to perform only a single jump to produce annealing behavior in our attenuation peaks.) We rewrite equation 10 as:

(12) $$c = c_0 \exp(-t/\tau) \quad \text{where}$$

(13) $$\tau^{-1} = f_0 \exp(-U/kT)$$

For a time of measurement, τ, of about 10^3 seconds (about 16 minutes) and a value for f_0 of 10^{13} sec^{-1}, we obtain the following linear relationship between U and T_A:

(14) $$T_A(K) = 320\ U(eV)$$

The trap marked .01 was used by Cannon and Sosin in their interpretation of the resistivity substage II_b at 60 K (see figure 2A). It was believed to be the shallow trap that fed into the deepest trap marked .21 in figure 2B. However, Table VII shows that this process should occur at 47 K (as an upper limit) so that this configuration probably cannot account for the 60 K substage. Also, this trap is probably unimportant for irradiation temperatures between 40 and 80 K. Therefore, we can simplify our discussion by dealing only with the remaining stable sites marked .21 and .09. We will use the numbers shown in figure 2B for identification of the different defect complexes treated in the following discussion.

A. Predictions of the Dederichs, et al. model

Dederichs, et al.[3] used simple potentials (the Born-Mayer, Morse, and Modified Morse) to describe the interactions between the interstitial and the impurity atom. These potentials would be expected to give good results for Cu and Ag which have hard core closed electron shells. Also, these potentials have given a good quantitative account of the interstitial and vacancy properties in pure copper. Therefore, it is expected that the calculations by Dederichs, et al. should apply best to Cu-Ag among all of the interstitial-impurity systems investigated to date.

To see the implications of these calculations for the present measurements, we first take note of the fact that there exist several independent "tracks" for the motion of the interstitial, so that not every configuration is available to a given interstitial at a given impurity atom. This has certain consequences upon the annealing behavior which will be discussed below. The concept of the tracks arises from consideration of the stable defect configurations indicated in figure 2B with the binding energies .21 and .09. If the dumbbell can only migrate via the elementary jump shown in figure 1B (i.e., the initial and final positions of the dumbbell atoms all lie in a (100) plane), then the site marked .21 is inaccessible to the site marked .09. In fact, if the system is allowed to change only via the elementary jump specified, then at a given impurity, the migration paths or "tracks" including the sites marked .09, 0.0, -.04, -.13, and -.4 are completely inaccessible to the path that includes the sites .01

and .21.

These tracks are drawn in figure 27. The impurity atom is stationary, while the dumbbell can migrate between the positions and orientations shown for each track. Two types of tracks are shown, track A (containing the stable site marked .21) and track B (containing the stable site marked .09). "Track B" actually consists of three independent tracks; For example, each position marked .09 for one orientation of the dumbbell is marked 0.0 for the other two orientations. Dederichs, et al.[3] have shown that a simple rotation of the dumbbell at the same site requires an energy greater than the migration energy, so that the dumbbell cannot get from 0.0 to .09 at the same site by simply rotating. Therefore, the three tracks passing through the position marked .09 are independent. A similar situation exists for every position shown in the figure, so that a total of four independent tracks exist for each impurity atom in the crystal (although tracks B1-B3 are related by 90° rotations around a <100>-axis passing through the impurity).

After irradiation at low temperatures, 25% of the induced defects are in track A, trapped at the sites marked .21. 75% of the defects are divided among tracks B1-B3, trapped at the sites marked .09. As the annealing program reaches about 120 K (in Cu-Ag or Al-Mg, see table VII), the sites marked .09 release their trapped dumbbells and tracks B1-B3 become depopulated. The track B interstitials migrate away from their own impurities, enter track A at other impurities, and are deeply trapped in the sites marked .21. In the process of changing tracks,

Figure 27. Four independent tracks are shown for each impurity. Only the sites on a single track are mutually accessible. Most of the sites are marked by their binding energy as calculated by Dederichs, et al.[3] in units of the mixed dumbbell binding energy. Positive values are binding. Note that the deepest trap (marked .21) lies in track A, while the .09 trap lies on tracks B1 through B3.

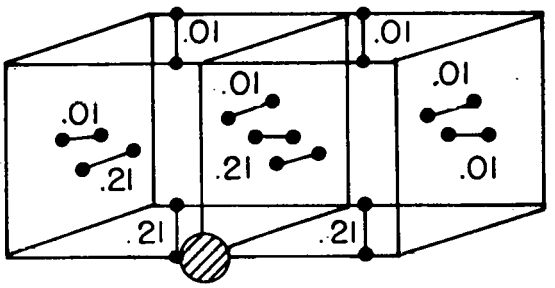

track A

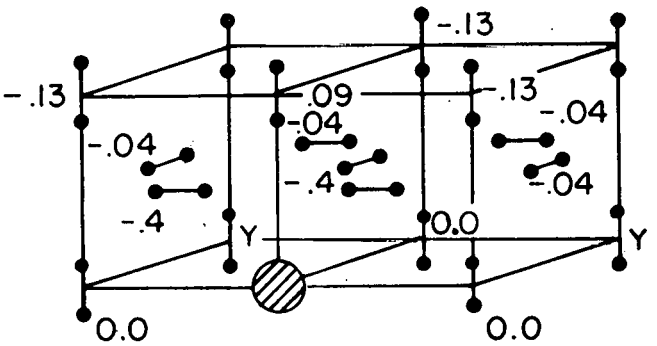

track B_1

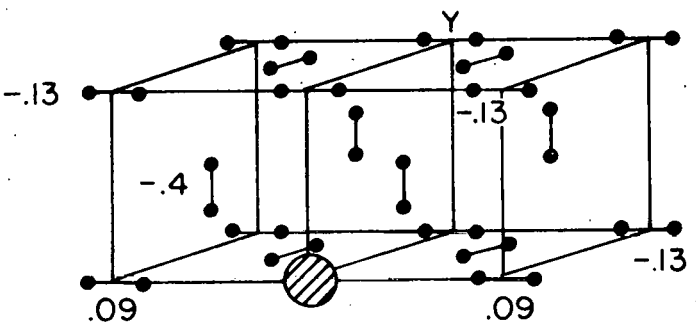

track B_2

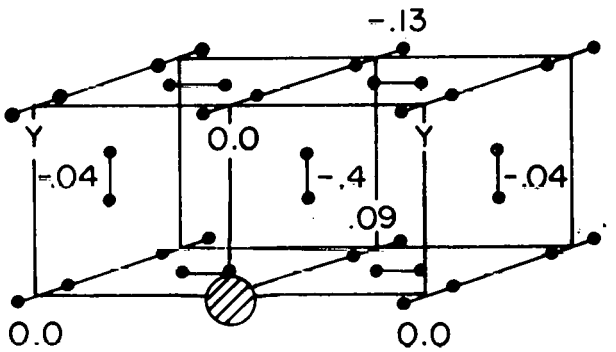

track B_3

some of the interstitials recombine with nearby correlated vacancies and produce resistivity recovery. After the 230 K anneal (see table VII), the sites marked .21 detrap and finally release their interstitials. Both correlated and uncorrelated resistivity recovery should occur at this time.

Dederichs, et al.[3] chose the deepest trap (.21) in track A to illustrate a possible reorientation process in oversized materials. The relaxation is between the equivalent sites shown in figure 3A. The relaxing defect complex possesses <110>-orthorhombic symmetry and should produce an attenuation peak visible in both the C' and C_{44} acoustic modes[37](see figure 3B). Since the C' relaxation requires the same elementary jump of the dumbbell that is required for the C_{44} relaxation, we expect the frequency factor and the activation energy for the relaxation to be the same in both modes. The relaxation peak should therefore appear at the same temperature in both C' and C_{44} modes. Because the reorientation jump is similar to the motion of the interstitial when freely migrating though the crystal, the reorientation energy should be on the order of the migration energy: about .1 eV in copper. This results in a peak temperature of 100 K or possibly higher at 10 MHz. Finally, since a single defect type is causing the peak in both modes, the peak should display identical annealing behavior in both modes.

The defect trapped in the site marked .09 does not appear to relax. On a given track, there are only two equivalent positions located on opposite sides of the impurity. Neither a <100> nor a <111>

uniaxial stress removes the degeneracy of these two sites. Therefore, no attenuation peak is expected for this trapping position.

We summarize the predictions of Dederichs, et al.'s model as follows:

1) Following irradiation, 25% of the induced defects should be in the deepest trap, marked .21 in track A. Relaxation of the trapped dumbbell should be visible as an attenuation peak located at about 100 K in both the C' and C_{44} modes.

2) At the same time, 75% of the induced defects should be trapped at the sites marked .09 in tracks B1-B3. No relaxation due to these defects is expected.

3) After the 100 K anneal, the ".09" defects (with a binding energy of only .25 eV, see table VII) dissociate. The shallow trapped interstitials leave their impurities and find the deepest trap (.21) in track A or recombine with correlated vacancies. This causes the high temperature attenuation peak in both modes to grow by at most a factor of 4, decreased by the correlated recovery which occurs.

4) The attenuation peak(at about 100 K) should remain until the 230 K anneal. The binding energy of the .21 trap (which causes the peak) is about .6 eV so that at 230 K, these traps finally release their interstitials causing the attenuation peak to disappear. Long range migration of the interstitials takes place, resulting in both correlated and uncorrelated recovery.

B. Cu-Ag discussion

The principal results which need to be accounted for by a model can be summarized as the following:

1) Three peaks were seen, including the main one (peak 1), all with trigonal symmetry (that is, all in the C_{44} acoustic mode).

2) Peak 1 was seen at 16 K, so that the defect responsible requires a low activation energy of about .014 eV for relaxation.

3) Peak 1 anneals away without an accompanying resistivity substage at 110 K, at a temperature close to but distinct from the resistivity substage II_c seen by Cannon and Sosin[4] at 127 K.

4) Peak 1 grows at 60 K, corresponding with the resistivity substage II_b seen by Cannon and Sosin.

5) The smaller peaks 2 and 3 grow at about 127 K. Their growth corresponds with the resistivity substage II_c.

None of the peaks observed in Cu-Ag can be identified with the <110>-orthorhombic defect predicted by Dederichs, et al.[3] Point 1 of the summarized results indicates that only peaks of trigonal symmetry were seen. None of them possessed a counterpart in C', which would be required for the predicted relaxation. We examined the C' mode carefully for a peak that might be associated directly with peak 1, our main peak in C_{44}. The relaxation strength of such a peak would have to be more than 30 times less than the relaxation strength found for peak 1. This in turn would require a condition on the principal values of

the λ-tensor (see equation 9) that we believe to be improbably restrictive. Furthermore, point 2 of our summarized results states that the temperature of peak 1 was only 16 K, much lower than the predicted peak temperature (100 K) for the <110>-orthorhombic defect. We conclude that peak 1 is not due to the deep-trapped defect predicted in Dederichs, et al.'s model. The remaining peaks 2 and 3 are also at low temperature (15 and 10 K) and possess trigonal symmetry. We therefore conclude that none of the peaks are caused by the predicted defect.

The annealing behavior predicted by Dederichs, et al.'s treatment does not fit the annealing behavior outlined in points 3, 4, and 5. The annealing of peak 1 near 110 K without any distinct resitivity substage occurring cannot be explained by the emptying out near 100 K of the .09 sites into the deep .21 sites. This emptying out must be accompanied by correlated resistivity recovery which, in this case, is not seen. The growth of peak 1 at 60 K (mentioned in point 4) does not correspond with any annealing at 60 K predicted by the model unless one makes a major modification in the calculated numbers. The model as it stands, however, does not predict any annealing at 60 K. Finally, the behavior described in point 5 might be explained by migrating interstitials encountering deep traps at trace impurities or Ag doublets. Such traps may produce relaxation peaks and would grow due to long range interstitial migration following final detrapping at single Ag atoms. However, final detrapping in the model does not take place until about 235 K when the deep traps marked .21 finally release

their interstitials.

To summarize, the symmetry and temperature of our main Cu-Ag peak do not match with those predicted for the most deeply trapped defect. In fact, no evidence for the predicted defect symmetry is found in our measurements. The annealing behavior observed by us is also not well explained by the model without major modification of the results calculated by Dederichs, et al. Our results force us to suggest certain extensions of and changes to the model by Dederichs, et al., resulting in two new models that can better explain the principal features seen in our measurements. These models are outlined in the next section.

C. Two possible models for Cu-Ag

Since the model by Dederichs, et al. should apply best for Cu-Ag as noted earlier, it is surprising that there exists such a discrepancy between the predictions and the results. Nevertheless, we would first like to make the smallest possible changes to the model that are necessary in trying to account for our results. We assume that the binding energies for the limited number of configurations considered are correct, but that other stable configurations have not yet been treated and that some of the equilibrium configurations proposed may be, in fact, saddle point configurations. Therefore, our initial suggestions are in the nature of extensions rather than corrections to the model.

1. Model A: First, in explaining points 1 and 2 of our Cu-Ag summary of results, we require a defect with a low energy of relaxation, a trigonal symmetry which produces only a C_{44} peak, and a binding energy that causes the peak to disappear at 110 K. The only defect in the basic model which has the proper binding energy is a dumbbell located at site .09 which has a calculated annealing temperature (table VII) of 122 K in Cu-Ag. The .09 configuration for which the binding energy was calculated is an equilibrium configuration by symmetry, but the equilibrium of the <100> orientation could be unstable. Therefore, in order to obtain a low temperature C_{44} relaxation, we postulate that the dumbbell be tilted slightly away from the <100> axis and into the (110) plane, as shown in figure 28. Such a tilt is reasonable when one assumes a strong repulsion of the bottom atom of the dumbbell both from the oversized impurity and from the face-centered host atoms. This dumbbell can occupy one of the equivalent positions A-D shown in figure 28. The distance between equivalent sites is short and no motion of the center of mass is required. This means that the activation energy for relaxation and therefore the peak temperature can be quite low. This satisfies point 2 of our Cu-Ag results. By applying a <100> uniaxial stress, the degeneracy of positions A-D is left unchanged: no C' relaxation takes place. A <111> uniaxial stress does remove the degeneracy so that relaxation occurs between the positions shown, producing a peak in the C_{44} mode. This satisfies point 1 of our main results in Cu-Ag. Thus, the canted dumbbell can explain two of the principal features observed

Figure 28. The .09 site occupied by a canted dumbbell. Equivalent positions are labeled A through D. The oversized impurity lies at the bottom of the face-centered cube. Open circles represent host-type atoms.

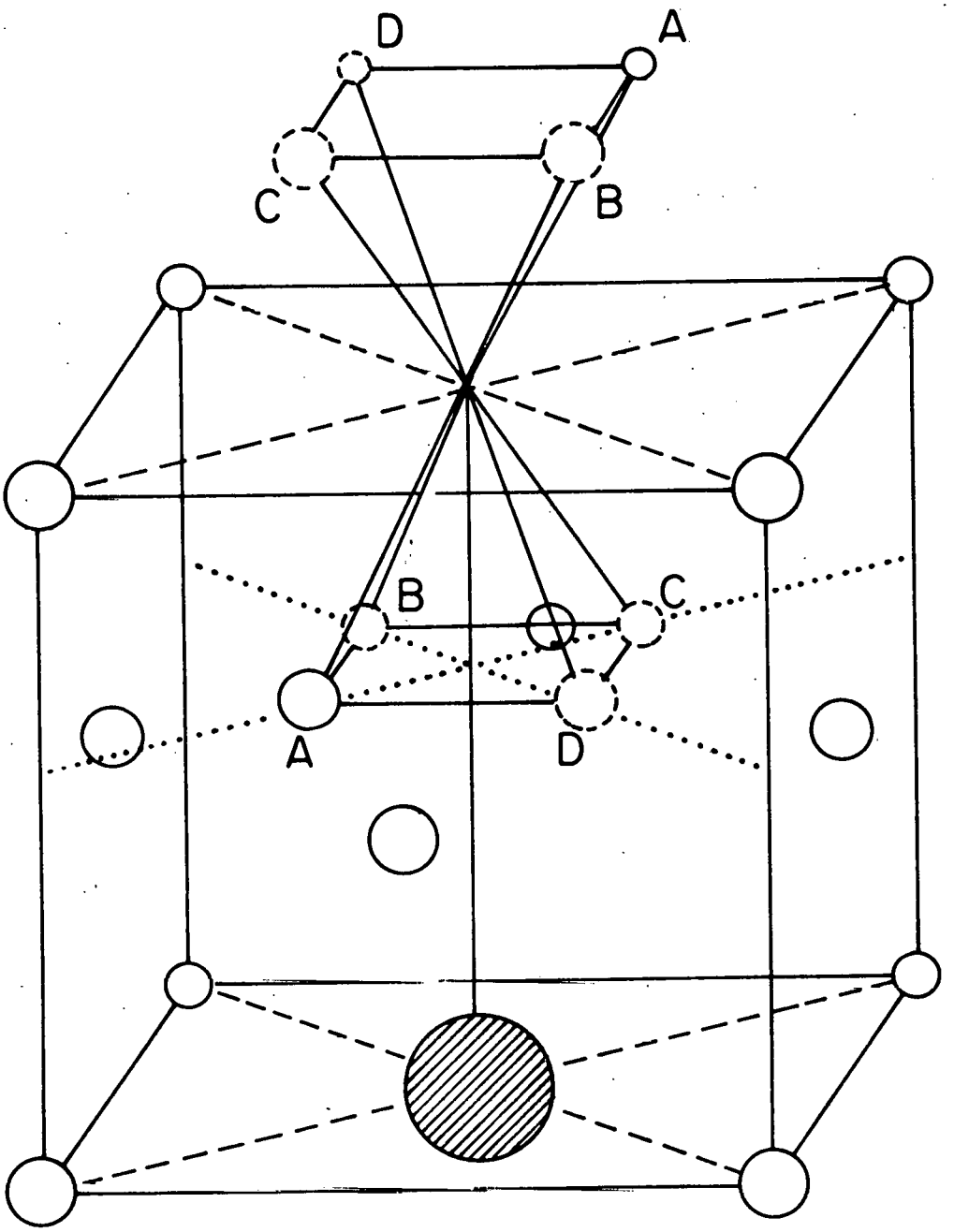
D
A
C
B
B
C
A
D

in Cu-Ag: 1) a peak in the C_{44} mode only, and 2) a low activation energy for relaxation.

We note here that up to now, not very much attention in the theoretical models has fallen on the interstitial traps marked .09 in tracks B1-B3. This is a little surprising considering that the track model predicts that three times the number of defects initially enter track B as enter track A. Calculations in the vicinity of the .09 site should be extended to test for the possibility of the proposed canted dumbbell.

Our second suggestion is directed at an explanation for the disappearance of peak 1 at 110 K without an associated resistivity substage. This behavior can be explained if the defect causing peak 1 (the canted dumbbell in our new model) dissociates and is trapped again at the same impurity so that no recovery with nearby or distant vacancies has a chance to occur. We require this new trap to be only somewhat deeper than the .09 site so that it may release interstitials at 127 K in stage II_c (this corresponds to a binding energy of .095 compared to .09 for the canted dumbbell.) Also, this trap must lie on track B so that it is accessible to the detrapped dumbbell from the .09 site. Examining the available sites on track B (figure 27), we see that none of the other sites which have been treated by Dederichs, et al. have positive binding energies. However, the site marked Y was apparently not considered for calculation so that the binding energy for this position is unknown. If one groups the known stable sites together (.21, .09, and .01) they all lie on the same (110) plane that

includes site Y. Therefore, our second suggested extension of the model is that site Y may be a stable trapping site for a dumbbell. After 110 K, the dumbbell leaves the .09 site and can migrate to site Y without encountering a vacancy. The result is that peak 1 disappears at 110 K without producing a resistivity substage and thus accounts for point 3 of our main results. This is in contrast to Cannon and Sosin's interpretation[4] of an earlier resistivity substage II_b (60 K) as being caused by the same sort of process: a reconfiguration of the interstitial from a shallow trap to a deeper one. It is possible that not all reconfigurations produce resistivity changes. It is also possible that the interpretation of II_b in terms of deeper trapping was incorrect. More will appear on this point later in the discussion.

A dumbbell trapped at site Y may be capable of producing a relaxation peak in C_{44}, but the required reorientation energy would be on the order of the migration energy (.1 eV), and the resulting peak temperature would be high (about 100 K at 10 MHz). Therefore, this site is not itself a candidate for the low temperature C_{44} peaks observed. The observation temperature of the peak at 10 MHz may be higher than the annealing temperature and might be missed for this reason.

Thus, we offer two suggestions for possible extensions of the model by Dederichs, *et al.*[3] to form what we call model A: 1) The dumbbell trapped at the .09 site is canted away from the impurity atom and into the (110) plane. This can produce a low temperature, C_{44} relaxation which accounts for points 1 and 2 of the main results

observed in Cu-Ag. 2) Site Y is a deeper trap than the .09 trap (with a binding energy in these units of about .095). This accounts for the early disappearance of peak 1 without an accompanying resistivity substage at 110 K (point 3 of our main results in Cu-Ag).

In summary, Model A makes the following predictions:

1) After irradiation, a low temperature attenuation peak appears in the C_{44} mode which is caused by the canted dumbbell. 75% of the induced defects are divided among the canted dumbbell sites (binding energy .09) and the deeper traps marked Y on track B (binding energy .095). Site Y may also produce an attenuation peak in the C_{44} mode whose observation temperature may be higher than its annealing temperature (127 K). The remaining 25% of the induced defects lie in the deepest traps marked .21 in track A. These produce a high temperature attenuation peak in both C' and C_{44} modes.

2) At 110 K, the low temperature peak anneals away as the canted dumbbell leaves the .09 site and migrates to site Y at the same impurity atom. Very little resistivity recovery occurs because the interstitials do not leave the impurity atom, and recovery with nearby correlated vacancies does not take place. If an attenuation peak is associated with site Y, it grows while the peak associated with the .21 site remains unchanged.

3) At about 127 K, site Y finally detraps, and the interstitials leave the impurity atoms to migrate freely through the crystal. Some correlated recovery takes place, but most of the interstitials enter

track A and are deeply trapped. Almost all of the induced defects now reside in the deepest trap and the high temperature peak grows by at most a factor of 4, decreased by the correlated recovery that occurs.

4) Finally, at about 235 K, the deepest traps (at the .21 sites) release their interstitials and the high temperature peak disappears in both modes simultaneously.

We see that in model A, the growth of peak 1 at 60 K (point 4 of our main results) is still unexplained, although the canted dumbbell accounts for the peak itself. We can explain its growth by using Cannon and Sosin's general view of resistivity substage II_c at 60 K as being caused by a reconfiguration of defects from shallow traps into deeper ones. The shallow and deep traps involved, however, are different from the ones chosen by Cannon and Sosin (see figure 2A). In our model A, the deep trap at 60 K can be either the site marked .09 (the canted dumbbell) or the site marked Y. The location of the shallow traps remains unknown. Cannon and Sosin believed such a reconfiguration could cause the resistivity change they observed,[4] but Lennartz, Dworschak, and Wollenberger[43] concluded otherwise after performing damage rate measurements in copper alloys. They found that deeper trapping at an impurity did not seem to change the resistivity contribution of the interstitial compared to no trapping at all. Later in this chapter, we present an alternative explanation for the resistivity substage that is more consistent with the results of Lennartz, Dworschak, and Wollenberger.

The greatest difficulty with this strict adherence to the

calculated binding energies of Dederichs, et al. arises in accounting for the reciprocal damage rate measurements of Dworschak, Lennartz, and Wollenberger.[44] They showed that in dilute copper alloys with Au, Ge, Ni, Pd, Sb, and Zn, final detrapping by the impurity atoms occurs around 110 K. Only the undersized inpurity Be displayed evidence of trapping to higher temperatures. Cannon and Sosin observed that Au and Ag displayed similar properties in their resistivity measurements[4], and, citing Dworschak, Lennartz, and Wollenberger's results, concluded that the substage II_c at 127 K in Cu-Ag was due to the final detrapping of interstitials from single Ag atoms. This directly contradicts the prediction that the deepest trapping site marked .21 is stable to 235 K and forces a major modification of the model. Recognizing that this represents a departure from our earlier attempt to make only small extensions of the model, let us examine some of the consequences of revising the binding energy of the .21 site.

If the defect configuration associated with the .21 site exists at all, it must detrap by 127 K, and its binding energy must therefore be reduced by a factor of 2 or more. (In Cu-Ag, this represents a change from .62 eV to .28 eV.) The annealing temperature may then become lower than the observation temperature of the predicted attenuation peak in C' and C_{44}, thus accounting for the absence of the peak in our measurements. If we assume that the .21 site detraps at 127 K, then point 5 of our results (the growth of peaks 2 and 3 near 127 K) may be explained by the long range migration of interstitials resulting from the final release of defects from the impurity.

This also raises the possibility that the revised .21 site is the deep trap into which the canted dumbbell disappears (at 110 K) instead of our proposed site Y. Otherwise, one has the awkward situation of three separate sites (.09, Y, and the revised .21) all detrapping between 100 and 130 K with site Y and the revised .21 site detrapping at almost the same temperature. The canted dumbbell cannot reach the .21 site via the usual elementary jump, but this constraint on its motion may be lifted due to the pre-existing tilt of the dumbbell into the (110) plane. The canted dumbbell might then be able to reach the .21 site directly via a jump within the (110) plane. On the other hand, it is just as likely that the .21 site does not bind at all and that site Y is the proper choice for the deep trap into which the canted dumbbell disappears. Based on the available evidence, we are unable to favor one over the other.

Thus, we have found that while model A can explain points 1, 2, and 3 from our summary of main results in Cu-Ag, it fails to fully account for the growth of peak 1 at 60 K and the growth of peaks 2 and 3 at 127 K. In fact, strict adherence to the calculated values for the binding energies leads to a strongly bound defect configuration that contradicts the observation that there is no further trapping by single Ag atoms above 127 K.[44] This forces a major departure from our earlier attempt to merely extend the model of Dederichs, et al. instead of revising it. To conform with the experimental observations reported,[4,44] the binding energy of the site .21 must be reduced drastically while leaving the binding energies of the other sites

unchanged. With this drastic change of the estimated binding energy of the .21 configuration, model A remains a possible model, but it can no longer be considered to be a simple extension of the model by Dederichs, et al. This leads us to consider an alternative model, model B.

2. Model B: To explain the observation by Dworschak, et al.[44] that final detrapping by most impurities in copper takes place near 110 K, we require the binding energy of the deepest trap (marked .21) to be decreased by about a factor of 2. In the case of Cu-Ag, the final detrapping is believed[4] to take place near 127 K, corresponding to the resistivity substage II_c seen by Cannon and Sosin. This is also the annealing region where the attenuation peaks 2 and 3 were seen to grow in our measurements, behavior which is consistent with the long range migration of interstitials. We wish to force the deepest trap to release its defects near 127 K, so we change the binding energy of the .21 site from .62 eV to .28 eV (see table VII). It is reasonable to expect that even if the absolute values of the calculated binding energies are wrong, the ratio of their values might still be correct so that the annealing temperature of the .09 site is also scaled down by about the same factor to 76 K. The new binding energies and annealing temperatures for model B are listed in table VII.

The defect responsible for peak 1 in Cu-Ag must still satisfy the requirements outlined earlier. In model B, the only defect which anneals near 110 K is trapped in the .21 site. We require a simple

modification of the dumbbell trapped at the .21 site that can meet the requirements for peak 1. One such configuration is shown in figure 29. The figure shows the motion of a single point interstitial atom from one octahedral site to another, with the trapped dumbbell at the .21 site acting as the saddle-point configuration between the two stable octahedral configurations. We require the octahedral sites to be only slightly more binding than the .21 site so as not to deviate too far from the original assignment of the .21 sites as being the most binding position. This results in a low activation energy for relaxation, satisfying the requirement for a low temperature attenuation peak. There are eight equivalent octahedral sites located at the corners of the cube shown in figure 29 whose degeneracy is removed by a <111> uniaxial stress but not by a <100> uniaxial stress. This produces a peak in C_{44} but not in C'. Therefore, the octahedral defect can account for the symmetry and the temperature of the main attenuation peak observed in Cu-Ag (points 1 and 2 of the Cu-Ag results). In fact, the octahedral position lies at the body center of the face-centered cube where an extra atom is easily accomodated. Hasiguti(1960)[16], after performing a simple elasticity calculation, suggested that this particular configuration was the deepest trap near an oversized impurity in irradiated copper. Our introduction of this configuration is therefore not new.

The binding energy of the .09 site is given in table VII as .12 eV, which corresponds to anannealing temperature of about 76 K. A defect trapped at the shallow .09 site will be released near 76 K,

Figure 29. A(top): A point interstitial is located at the octahedral site in a <111> direction from the oversized impurity.

B(middle): As movement proceeds from one equivalent site to another, a dumbbell forms as a saddle configuration, pushing the normal atom from its site.

C(bottom): Normal atom becomes the interstitial at octahedral site.

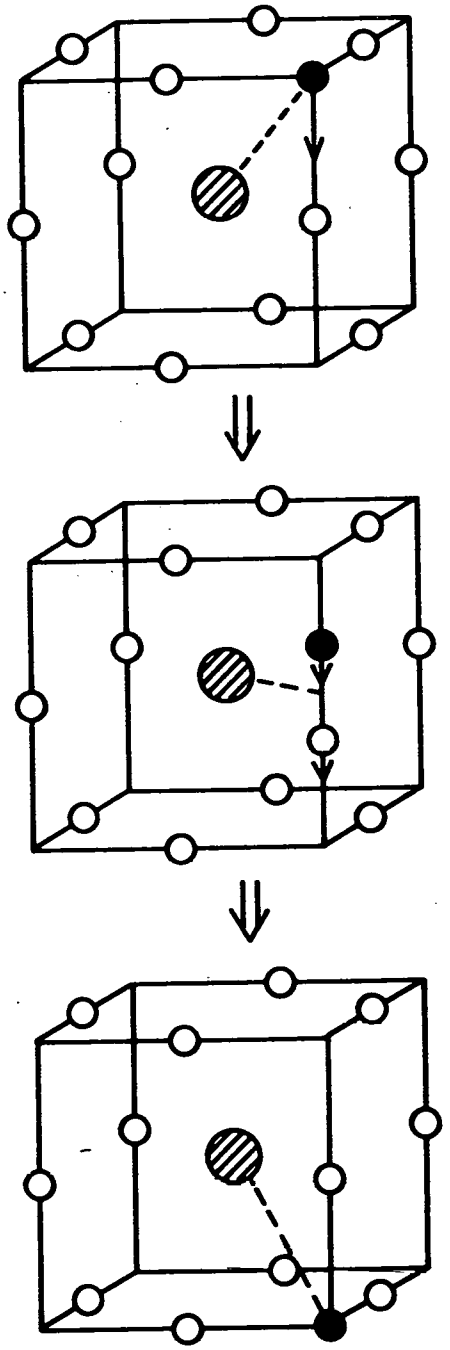

migrate away from the impurity and track B, and either recombine with a correlated vacancy or be deeply trapped at the (new) octahedral site in track A, causing an increase in the height of the low temperature attenuation peak. This gives an account of the growth of peak 1 at 60 K (which is consistent with an estimate of 76 K when one recalls that 76 K should be considered an upper limit) and may explain the resistivity change observed by Cannon and Sosin.[4] However, the process described here is quite different from the one used by Cannon and Sosin. This point will be discussed below in more detail.

Thus, model B consists of three main parts:

1) The .21 site must have a binding energy consistent with the final detrapping of interstitials at 127 K in Cu-Ag; this energy can be no greater than about .28 eV.

2) The trapped dumbbell at the .21 site is actually the saddle-point configuration and the stable position for the interstitial atom is the octahedral site at the center of the face-centered cube. This configuration can produce a relaxation at low temperatures in the C_{44} mode, satisfying points 1 and 2 of our main Cu-Ag results.

3) Even though the magnitudes of the calculated binding energies are wrong, the ratios between them should still be reliable. We find therefore that the .09 site can act as a shallow trap which empties near 76 K and causes the low temperature C_{44} peak to grow. This accounts for point 4 of our main results.

In summary, model B makes the following predictions:

1) After irradiation, a low temperature peak in C_{44} is immediately

visible, due to one-fourth of the induced defects being trapped at the octahedral site. The remaining three-fourths of the defects are located at site .09 and do not produce an attenuation peak.

2) At 60 K, the .09 site detraps. The migrating interstitials find either correlated vacancies or deep traps in track A at the octahedral sites. The attenuation peak grows by at most a factor of 4, decreased by the correlated recovery that occurs. The correlated recovery appears as a resistivity substage.

3) Near 127 K, the octahedral site finally detraps and releases interstitials into the crystal. Long range migration occurs, resulting in correlated and uncorrelated recovery and a resistivity substage.

The major problem with model B is that it does not explain the early disappearance of peak 1 at 110 K without an accompanying resistivity substage. This result was explained in model A by the presence of a deeper trap at site Y that would retain the detrapped defects at the same impurity and prevent correlated recovery from taking place. While it is required that there exists in model B a trap deeper than the trap which gives rise to peak 1, its location is not identified in the model. Therefore, we actually expect that the octahedral site will detrap at 110 K (with a new binding energy of .23) feeding the unidentified deeper trap. This deeper trap releases the interstitial at 127 K. If we recalculate the energy for the .09 site using this new binding energy for the .21 trap, we obtain a new annealing temperature of 69 K. This brings the predicted temperature

closer to the experimentally observed annealing temperature of 60 K.

Another possible difficulty is model B's account of the resistivity substage II_b at 60 K. In this model, the .09 site detraps at 60 K and interstitials are then free to leave track B. This results in some correlated recovery and a distinct substage. Mainly, the interstitials are trapped at octahedral sites at other impurities, which results in the growth of peak 1. Cannon and Sosin[4] discuss the possibility of correlated recovery in explaining the resistivity substage at 60 K, but they discount it in favor of reconfiguration into deeper traps at the same impurity. They based their conclusion in part upon a calculated dependence of the correlated recovery on impurity content. However, it is not clear that their measurements are accurate enough to rule out correlated recovery as a mechanism for explaining their results. For example, Lennartz, et al.[43] found that the resistivity contribution of a trapped interstitial in Cu is equal to the contribution from one which is isolated. This question could be settled by an experiment which could also be used to help select between Model A and model B. This will be discussed in more detail below.

Peaks 2 and 3 are not specifically explained by model B, but their behavior is consistent with one of model B's main assumptions: that the deepest trapping sites finally release their interstitials near 127 K. Long range migration follows this detrapping. Trace impurities or Ag doublets may be present which are still able to trap interstitials. If those traps have relaxation peaks associated with the resulting

defect complexes, then those peaks should increase, just as peaks 2 and 3 do. We do not know the origin of peak 3. However, because peak 2 disappears during the resistivity substage II_d, we make the same identification that Cannon and Sosin make: peak 2 may be due to the relaxation of a defect trapped at a Ag doublet. The defect configuration seems to possess trigonal symmetry, but beyond this comment, no more will be said about the origin of peak 2.

To summarize, model B is able to account for the symmetry and the temperature of peak 1 as well as its growth at 60 K. It accomplishes this by changing the magnitudes of the binding energies calculated by Dederichs, et al. but without changing the ratios between them. Model B is distinguished from model A by its prediction that interstitials change from track B to track A near 60 K, causing some correlated resistivity recovery to take place. The main problem is that model B does not identify the deep trap into which the peak 1 defect disappears at 110 K, though such a trap is still required to exist by our experimental results (see point 3 of our summary of results).

D. Concluding remarks on Cu-Ag

1) The model by Dederichs, et al.[3] fails to predict the appearance of peak 1 in the C_{44} mode or the annealing behavior of peak 1. Furthermore, no evidence is found for the existence of the predicted <110>-orthorhombic defect.

2) Model A. We introduce small extensions to the original model: a) We assume that the dumbbell trapped at site .09 in track B is

canted. b) We assume a positive binding energy for site Y which has previously escaped consideration.

3) Model A explains the low temperature of peak 1 as well as its symmetry and annealing behavior. It does not explain peaks 2 and 3, and it does not identify the shallow trap which feeds the .09 site at 60 K. Furthermore, to account for the evidence of final detrapping at 127 K, it is necessary to suppose that the computed binding energy for site .21 is greatly overestimated so that the ratios of the final set of binding energies are changed from the original.

4) Model B: We take as a starting point that final detrapping occurs at 127 K in Cu-Ag. The resulting model has three parts: a) The binding energy for the .21 site is no greater than .28 eV to account for the final detrapping observed at 127 K. b) The trapped dumbbell at the .21 site is a saddle point configuration between the stable octahedral sites. c) The ratios between the binding energies are as previously computed, so that the .09 site becomes the shallow trap that empties near 60 K.

5) Model B can explain the low temperature of peak 1, its symmetry, and its growth at 60 K. The growth of peaks 2 and 3 at 127 K is accounted for by model B while preserving the ratios of the earlier computed binding energies. This is something that model A fails to do. However, model B's explanation for the resistivity substage at 60 K conflicts with Cannon and Sosin's interpretation. Furthermore, the model does not give a good account of peak 1's early disappearance at 110 K without an accompanying resistivity substage; i.e., a deeper

trap at the same impurity is still required to explain this feature, but it is not identified in this model.

6) One experimentally testable feature distinguishing model A from model B is the prediction of the annealing temperature at which an interstitial first leaves the impurity at which it is trapped. In model A, this occurs near 127 K, when either site Y or the revised .21 site detraps. In model B, this takes place near 60 K when the .09 site detraps, allowing the interstitial to switch to track A at another impurity. We propose here an experiment which may provide additional evidence in support of one model or the other. The experiment requires the existence of an impurity which, when present in irradiated copper, gives rise to attenuation peaks which are distinguishable from those caused by Ag. This impurity can be used as a probe in Cu-Ag to determine when interstitials move from one impurity to another. The peaks caused by the "probe" impurity need to be stable above 60 K. This hypothetical impurity could be introduced in concentrations such that its own attenuation peaks as well as the peaks caused by Ag were large enough to be accurately measured. An example of this is presented in the Al-Mg discussion for the case of Fe as a probe for interstitial motion between Mg atoms. After irradiation at 40 K, an annealing program centered on 60 K could be performed. If the Non-Ag peaks grew at 60 K, then this would mean that interstitials had left the Ag impurities at which they were initially trapped. This would support model B. It would also mean that Cannon and Sosin's interpretation of the resistivity substage II_b (in terms of

reconfiguration at the same impurity) was wrong. On the other hand, if the Non-Ag peaks grew near 127 K, then both model A and Cannon and Sosin's interpretation would be given further support. Of course, further internal friction studies of different alloys need to be done in order to find an impurity which can be used in this fashion.

E. Al-Mg discussion

As in Cu-Ag, none of the peaks seen were consistent with the relaxation of a <110>-orthorhombic defect. This was decided on the basis of the symmetries displayed and by the different annealing behavior shown by each peak. In this discussion, we will focus first on peak 6 in the C_{44} mode because 1) it was the largest peak seen, and 2) it apparently was also seen by Kollers, Jacques, Rehn, and Robrock[27] in an internal friction study at low frequencies (20-70 Hz). This suggests that peak 6 represents the principal intrinsic defect in the system.

Just as for peak 1 in Cu-Ag, peak 6 had no counterpart in the C' mode (an upper limit being established for the C' relaxation strength which, again, was about a factor of 30 times less than the C_{44} relaxation strength observed for peak 6). Therefore, we concluded that peak 6 was not caused by the predicted <110>-orthorhombic defect.

The annealing behavior of peak 6 seemed to correlate well with the resistivity substage observed at 127 K by Garr and Sosin[28] and by Dimitrov, Moreau, and Dimitrov[41] in Al-Mg. Both groups attributed this substage to the final release of interstitials from Mg atoms. Our own

observation in this annealing region was that peak 6 annealed away and that all remaining peaks in both C' and C_{44} modes underwent growth simultaneously. There was no indication (as there was in Cu-Ag) of the presence of a deeper trap into which the peak 6 defect was disappearing.

To summarize the features of peak 6 that need to be accounted for by a model:

1) The peak is a C_{44} peak with no counterpart in C'.

2) It is a high temperature peak, requiring a high activation energy for relaxation.

3) It anneals away at 127 K in an annealing region that correlates well with a resistivity substage (labeled II_b by Garr and Sosin[28].)

4) The remaining peaks (1-5) grow while it anneals away.

5) There is no evidence of a deeper trap at the same impurity into which the peak 6 defect disappears; i.e., the disappearance of peak 6 seems to correspond to a resistivity substage, unlike peak 1 in Cu-Ag.

F. Proposed models for Al-Mg

Since the deepest trap predicted by Dederichs, et al. has the wrong symmetry to explain peak 6 (as do all the other predicted configurations), let us first try to apply model A as it was developed for Cu-Ag. This is desirable since model A still represents only a small deviation from the original model by Dederichs, et al. Therefore, let us suppose that the defect responsible for peak 6 is the canted dumbbell. Of course, the symmetry is correct (for the reasons

cited in the Cu-Ag discussion) but can the same defect type be used to explain two peaks which appear at such widely separated temperatures? Peak 1 in Cu-Ag appears at 16 K while peak 6 in Al-Mg appears at 135 K or higher. Another possible problem lies in a comparison of the temperature-and-dose compensated relaxation strengths, RT_m/c, from tables IV and VI. The value for peak 1(Cu-Ag) is 424 while the value for peak 6(Al-Mg) is almost 13,000, a factor of 30 greater.

Let us first examine the disparity in compensated relaxation strengths. This difference in strengths becomes smaller when one realizes that "c", the dose in terms of induced Frenkel pairs after irradiation, describes the <u>total</u> defect concentration in the crystal and not the concentration of defects specifically responsible for peak 1 or peak 6. In the case of peak 1(Cu-Ag), we believe that another trap exists near the Ag atom which is deeper than the trap associated with peak 1. As an interstitial approaches the Ag atom more closely, it can enter either the peak 1 trap or the other deeper trap. Therefore, this other trap probably accounts for a major proportion of the total defect concentration so that the value of "c" used in Rt_m/c is higher than the concentration of defects actually giving rise to peak 1. In Al-Mg on the other hand, there is no evidence of a deeper trap present near the Mg atom than the trap associated with peak 6. There is then no competition between the peak 6 trap and any other trap for migrating defects so that the value of "c" used in RT_m/c is closer to the actual concentration of defects responsible for peak 6. In any comparison between the two peaks, we need to increase the value of the

compensated strength for peak 1(Cu-Ag).

If we suppose arbitrarily that in Cu-Ag half of the defects go to the peak 1 trap and half to the competing deeper trap, then the difference between the compensated relaxation strengths is reduced to a factor of 15. This implies a difference in the shape factor λ of about a factor of 4 (see equation 9). Physically, this means that the anisotropy of the strain caused by the peak 6(Al-Mg) canted dumbbell is 4 times greater than the anisotropy caused by the peak 1(Cu-Ag) canted dumbbell. Whether this is reasonable or not depends upon the details of the atomic potential close to the impurity atom. However, if we accept that the strain anisotropy of the peak 6(Al-Mg) defect is greater than that of the peak 1(Cu-Ag) defect, then we would expect the relaxation time necessary for reorientation between equivalent sites to be longer for the peak 6 defect than for the peak 1 defect. A longer relaxation time would result in a higher observation temperature for peak 6(Al-Mg) than for peak 1(Cu-Ag). This is in agreement with our experimental results. Therefore, assigning the canted dumbbell of model A to both peak 6 in Al-Mg and peak 1 in Cu-Ag can explain the symmetries observed and does not result in any inconsistencies with our measurements.

Model A: The predictions of Model A are listed earlier (in the discussion of Cu-Ag) but should be modified for Al-Mg. There is now no need for site Y since point 5 in our summary of results states that there is no evidence for a deeper trap at the same impurity into which

the peak 6 defect disappears when the peak anneals away. Indeed, part of our plausibility argument for using the canted dumbbell to explain both peak 1(Cu-Ag) and peak 6(Al-Mg) depends on there not being any site Y in Al-Mg. On the other hand, site .21 needs to revised just as it was in Cu-Ag because reciprocal damage rate measurements by Dworschak, Monsau, and Wollenberger[44] have indicated that single Mg atoms lose their trapping ability above 127 K. The binding energy of the deepest trap (marked .21) must therefore be reduced by about a factor of 2, or the site must be done away with entirely. Table VII lists the calculated binding energies and expected annealing temperatures for the Mg traps in Al. Finally, we assume that the canted dumbbell is capable of a higher temperature relaxation (as outlined above).

The predictions of model A then become:

1) After irradiation, a high temperature attenuation peak appears in the C_{44} mode caused by the canted dumbbells at the .09 sites in track B. A high temperature peak also appears in both C' and C_{44} modes due to the induced defects stuck at the .21 sites in track A.

2) Near 116 K, the canted dumbbell is released from the .09 trap and the attenuation peak in C_{44} disappears. The dumbbell leaves the impurity atom and enters track A at another impurity to be trapped at the .21 site. Correlated resistivity recovery should occur and the high temperature peak in both modes should grow.

3) Near 120 K, the .21 site also releases its interstitials so that both correlated and uncorrelated resistivity recovery takes place.

The associated attenuation peak in both C' and C_{44} modes disappears.

We see that model A for Al-Mg must be changed somewhat to account for the differences between Al-Mg and Cu-Ag. With these changes, the symmetry and temperature of peak 6 can be explained (points 1 and 2 of our summary of results). Furthermore, by revising the .21 site's binding energy as we did for Cu-Ag, we are able to explain the growth of peaks 1-5 (mentioned in point 4) as being due to the resulting long range interstitial migration (similar to the growth of peaks 2 and 3 in Cu-Ag).

The temperature separation that the model predicts between the annealing point when the .09 site detraps and the annealing point when the .21 site detraps does not show up in our measurements. However, Dimitrov, et al.[41] performed resistivity measurements in neutron-irradiated Al-Mg and studied the effect of varying the Mg concentration. They saw two substages, labeled II_{B1} and II_{B2}, at 112 and 129 K respectively which were not evident in the Garr and Sosin electron-irradiation study.[28] Possibly II_{B1} can be associated with the detrapping of the .09 site and II_{B2} with the detrapping of the .21 site, but such an identification must remain uncertain at best. Our own measurements indicated very little change in peak 6 even after the 120 K anneal, and Garr and Sosin only saw a single stage at 127 K in their electron-irradiation study. In any case, no conclusive inconsistency exists here between model A and the experiment.

We still do not see any evidence of a relaxation peak attributable

to the <110>-orthorhombic defect predicted at the .21 site. However, as before in Cu-Ag, it is possible that the temperature of observation (at 10 MHz) was above the annealing temperature so that such a peak might have been missed.

We also note that any growth of peak 6 at lower temperatures similar to the growth of peak 1(Cu-Ag) at 60 K could not be seen by us because of the high temperature of observation for peak 6. A resistivity substage at about 80 K exists in Al-Mg, but its origin is still unknown[28,41] and may be quite different from the 60 K substage seen in Cu-Ag. Kollers, et al.[27], using 20-70 Hz measurements of the internal friction in Al-Mg, saw a set of relaxation peaks which we have tentatively identified with our peak 6. However, the main peak they saw experienced little growth between the 70 and 100 K annealing points (where the resistivity change mentioned above was seen). Therefore, there is little evidence in Al-Mg for a shallow trap that feeds the canted dumbbell sites at 80 K as there was in Cu-Ag (at 60 K).

In summary, a modified model A in which the canted dumbbell remains the major actor, gives a good account of the properties of peak 6 in Al-Mg (as expressed in points 1-5 of our summary of results). No evidence for the predicted <110>-orthorhombic defect was seen. Once again, the main difficulty with model A is that it requires a change in the ratios of the calculated binding energies to account for the detrapping observed at 127 K. This represents an unappealing feature if one wishes to make the smallest possible changes to the model by Dederichs, et al.[3]

Model B: In applying model B to Al-Mg, we need to use the same plausibility argument used for the canted dumbbell in order to establish that the octahedral defect can be used to explain both peak 1(Cu-Ag) and peak 6(Al-Mg). This argument is unchanged if one recalls that even though no deeper trap than the octahedral defect is explicitly identified in model B, such a trap must still exist (in the Cu-Ag case) in order to explain the disappearance of peak 1 without a resistivity substage.

The predictions for model B have been listed before in the discussion of Cu-Ag, and only the annealing temperatures and binding energies need to be changed to the values listed in table VII. We assumed that the binding energies were scaled down by the same factor used in Cu-Ag.

These predictions are:

1) After irradiation, a high temperature peak in C_{44} is visible, due to 25% of the induced defects being trapped at the octahedral site shown in figure 29. The other 75% reside at the .09 sites and do not produce a relaxation peak.

2) Near 72 K, the .09 site detraps and the interstitials migrate away from the impurity to enter track A and the octahedral sites. The high temperature peak grows by at most a factor of 4, decreased by the correlated recovery that also occurs.

3) Near 120 K, the octahedral site finally detraps, resulting in long range interstitial migration. Both correlated and uncorrelated recovery should take place.

The symmetry and temperature of peak 6 can be explained using the octahedral defect of model B. The disappearance of peak 6 near 127 K is in agreement with the detrapping at 120 K predicted for the octahedral site. The resulting long range migration is also consistent with the growth of peaks 1-5 near 127 K.

In Cu-Ag, the use of model B was awkward in the temperature region where the main peak disappeared. For Al-Mg, on the other hand, model B is less awkward than model A in explaining both peak 6's disappearance and the growth of peaks 1-5 with a single detrapping process from the octahedral site.

Earlier in the annealing program, however, model B makes a prediction which seems to contradict what is observed experimentally. It predicts that near 72 K, the .09 sites empty out, causing some correlated resistivity recovery and causing the high temperature C_{44} peak to grow. While some resistivity recovery is observed near 80K,[28,41] there seems to be little evidence for much growth in peak 6. We have tentatively identified our peak 6 with a set of peaks seen by Kollers, et al.[27] Their peak III was considered to be the main peak and was observable by them at about 75 K because of their lower measuring frequencies (20-70 Hz). Peak III grew no more than 10% between 70 and 110 K. The consequence of this upon model B is that the .09 site may no longer be a stable trapping position. It is also possible that a deeper trap on track B (like site Y in model A) is able to retain the detrapped defects and prevent them from feeding the octahedral sites until about 127 K. This too might explain the two resistivity

substages seen by Dimitrov, et al.[41] at 112 and 129 K. However, these suggestions must presently be regarded as speculations only, so that the reasons for the apparent disagreement around 80 K between the predictions of model B and the experimental results remain unclear.

However, an experiment can be performed like the one proposed for Cu-Ag to select between model A and model B. Again, a testable distinction between the two models is that model A predicts that detrapping from track B takes place near 127 K while model B predicts that it takes place near 72 K. It is known that the presence of Fe in electron-irradiated aluminum causes a very strong relaxation peak to appear at low temperatures in the C_{44} mode.[2] This peak does not normally grow at 72 K. If Fe were introduced at a concentration 20 times less than the Mg concentration, then about 1/20th of the induced defects would be trapped at Fe atoms and produce the characteristic 19 K peak (at 10 MHz) in C_{44} that should be visible even at low concentrations. One-fourth of the defects would get to the deep traps in track A (for Mg), and about three-fourths of the defects would get to the shallow traps in track B (if they existed in Al-Mg). After the 80 K anneal, model B predicts that defects are released from track B and migrate away from their impurities. The Fe impurity atoms should trap one interstitial for every five that are trapped in the A tracks of the Mg atoms. This should produce about a three-and-a-half-fold increase in the size of the Fe peak (decreased by whatever correlated recovery took place.) Therefore, if model B were correct, we would expect a significant increase in the size of the Fe peak after the 80 K

anneal. If model A were correct, we would not expect an increase until the 127 K anneal.

As in Cu-Ag, there are a number of peaks (1-5) whose origins lie outside both model A and model B. Since peaks 1-5 grew after the final detrapping at 127 K, the defects responsible for those peaks are not believed to be associated with single Mg atoms. These peaks may be due to impurities other than Mg, since they were apparently not seen by Kollers, et al.[27] For example, as has been mentioned, Fe displays a strong C_{44} peak in irradiated aluminum. Using data from Hultman[2], we estimate that only .1 ppm defects (or 1% of the total number of induced defects, at typical doses) need to be trapped at Fe in order to produce a peak the size of peak 3 at its maximum height. This would require an Fe concentration of only 10 ppm in our sample which is a high though not impossible level for a trace impurity. We did not test for possible saturation effects (i.e., by using different doses) so we have no indication of the concentration levels for the defects responsible for peaks 1-5. If peaks 1-5 were due to trace impurities, it could explain why they were not seen in the internal friction measurements of Kollers, et al.[27] Some of the peaks do appear to be related through their annealing behavior. Peaks 2 and 4 disappear while peak 5 undergoes partial annealing near 190 K which corresponds to a very small, impurity dependent resistivity change seen by Garr and Sosin.[47] However, the change could not be identified with a particular impurity. In this same region, peak 3 grew while peak 1 remained unchanged, but the possible reasons for this are unclear. In short, while a model for

the defect causing peak 6 has been developed, the sources of peaks 1-5 remain more doubtful.

We note here that another calculation of trapping configurations in Al based on the pseudopotential method has been presented by Lam, et al.[46] for several impurities, including Mg. However, they find no traps strong enough to account for complexes surviving to 100 K and above as we see in our own results.

To summarize the Al-Mg discussion:

1) The model by Dederichs, et al.[3] fails to predict the appearance of peak 6 in the C_{44} mode and it also fails to account for the growth of peaks 1-5 at 127 K. Again, as in Cu-Ag, no evidence was found for the predicted <110>-orthorhombic defect.

2) We are forced to modify model A by eliminating site Y. The new version of model A uses the canted dumbbell to account for peak 6. Points 1-5 in our summary of peak 6 characteristics were well accounted for by model A. However, the same difficulty exists as in Cu-Ag that the binding energy of the .21 site must be changed relative to the energy of the .09 site.

3) Model B uses the octahedral defect to provide an explanation for points 1-5 of our summary of results, but it does so by keeping the ratios between the calculated binding energies unchanged. However, there appears to be no experimental evidence in support of the prediction that at about 72 K, the interstitials leave their own impurity atoms and change to a deeper trap on another track at a

different impurity atom.

4) An experiment is proposed to help select between model A and model B. It is the same as the one proposed for for Cu-Ag, with the difference that Fe is already known to be a good candidate for the "probe" atom in aluminum. This is because it exhibits a strong stable, low temperature peak in C_{44} when present in irradiated samples of aluminum. It can therefore provide a test for movement of interstitials from one impurity to another.

G. Future experiments

It is possible in Cu-Ag that the deep trap into which the canted dumbbell disappears produces a relaxation peak which we missed because of our use of MHz frequencies. In fact, the <110>-orthorhombic defect may also have been missed for this reason. Therefore, a low frequency experiment could be performed in single crystals of Cu-Ag to determine whether or not this is the case. Symmetry information from such a study might also help to select one of the possible deep traps mentioned in the Cu-Ag discussion.

A verification of our belief that no such deep trap exists in Al-Mg might be made by introducing Fe as an impurity, but at concentrations perhaps 20 times lower than the Mg concentration so as not to swamp out entirely the Mg effects. Fe in aluminum produces a very strong relaxation peak in C_{44} at 20 K (stable to stage III)[2]. Its growth could act as an indicator for interstitial movement away from their impurities. If this growth took place as peak 6 disappeared,

then this would verify that no deeper trap existed at the same impurity atom. The effect of the Fe impurity upon the heights of the other peaks would also be very informative.

Fe could also be used in the experiment mentioned earlier in the Al-Mg discussion to help select between model A and model B. The test would be of the annealing temperature at which the interstitial first left their impurity atoms. In model A, this happens at 127 K. In model B, this migration takes place between 60 and 80 K. Ultrasonic experiments should be performed in various alloys of copper to find a suitable probe impurity equivalent to Fe in aluminum so that the same experiment may be performed.

Future investigations of Cu-Ag should include a study of the peak heights as a function of Ag concentration. The question of whether peak 2 is connected to Ag doublets might then be resolved by the dependence of its maximum height on decreasing Ag concentration. A similar study on Al-Mg would help in deciding upon the origins of peaks 1-5.

The calculations of Dedcriohs, et al. need to be extended in the directions suggested in our discussion. The possibility of the canted dumbbell should be checked, as well as its modes of migration to possible deeper traps. Site Y should be established as either a binding or an unbinding position for the dumbbell. The deepest trap (.21) should be examined more closely to see why it does not appear to trap above about 127 K in either Cu or Al.

Finally, we hope that a better theoretical understanding of the

diaelastic effect will allow us to determine the validity of the canted dumbbell. It is conceivable that the diaelastic results already seen rule out the presence of such a configuration in favor of some other defect that gives a peak in C_{44} but none in C'. At any rate, more work, both theoretical and experimental, needs to be done.

CHAPTER 5

SUMMARY

A) Measurements were taken of the ultrasonic attenuation and resonant frequency in two oversized systems, Cu-Ag and Al-Mg, which had undergone electron-irradiation. The principal results were the following:

Three peaks were seen in Cu-Ag, all in the C_{44} mode; six peaks were seen in Al-Mg, two in the C' mode and four in the C_{44} mode. Different annealing behavior was displayed by each peak so that we concluded that three different defect types were present in Cu-Ag while six different defect types were present in Al-Mg. The annealing behavior of the peaks in these oversized systems can be compared with the behavior found in undersized systems[2]. A trend toward weaker interstitial trapping by the oversized impurities was noticed. This was found to be roughly consistent with the model calculations by Dederichs, et al.[3]

B) The principal features observed in Cu-Ag that must be accounted for by a model are the following:

1) Three peaks were seen, including the main one (peak 1), all possessing trigonal symmetry (all in the C_{44} mode).

2) Peak 1 was seen at 16 K, so that the defects require a low activation energy of about .014 eV for relaxation.

3) Peak 1 annealed away without an accompanying resistivity substage at 110 K, close to but distinct from the resistivity substage II_c seen by Cannon and Sosin[4] at 127 K.

4) Peak 1 grew at 60 K, corresponding to the resistivity substage II_b seen by Cannon and Sosin.

5) The smaller peaks 2 and 3 grew at about 127 K. Their growth corresponds with the resistivity substage II_c.

C) The principal features of our main peak in Al-Mg (peak 6) are the following:

1) It was seen only in the C_{44} mode, with no counterpart in the C' mode.

2) It was a high temperature peak (> 135 K).

3) It annealed away at 127 K in an annealing region that correlates well with a resistivity substage.

4) The remaining peaks (1-5) grew while peak 6 annealed away.

5) There was no evidence of a deeper trap at the same impurity into which the peak 6 defect disappeared; i.e., the disappearance of peak 6 does seem to correspond to a resistivity substage.

D) The implications of a model by Dederichs, et al., based on the predominant influence of size effects in determining impurity-interstitial interactions, were developed. Predictions were compared with the experimental results. In neither Cu-Ag (which was expected to give the closest agreement to the model) nor Al-Mg was

there found any evidence for the deeply trapped <110>-orthorhombic defect predicted by Dederichs, et al. and by Cannon and Sosin. In both materials peaks of trigonal symmetry occurred instead. Also, the growth with annealing of the smaller peaks was not consistent with the presence of a deep trap like the one predicted by the Dederichs et al. model. Therefore, two alternative models were developed: model A and model B.

E) Small extensions to the original model were made initially, in order to obtain better agreement between prediction and experiment. Model A proposed a) that the dumbbell in the shallow .09 trap be canted slightly, and b) that site Y (see figure 27) is also a trap with a binding energy slightly higher than the canted dumbbell trap. This model was able to account for the symmetry and temperature of peak 1 in Cu-Ag and peak 6 in Al-Mg. It was also able to explain the early disappearance of peak 1 without an associated resistivity substage. However, it did not identify the shallow trap whose detrapping at 60 K is presumed to result in peak 1's growth in Cu-Ag. Furthermore, the binding energy of the deepest trap had to be reduced by a factor of 2 to account for the final detrapping by Ag which was observed at 127 K[44]. This represented a change in the ratio of the calculated binding energies, which constitutes a major modification of the original model.

F) Model B proposed a) that the binding energy of the deepest trap be changed to agree with the final detrapping seen at 127 K, but that

the ratios of the energies remain unchanged, and b) that the stable configuration be an octahedral defect as shown in figure 29, instead of the dumbbell trapped at site .21. This model was also able to account for the symmetry and temperature of peak 1 in Cu-Ag and peak 6 in Al-Mg. It was able to explain the growth of peak 1 at 60 K as well. However, it was not able to identify the deeper trap into which the peak 1 (Cu-Ag) defect disappeared at 110 K.

G) One testable feature that distinguishes model A from model B is the predicted temperature at which the trapped interstitials first leave their impurities. This leads to a possible experiment in which a probe atom (like Fe in aluminum) can be used to determine when interstitial motion between impurities occurs. Such an experiment should be able to provide additional support for one model or the other.

H) Both Cu-Ag and Al-Mg represent systems in which the impurity atoms are oversized by a similar amount within their host crystals. Dederichs, et al.'s model assumes the predominance of size effects and predicts that very similar impurity-interstitial interactions should occur. Our measurements indicate that while similarities exist, there also appear to be significant differences which such a model fails to predict.

REFERENCES

1. D.L. Johnson, Ph.D. Thesis, University of Illinois (1978).

2. K.L. Hultman, Ph.D. Thesis, University of Illinois (1979).

3. P.H. Dederichs, C. Lehmann, H.R. Schober, A. Scholz, and R. Zeller, J. Nucl. Mater. 69 and 70, 176 (1978).

4. C.P. Cannon and A. Sosin, Radiat. Eff. 25, 253 (1975).

5. M.L. Swanson and F. Maury, Can. J. Phys. 53, 1117 (1975).

6. L.E. Rehn, K.-H. Robrock, and H. Jacques, J. Phys F. 8, 1835 (1978).

7. W. Schilling, G. Burger, K. Isebeck, and H. Wenzl, Vacancies and Interstitials in Metals, North-Holland, Amsterdam (1969).

8. G.D. Magnuson, W. Palmer, and J.S. Koehler, Phys. Rev. 109, 1990 (1958).

9. J.W. Corbett, R.B. Smith, and R.M. Walker, Phys. Rev. 114, 1452 and 1460 (1959). Also, J.W. Corbett and R.M. Walker, Phys. Rev. 110, 767 (1958).

10. A.V. Granato, and T.G. Nilan, Phys. Rev. 137, A1250 (1965).

11. D.G. Martin, Phil. Mag. 6, 839 (1961).

12. A. Sosin and L.H. Rachal, Phys. Rev. 130, 2238 (1963).

13. F. Dworschak, A. Kraut, K. Sonnenberg, and H. Wollenberger, Radiat. Eff. 19, 119 (1973).

14. H. Wollenberger, J. Nucl. Mater. 69 and 70, 362 (1978).

15. J.D. Eshelby, Acta. Met. 3, 487 (1955).

16. R.R. Hasiguti, J. Phys. Soc. Jpn. 15, 1807 (1960).

17. A. Sosin, in: Lattice Defects and Their Interactions, R.R. Hasiguti, ed. Gordon and Breach, New York, N.Y. (1967).

18. J.B. Gibson, A.N. Goland, M. Milgram, and G.H. Vineyard, Phys. Rev. 120, 1229 (1960).

19. R.A. Johnson, Phys. Rev. 145, 423 (1966).

20. J. Holder, A.V. Granato, and L.E. Rehn, Phys. Rev. B 10, 363 (1974), Phys. Rev. Lett. 32, 1054 (1974), L.E. Rehn, J. Holder, A.V. Granato, R.R. Coltman, and F.W. Young, Jr., Phys. Rev. B 10, 349 (1974).

21. P.H. Dederichs, C. Lehmann, and A. Scholz, Phys. Rev. Lett. 31, 1130 (1973).

22. K.-H. Robrock and W. Schilling, J. Phys F: Metal Phys. 6 1598 (1976), and V. Spiric, K.-H. Robrock, and L.E. Rehn, in Fundamental Aspects of Radiation Damage in Metals, ed. by M.T. Robinson and F.W. Young, Jr. (National Technical Information Service, Springfield, VA, USA) 240 (1975).

23. H.G. Haubold, loc.cit., 268. See also earlier work in which all but the cubic [100] split octahedral and tetrahedral symmetries had been ruled out for Al. [P. Ehrhart and W. Schilling, Phys. Rev. B8, 2604 (1974)] and for copper [P. Ehrhart and U. Schlagheck, J. Phys. F: Metal Phys. 4, 1575 and 1589 (1974)].

24. M.L. Swanson, F. Maury, and A.F. Quenneville, Phys. Rev. Lett. 31, 1057 (1973).

25. M.L. Swanson, L.M. Howe, and A.F. Quenneville, J. Nucl. Mater. 69 and 70, 372 (1978).

26. G. Vogl, W. Mansel, P.H. Dederichs, Phys. Rev. Lett. 36, 1497 (1976).

27. G. Kollers, H. Jacques, L.E. Rehn, and K.-H. Robrock, Proceedings of the Seventh International Conference on Internal Friction and Ultrasonic Attenuation in Solids at Lausanne, Switzerland, July 1981, published in Journal de Physique, Colloque No. 5, C5-729 (1981).

28. K.R. Garr and A. Sosin, Phys. Rev. 162, 669 (1967).

29. A.S. Nowick and B.S. Berry, Anelastic Relaxation in Crystalline Solids, Academic Press, New York, N.Y. (1972).

30. Device from South Bay Technology of El Monte, California.

31. T. Ochs, J. Phys. E: Sci. Instrum. 1, 1122 (1968).

32. H.E. Bömmel, Phys. Rev. 96, 200 (1954).

33. W.P. Mason, Phys. Rev. 97, 555 (1955).

34. R.W. Morse, Phys. Rev. 97, 1716 (1955).

35. A.B. Pippard, Rep. Prog. Phys. 23, 176 (1960).

36. E. Lax, Phys. Rev. 115, 1591 (1959).

37. A.S. Nowick and W.R. Heller, Adv. Phys. 12, 251 (1963).

38. W. Schilling, J. Nucl. Mater. 69 and 70, 465 (1978).

39. F.R. Fickett, Cryogenics 11, 349 (1971).

40. F.J. Blatt, a table on p. 318 in: Solid State Physics, Vol. 4, Ed. by F. Seitz and D. Turnbull, Academic Press Inc., New York, N.Y. (1957).

41. C. Dimitrov, F. Moreau, and O. Dimitrov, J. Phys. F: Metal Phys. 5, 385 (1975).

42. F.W. Young, Jr., J. Nucl. Mater. 69 and 70, 310 (1978).

43. R. Lennartz, F. Dworschak, and H. Wollenberger, J. Phys. F: Metal Phys. 7, 2011 (1977).

44. F. Dworschak, R. Lennartz, and H. Wollenberger, J. Phys. F: Metal Phys. 5, 400 (1975).

45. F. Dworschak, Th. Monsau, and H. Wollenberger, J. Phys. F: Metal Phys. 6 2207 (1976).

46. K.R. Garr and A. Sosin, Phys. Rev. 162, 681 (1967).

47. N.Q. Lam, N. Van Doan, L. Dagens, and Y. Adda, J. Phys. F: Metal Phys. 11, 2231 (1981).